Differential regulation of mouse hippocampal gene expression sex differences by chromosomal content and gonadal sex

Authors: Sarah R. Ocañas[1,2], Victor A. Ansere[1,2], Kyla B. Tooley[1,2], Niran Hadad[3], Ana J. Chucair-Elliott[1], David R. Stanford[1], Shannon Rice[1], Benjamin Wronowski[2], Kevin D. Pham[1], Jessica M. Hoffman[4], Steven N. Austad[4], Michael B. Stout[5], Willard M. Freeman[1,6*]

[1]Genes & Human Disease Program, Oklahoma Medical Research Foundation, Oklahoma City, OK USA, [2]Department of Physiology, University of Oklahoma Health Sciences Center, Oklahoma City, OK USA, [3]The Jackson Laboratory, Bar Harbor, ME, [4]Department of Biology, The University of Alabama at Birmingham, Birmingham, AL USA, [5]Aging & Metabolism Program, Oklahoma Medical Research Foundation, Oklahoma City, OK USA, [6]Oklahoma City Veterans Affairs Medical Center, Oklahoma City, OK USA

To whom correspondence should be addressed: [*]Willard M. Freeman, Genes & Human Disease Program, Oklahoma Medical Research Foundation, 825 NE 13th Street, Oklahoma City, OK 73104, USA.
Tel: 405-271-3139
Fax: 405-271-2536
E-mail address: bill-freeman@omrf.org

ORCID:
Sarah R. Ocañas: 0000-0003-4281-0303
Victor A. Ansere: 0000-0002-4874-3802
Kyla B. Tooley: 0000-0001-7484-0991
Niran Hadad: 0000-0001-8839-7011
Ana J. Chucair-Elliott: 0000-0002-0172-1876
David R. Stanford: 0000-0002-9232-4074
Shannon Rice: N/A
Benjamin Wronowski: 0000-0002-5954-0736
Kevin D. Pham: N/A
Jessica M. Hoffman: 0000-0002-9487-1629
Steven N. Austad: 0000-0003-4798-8442
Michael B. Stout: 0000-0002-9996-9123
Willard M. Freeman: 0000-0001-7027-999X

Acknowledgments: This work was supported by grants from the National Institutes of Health (NIH) P30AG050911, R01AG059430, R56AG067754, T32AG052363, F31AG064861, P30EY021725, P30AG050886, R21AG058811, R01AG057434, R01AG070035, R01AG069742, Oklahoma Center for Adult Stem Cell Research (OCASCR), a program of the Oklahoma Tobacco Settlement Endowment Trust, BrightFocus Foundation (M2020207), and Presbyterian Health Foundation. This work was also supported in part by the MERIT award I01BX003906 and a Shared Equipment Evaluation Program (ShEEP) award ISIBX004797 from the United States (U.S.) Department of Veterans Affairs, Biomedical Laboratory Research and Development Service. The authors would also like to thank the Clinical Genomics Center (OMRF) for assistance and instrument usage. The authors also acknowledge Robyn Berent (administrative support and lab management), Adeline Machalinski (animal colony management), Ashley Martin (manuscript review), and Hunter Porter (scientific discussions).

Abstract

Common neurological disorders, like Alzheimer's disease (AD), multiple sclerosis (MS), and autism, display profound sex differences in prevalence and clinical presentation. However, sex differences in the brain with health and disease are often overlooked in experimental models. Sex effects originate, either directly or indirectly, from hormonal or sex chromosomal mechanisms. To delineate the contributions of genetic sex (XX v. XY) versus gonadal sex (ovaries v. testes) to the epigenomic regulation of hippocampal sex differences, we use the Four Core Genotypes (FCG) mouse model to uncouple chromosomal and gonadal sex. Transcriptomic and epigenomic analyses of ~12-month-old FCG mice hippocampi, revealed genomic context-specific regulatory effects of genotypic and gonadal sex on X- and autosome-encoded gene expression and DNA modification patterns. X-chromosomal epigenomic patterns, classically associated with X-inactivation, were established almost entirely by genotypic sex, independent of gonadal sex. Differences in X-chromosome methylation were primarily localized to gene regulatory regions including promoters, CpG islands, CTCF binding sites, and active/poised chromatin, with an inverse relationship between methylation and gene expression. Whereas, autosomal gene expression demonstrated regulation by both genotypic and gonadal sex, particularly in immune processes. These data demonstrate an important regulatory role of sex chromosomes, independent of gonadal sex, on sex-biased hippocampal transcriptomic and epigenomic profiles. Future studies will need to further interrogate specific CNS cell types, identify the mechanisms by which sex chromosomes regulate autosomes, and differentiate organizational from activational hormonal effects.

Keywords

Sex difference; hippocampus; epigenome; transcriptome; four core genotypes; sex chromosome

Introduction

Sex is a major risk factor for many neurological diseases and disorders, including Alzheimer's disease (AD) [1, 2], multiple sclerosis [3, 4], autism [5], attention-deficit/hyperactivity disorder (ADHD) [6], depression [7], and age-related cognitive decline [8, 9]. Of particular importance in modulating the cognitive effects seen in many sex-biased diseases is the hippocampus, the learning center of the brain [10]. Females tend to outperform males on hippocampal-dependent learning tasks and are more impacted by many diseases/disorders of hippocampal dysfunction (i.e. AD, depression) [11]. Understanding basal sex differences and their regulation in the hippocampus can help gain insight into the etiology of sex differences in hippocampal dysfunction in common neurological diseases. The goal of this study is to separate the effects of gonadal and chromosomal sex on the sex differential regulation of mouse hippocampal gene expression through epigenomic mechanisms.

Sex characteristics can be influenced by genotypic sex, gonadal sex, and gender. Generally, in mammals, a genotypic female has two X-chromosomes (and no Y-chromosome), while a genotypic male has one X-chromosome and one Y-chromosome. Gonadal sex is classified based on the individual's genitalia, which can influence expression of secondary sex characteristics [12]. Gonadal sex determination is driven by the presence or absence of the Y-chromosome encoded sex-determining region of Y (*Sry*) gene. *Sry* is necessary and sufficient for development of testes, and in the absence of *Sry* mammals develop ovaries [13]. As such, genotypic and gonadal sex are causally linked and the relative contributions of chromosomal and gonadal sex to sex-biases in health and disease are difficult to disentangle.

On the other hand, gender is a societal construct that can be molded by an individual's perception of their sex, as well as influences from their social and physical environments. Although gender, including behavioral and societal influences, likely impacts health and disease outcomes [14], it is not possible to discern gender in non-human animal models. Here we focus on the relative contributions of genotypic and gonadal sex to sex differences in the adult mouse hippocampus.

After gonad differentiation, hormonal secretions influence the organism's sexual phenotype. Gonadal hormonal secretions lead to organizational effects that cause sex differentiation during development, as well as activational effects that may be temporary and reversible and can occur at any stage of life [15]. In a seminal paper, Phoenix et al (1959) [16] described the organizational-activational theory of sexual differentiation in which during early development, hormones have an organizational effect on neural tissue development and circuitry that mediates mating (and likely other behaviors). After the organizational framework is established during development,

activational effects are mediated by levels of gonadal and non-gonadal sex hormones. As such, the direct contributors to phenotypic sex effects are: (1) activational effects of gonadal hormones, (2) organizational effects of gonadal hormones, and (3) sex chromosomal effects [17].

Since the onset of developmental and age-related brain diseases correlate to critical windows of hormonal transition, gonadal hormone effects have been widely studied in brain diseases [18-22]. However, inconsistent efficacy of hormonal replacement therapies (HRT) in diseases like AD [23-25], potential adverse outcomes [26, 27], and the feminizing/masculinizing effects of gonadal hormones have diminished enthusiasm for HRT approaches. On the other hand, several studies have also pointed to distinct contributions of sex chromosomes to brain development [28, 29] and pathology [30-32]. Thus, establishing the contributions of sex chromosomes, independent of gonadal hormones, to brain diseases have come to the forefront of the neurobiology of sex differences.

Despite being the largest genomic difference between humans, the role of sex chromosomes in regulating sex effects is complex and still mostly unclear. Although the human Y-chromosome only contains 568 genes (71 protein-coding) [33], mosaic loss of Y with age has been linked to cancer [34] as well as AD [35]. In comparison, the X-chromosome has between 900 and 1500 genes, but its expression profile is complicated by the random inactivation in females of one X-chromosome on a cell-by-cell basis due to dosage compensation [36]. In fact, the complex nature of sex chromosome genomic regulation led to standardized exclusion of sex chromosomes from genome wide association studies (GWAS) [37], even those specifically interested in sex effects with brain disease [38]. X-chromosome gene dosage effects are evident in human sex chromosome aneuploidies, including Turner syndrome (XO), Triple X Syndrome (XXX), and Klinefelter syndrome (XXY), each with a wide array of CNS symptomology [39-41]. Thus, in humans it appears that genotypic sex, especially the number of X-chromosomes, plays an important role in proper brain development and function. However, sex chromosomal aneuploidies in humans are often confounded by different levels of gonadal hormones. Whereas, in mouse models the levels of hormones are more easily controlled, and can be dissociated from the effects of different numbers of sex chromosomes.

To disentangle the effects of gonadal sex (testes v. ovaries; M v. F) and sex chromosome complement (XX v. XY) on the steady state gene expression and DNA modification patterning of the hippocampus, we use the Four Core Genotypes (FCG) mouse model [42]. The FCG male (XYM) originated through two sequential genetic changes [43]: 1) a spontaneous deletion of the testis-determining *Sry* gene from the Y-chromosome (Y^{-Sry}) [44] and 2) transgenic insertion of the

135 *Sry* gene onto an autosome (A^{Sry}) [45] resulting in $XY^{-Sry}A^{Sry}$ (XYM). Crossing the XYM with a wild-
136 type C57BL/6J XX female (XXF), results in the uncoupling of gonadal and chromosomal sex: XX
137 and XY^{-Sry} mice with ovaries (XXF/XYF) and XXA^{Sry} and $XY^{-Sry}A^{Sry}$ mice with testes (XXM/XYM)
138 (**Fig. 1A**). This allows for 2-way statistical comparisons to assess the contributions of gonadal
139 and chromosomal sex, as well as interactive effects, on molecular and phenotypic outcomes (**Fig.**
140 **1B**).

141 Early FCG mouse studies were aimed at determining if sex chromosome complement (XX v. XY)
142 contributed to development of well-established sexually dimorphic phenotypes [43, 46-48] [49]
143 [50, 51]. Later FCG studies have brought to light distinct contributions of genotypic sex to disease-
144 associated phenotypes seen in Experimental Autoimmune Encephalomyelitis (EAE) and pristane-
145 induced Systemic Lupus Erythematosus (SLE) mouse models [30]. Additionally, XX mice have
146 longer lifespans than their XY counterparts, regardless of gonadal sex [31], and XX mice show
147 resiliency to death in an AD mouse model [32].

148 Although hippocampal sex differences in the transcriptome and epigenome are well-established
149 across development, aging, and disease in mice and humans, the relative contributions of sex
150 chromosome complement (XX v. XY) and gonadal sex (M v. F) to the steady state and stimulus
151 responsive transcriptome and epigenome are not fully defined. Given its influence on X-
152 chromosome inactivation (XCI), genome accessibility, and regulation of gene expression, specific
153 methylation of the fifth carbon of a cytosine residue, resulting in the DNA modification 5-methyl-
154 cytosine (mC) is a particularly interesting epigenetic factor. In this study, we use transcriptomic
155 and epigenetic approaches to examine the hippocampal transcriptome and methylome in adult
156 FCG mice. We then compare our findings to previously identified hippocampal sex differences to
157 begin to separate contributions of sex chromosome complement (XX v. XY) and gonadal sex
158 (testes v. ovaries; M v. F) to sex differences in transcriptional programming.

159 **Results**

160 ***Sry* copy number and localization in adult FCG hippocampi.**

161 The testis-determining *Sry* gene is considered the "master switch" in mammalian gonadal sex
162 determination [52]. In the FCG model, *Sry* is absent from the Y-chromosome and inserted onto
163 an autosome, uncoupling gonadal and genetic sex. Previous initial reports [53] used fluorescence
164 *in situ* hybridization (FISH) and PCR amplicon sequencing to localize a concatemer (12-14
165 copies) of *Sry* on chromosome 3 (Chr3: 70673749-70673824) in FCG XX and XY males. To verify
166 *Sry* copy number, we designed a digital PCR *Sry* copy number assay and confirmed 12-14 copies

167 of *Sry* in FCG males (XXM/XYM), as compared to one copy in WT males (**Fig. 1C**). To confirm
168 the localization of *Sry,* a form of linked-read sequencing was used, which barcodes sequence
169 reads that come from the long DNA fragments with the same oligo tag. Within the visualization, a
170 darker amber color indicates more linked reads between the regions on the X and Y axes (**Fig.**
171 **1D**). There was no linkage between *Sry* and the adjacent region of the Y-chromosome, indicating
172 deletion of *Sry* from the Y-chromosome. Strong linkage of the *Sry* gene with the previously-
173 identified [53] region of chromosome 3 (**Fig. 1E**) within a region with no known gene annotation.
174 No other linked regions were identified indicating that this is the only autosomal insertion site of
175 *Sry*. To examine if *Sry* insertion alters expression of genes on Chr3, hippocampal RNA-Seq data
176 from and wild-type C57Bl/6J mice was compared for genes adjacent (+/- 10Mbp) to the *Sry*
177 insertion site **(Fig. 1F)**. Forty genes were expressed at detectable levels (>20 reads) in male and
178 female hippocampi in all three previous sex difference studies examined [54-56], and each of
179 these 40 genes were also expressed across all four groups in the FCG hippocampi
180 (**Supplemental Table 1**). No sex differences were identified across the three previously published
181 studies. Only a single gene (*Fam198b*) ~9.2 Mbp from the *Sry* insertion was differentially
182 expressed by sex in the FCG hippocampi. Due to the distance from the insertion site and
183 variability in autosomal sex differences, this sex difference is unlikely a result of the *Sry* insertion.
184 Further, there was no ectopic expression of *Sry* in the hippocampi of male FCG mice.

185 **Transcriptomic analysis of sex chromosomal (X/Y) differential expression from adult FCG**
186 **hippocampi.**

187 Despite X-inactivation compensatory mechanisms, there are a number of X-chromosome genes
188 whose expression is imbalanced between males and females in the mouse hippocampus.
189 Previous reports have established differentially expressed sex chromosomally-encoded genes in
190 the mouse hippocampus throughout development and aging [54-57] (**Supplemental Table 2;**
191 **GEO Accession:** GSE83931, GSE135752, GSE76567**; SRA bioProject:** PRJNA523985).
192 Intersecting sex chromosomally-encoded (X/Y) differentially expressed genes by sex across
193 studies identified eight common genes (**Fig. 2A, Supplemental Table 2**), including X-
194 chromosome genes (*Xist, Ddx3x, Kdm6a,* and *Eif2s3x*) and Y-chromosome genes (*Kdm5d,*
195 *Eif2s3y, Uty, Ddx3y*). The four common ChrX genes (*Xist, Ddx3x, Kdm6a,* and *Eif2s3x*) have all
196 been identified as genes likely to escape XCI [58]. XCI escape of *Ddx3x*, *Kdm6a*, and *Eif2s3x* are
197 likely due to intolerance of haploinsufficiency, as each of these genes have Y-encoded paralogs
198 *Ddx3y, Uty, and Eif2s3y*, respectively.

199 Common sexually dimorphic genes from these previous studies were examined in FCG (XXF,
200 XYF, XXM, XYM) hippocampi (n=10-16/group) by RT-qPCR to examine gonadal versus
201 chromosomal sex regulation. X-inactive specific transcript (*Xist*), a non-coding RNA, stabilizes the
202 inactive X-chromosome (Xi) and interacts with various silencing factors to alter chromatin
203 accessibility through a variety of epigenetic mechanisms [59]. In the FCG hippocampus, *Xist* was
204 differentially expressed by sex chromosome complement (XX v. XY) regardless of gonadal sex,
205 with no detected expression in XY genotypes (**Fig. 2B**; Two-way ANOVA, Main effect of sex
206 chromosome complement (XX v. XY), ***$p<0.001$) and no effect of gonadal sex or interactive
207 effect of gonadal and chromosomal sex showing a clear influence of sex chromosome
208 complement in the modulation of X-chromosome dosage compensation.

209 Y-encoded lysine demethylase 5D (*Kdm5d*) mediates H3K4 demethylation and regulates sexually
210 dimorphic gene expression [60]. DEAD-Box Helicase 3 Y-Linked (*Ddx3y*) is part of the male-
211 specific region of the Y-chromosome and contains a conserved Asp-Glu-Ala-Asp (DEAD) motif
212 that is used by ATP-dependent RNA helicases [61]. Expression of Y-chromosome encoded genes
213 *Kdm5d* and *Ddx3y* were assessed by RT-qPCR. In the FCG hippocampus, there was a main
214 effect of chromosome (XX v. XY) on *Kdm5d* and *Ddx3y* expression, with higher expression in XY
215 and no detected expression in XX genotypes (**Fig. 2C-D**; Two-way ANOVA, main effect of sex
216 chromosome complement (XX v. XY), ***$p<0.001$). There was no main effect of gonadal sex (M
217 v. F) or interactive effect of gonadal and chromosomal sex on the expression of *Kdm5d* or *Ddx3y*
218 in the FCG hippocampus.

219 To assess the transcriptome in an unbiased manner, directional RNA Sequencing (RNA-Seq)
220 libraries were prepared from FCG hippocampal RNA (n=5-6/group). After aligning, quantifying,
221 and calling differentially expressed genes, twenty differentially expressed X-chromosome genes
222 were identified with a main effect of sex chromosome (XX v. XY) regardless of gonadal sex (M v.
223 F) with nine genes higher and 11 genes lower in XX vs. XY (**Fig. 2E, Supplemental Table 3**;
224 Two-Way ANOVA, BHMTC, FC>=1.25, FDR<0.1). Only two X-chromosome genes (*Ace2, Aff2*)
225 were differentially expressed by gonadal sex (M v. F) (**Fig. 2F-G, Supplemental Table 3**; Two-
226 Way ANOVA, BHMTC, FC>=1.25, FDR<0.1). Four Y-encoded genes were found to be expressed
227 and each of the four Y-chromosome genes were differentially expressed by chromosome (XX v.
228 XY) (**Fig. 2H, Supplemental Table 3**; Two-Way ANOVA, BHMTC, FC>=1.25, FDR<0.1). There
229 were no Y-chromosome genes differentially expressed by gonadal sex (M v. F). There were no
230 X- or Y-chromosomal genes identified with interactive effects of gonadal and chromosomal sex in
231 the FCG hippocampi.

232 Erythroid differentiation regulator 1 (*Erdr1*) is part of X- and Y-chromosome pseudoautosomal
233 region (PAR) that is able to crossover and recombine during meiosis [62]. As such, genes within
234 the PAR have the same sequence on the X- and Y-chromosome and the chromosomal origin (X
235 or Y) of these transcripts cannot be determined with traditional RNA-Seq. In FCG hippocampi,
236 *Erdr1* is differentially expressed by sex chromosome complement (XX v. XY), with higher levels
237 in XX animals (**Fig. 2I**).

238 The eight common previously identified X/Y-chromosome sex differences (**Fig. 2A,**
239 **Supplemental Table 2 (Intersection)**) were all differentially expressed by sex chromosome
240 complement (XX v. XY) but not gonadal sex in the adult FCG hippocampus. When comparing the
241 union of all sex differentially expressed genes from previous hippocampal studies (**Fig. 2A,**
242 **Supplemental Table 2 (Union)**) to the differentially expressed genes by sex chromosome
243 complement (XX vs. XY) in the FCG hippocampus (**Fig. 2B-I, Supplemental Table 3**) there were
244 18 genes in common (**Fig. 2J**). Functional analysis of differentially expressed genes by sex across
245 all studies revealed enrichment in four overrepresented biological processes (Fisher's Exact,
246 FDR<0.05), including: 1) positive regulation of translational fidelity, 2) histone H3-K27
247 demethylation, 3) histone H3-K4 demethylation, and 4) formation of translation preinitiation
248 complex (**Fig. 2K**). Regulation of histone H3-K27 and H3-K4 methylation have both been
249 implicated in the initiation and maintenance of XCI [63].

250 Together, these data suggest that sex chromosome gene expression is tightly regulated by the
251 sex chromosomes themselves, independent of gonadal sex. Further, sex chromosomally-
252 encoded histone modifiers are likely involved in the maintenance of XCI and also may alter the
253 autosomal epigenome.

254 **Sex chromosome (X/Y) methylation patterns by Whole Genome Oxidative Bisulfite**
255 **Sequencing (WGoxBS) in FCG hippocampi.**

256 DNA methylation can regulate gene expression by a variety of mechanisms, including (but not
257 limited to): 1) direct transcription inhibition by blocking transcription factor binding [64], 2) indirect
258 transcription regulation by recruitment of chromatin modifiers and methyl binding proteins [65-68],
259 3) genomic imprinting [69], and 4) XCI [70-72]. Although methylated DNA is generally associated
260 with transcriptional silencing, there are reported cases where DNA methylation may also serve
261 an activational role [73].

262 In females, XCI occurs through multi-layer epigenetic mechanisms that ultimately compact the
263 inactive X-chromosome (Xi) into a heterochromatic Barr Body. Early in development, the long-

264 noncoding RNA (lncRNA) *Xist* is expressed from Xi and provides a *cis*-coating that recruits protein
265 complexes, leading to changes in chromatin accessibility and DNA modifications [36]. Changes
266 in histone modifications [63] and DNA methylation stabilizes Xi in the inactive state [74]. In this
267 study, we assessed the efficacy of Xi epigenetic silencing in the FCG mouse model by analyzing
268 the X chromosome DNA methylation patterning in FCG hippocampal DNA. DNA isolated from
269 FCG hippocampi (n=3/group) was oxidized and bisulfite-converted prior to constructing whole
270 genome libraries for sequencing. Oxidative bisulfite sequencing provides a specific methylation
271 quantitation, avoiding comingling of hydroxymethylation signal. After aligning and calling
272 methylation values, the whole genome methylation levels in both CG and non-CG (CH) contexts
273 were calculated. There were no observed differences in overall whole genome (including
274 autosomes and sex chromosomes) methylation in CG context (mCG) (**Fig. 3A**) by gonadal sex
275 (M v. F) or sex chromosome complement (XX v. XY), consistent examinations of sex differences
276 in mCG in WT mouse hippocampi [55].

277 When focused on the X chromosome alone, XX genotypes had higher mCG levels than XY
278 genotypes, regardless of gonadal sex (M v. F) (**Fig. 3B**; Two-way ANOVA, main effect sex
279 chromosome complement (XX v. XY), ***$p<0.001$), with a significant interactive effect of
280 chromosomal and gonadal sex ($p=0.0206$). The difference in X-chromosome mCG load between
281 XX and XY genotypes was primarily driven by non-repeat regions (**Fig. 3D**; Two-way ANOVA,
282 main effect sex chromosome complement (XX v. XY), ***$p<0.001$), and was not observed in
283 repetitive elements (**Fig. 3C**; Two-way ANOVA). However, there was a small, but significant effect
284 of gonadal sex on the average mCG in X-chromosomal repetitive elements (Two-way ANOVA,
285 main effect gonadal sex, #$p<0.05$).

286 In non-CpG (CH) context, there was no genome-wide difference in methylation (**Fig. 3E**).
287 However, there were higher levels of X-chromosome mCH in XY than XX, regardless of gonadal
288 sex (**Fig.3F;** Two-way ANOVA, main effect sex chromosome complement (XX v. XY),
289 ***$p<0.001$). Conversely to mCG, higher mCH was seen in both repetitive (**Fig. 3G**) and non-
290 repetitive (**Fig. 3H**) elements of the X-chromosome in XY genotypes as compared to XX (Two-
291 way ANOVA, main effect sex chromosome complement (XX v. XY), ***$p<0.001$), regardless of
292 gonadal sex, with no interaction of gonadal and chromosomal sex. These X-chromosomal
293 methylations trends are consistent with previous reports from wild-type C57Bl/6 mice [75].

294 Since the sex-chromosomally driven (XX v. XY) difference in X chromosomal mCG appeared to
295 be concentrated in non-repetitive elements of the X chromosome, we assessed the mCG
296 patterning in and around important gene regulatory regions, including CpG islands, gene bodies,

297 and CTCF binding sites. CpG islands (CGIs) are relatively long stretches (500-2000nt) of GC-rich
298 DNA that are predominantly unmethylated [76]. CGIs have higher methylation on the Xi [77]. In
299 the FCG hippocampi, XX genotypes have higher levels of mCG within CGIs, shores, and shelves
300 than XY genotypes, regardless of gonadal sex. The largest average mCG difference occurred in
301 the CGI followed by the shores and then shelves (**Fig. 3I**; Two-way ANOVA, main effect
302 chromosome (XX v. XY)). While on average most CGIs are hypermethylated in XX (over XY)
303 genotypes, there was a small subset of genes which show hypomethylation of CGIs in XX (vs.
304 XY).

305 Similarly, gene bodies and the regions 4 kilobases upstream from the transcription start site (TSS)
306 and 4 kb downstream of the transcription end site (TES) had higher percentage of mCG in XX
307 than in XY genotypes (**Fig. 3J**; Two-way ANOVA, main effect chromosome (XX v. XY)). The
308 largest difference in mCG was in the regions 4 kilobases upstream from the transcription start site
309 (TSS), inclusive of the gene promoter.

310 CCCTC-binding factor (*CTCF*) is a zinc-finger protein that mediates chromatin insulation and
311 gene expression by binding 12- to 20-bp DNA motifs (CTCF binding sites) and altering the 3-
312 dimensional chromatin structure. CTCF has high affinity for certain RNA transcripts, including *Xist*
313 and anti-sense transcript *Tsix* [78] which may help to differentially package the inactive and active
314 X chromatin. In the FCG hippocampus, there was lower percentage of mCG in X Chromosome
315 CTCF binding sites as compared to mCG on the whole X chromosome in all genotypes (XXF,
316 XXM, XYF, XYM). There were higher mCG levels in XX hippocampi than XY, regardless of
317 gonadal sex (**Fig. 3K**). The magnitude of difference between XX and XY mCG in CTCF binding
318 sites (~10%) was much greater than the average difference seen across the X chromosome
319 (~3%). Together, the methylation analysis of the X chromosome in FCG hippocampi suggests
320 that X chromosome methylation in non-repetitive regions is regulated by sex chromosome
321 complement (XX v. XY) and likely not influenced by gonadal status.

322 **X-chromosomal repeat element methylation**

323 Within repetitive regions of the X-chromosome, the regulation of DNA methylation is complex.
324 Here we present evidence that gonadal sex impacts X-chromosomal repetitive element DNA
325 methylation and suggest a hormonally-driven mechanism that may contribute to the gonadal sex
326 effect seen in X-chromosomal repetitive element DNA methylation. The mouse X chromosome is
327 made up of ~35% LINE-1 (L1) repeats, as opposed to ~20% on autosomes. The "Lyon Repeat
328 Hypothesis" [79] proposed that LINE-1 (L1) elements promote X-chromosome

329 heterochromatization during XCI. In the FCG hippocampus, LINE-1 elements had higher
330 methylation than LINE-2 (L2) and SINE elements (Alu, B2, B4, MIR) (**Fig. 4A**). Interestingly, the
331 average mCG across X-chromosomal L1 elements was higher in XY genotypes than XX (Two-
332 way ANOVA, main effect sex chromosome complement (XX v. XY), ***p<0.001), indicating that
333 there might be some L1 elements that are not entirely silenced on the inactive X.

334 In contrast, X-chromosomal LINE-L2, SINE-B2, and SINE-MIR elements have lower mCG in XY
335 genotypes as compared to their XX counterparts (**Fig. 4A**; Two-way ANOVA, main effect sex
336 chromosome complement (XX v. XY)), consistent with differences seen in whole X-chromosomal
337 methylation. SINE-*Alu* repeats were the only repetitive element examined that showed a main
338 effect of gonadal sex on X-chromosomal mCG levels, with higher methylation in females than in
339 males (**Fig. 4A**; Two-way ANOVA, main effect gonadal sex (M v. F), #p<0.05). SINE-B4 elements
340 showed no difference in mCG by chromosomal or gonadal sex.

341 Correlation of the degree of overlap (Jaccard distance) between LINE (L1, L2) and SINE (Alu, B2,
342 B4, MIR) repeat elements on the X-chromosome with important gene regulatory features
343 (Promoters, Gene Bodies, Enhancers, Promoter flanks, Transcription factor binding sites)
344 revealed that SINE-Alu and SINE-B4 elements were most strongly correlated with gene promoters
345 and bodies (**Fig. 4B**). L1 elements were associated with promoter flanks and L2 with enhancers,
346 suggesting that LINE elements serve distal regulatory functions in X-inactivation, perhaps through
347 chromatin looping [80]. On the other hand, SINE elements seem tightly correlated with proximate
348 gene regulatory factors, including promoters and transcription factor binding sites. We
349 hypothesize that, in addition to serving as boundary for heterochromatic domains, SINE-*Alu*
350 elements serve as a template to recruit epigenome modifiers to regulate gene transcription
351 (especially in genes that escape X-inactivation) in response to gonadal hormone signals. Motif
352 analysis of X-chromosomal SINE-*Alu* repeat sequences identified SP1 as a potential transcription
353 factor related to these sequences (**Fig. 4C**). STRING protein network analysis [81] identified
354 estrogen receptor 1 (ESR1) and histone deacetylase 1 (HDAC1) as predicted interactors to SP1
355 (**Fig. 4D**).

356 In the adult FCG hippocampus, *Aff2* was differentially expressed by gonadal sex (M v. F), with
357 higher expression in gonadal males as compared to females (**Fig. 1F**), regardless of sex
358 chromosome complement. Investigation of the *Aff2* promoter region revealed TSS flanking by
359 SINE-*Alu* repeats, as well as transcription factor binding sites for SP1, ESR1, ESR2, and JUN
360 (**Fig. 4E**). To better understand the epigenomic regulation of *Aff2*, we examined representative
361 genome tracks of FCG hippocampal methylation alongside publicly available methylation and

362 chromatin data, as well as positioning of CpG islands (CGI) and L1/Alu repeats (**Fig. 4F**). *Aff2*
363 has a CGI-containing promoter that coincides with active histone marks (H3K4me2, H3K4me3,
364 H3K27ac, H3K9ac) and open chromatin (ATAC-Seq) peaks from P0 forebrain [82]. Flanking the
365 *Aff2* TSS are *Alu* repeats (both up and down stream), with L1 elements completely absent from
366 the promoter region, but densely populating the region up and downstream of the flanking *Alu*
367 repeats. Considering only CpG sites between the two *Alu* repeats flanking the TSS, we quantified
368 the site-specific methylation within each of the FCG groups. Within this region, mCG was higher
369 in XX compared to XY (**Fig. 4G;** Two-way ANOVA, main effect sex chromosome complement,
370 ***p<0.001) and higher in gonadal females compared to males (**Fig. 4F**; Two-way ANOVA, main
371 effect gonadal sex, #p<0.001), as well as a significant interaction between chromosomal and
372 gonadal sex (p=0.001). Consistent with these results, the *Aff2* promoter was hypomethylated in
373 WT males (compared to female) [83] mirroring the patterning seen in the FCG hippocampus.
374 These data suggest that gonadal sex (and potentially gonadal hormones) may contribute to X-
375 chromosomal DNA methylation and have implications in escape from X-inactivation. Based on
376 the associations observed here, we propose that circulating estradiol binds to ESR1 and in the
377 nucleus complexes with SP1 and HDAC1. The complex interacts with the SINE-*Alu* repeats
378 flanking active promoters to induce changes in the chromatin landscape, including
379 hypermethylation and heterochromatization (**Fig. 4H).**

380 **Epigenomic patterning in genes that consistently escape X-chromosome inactivation in**
381 **mouse hippocampus**

382 There were four X-chromosomal genes (*Kdm6a*, *Ddx3x*, *Eif2s3x*, *Xist*) that were found to
383 consistently escape X-inactivation across all previously published hippocampal transcriptomic
384 studies examined in **Fig. 2A** and in the present FCG hippocampal study. *Kdm6a*, *Ddx3x*, and
385 *Eif2s3x* are expressed in all FCG groups (XXF, XXM, XYF, XYM) and wildtype (WT-XXF, WT-
386 XYM) with higher expression in XX genotypes regardless of gonadal sex, whereas *Xist* expression
387 is only detected in FCG XXF, FCG XXM, and WT-XXF. Thus, we consider the epigenomic
388 regulation of *Kdm6a*, *Ddx3x*, and *Eif2s3x* separate from *Xist*.

389 Examining the genome tracks for *Kdm6a*, *Ddx3x*, and *Eif2s3x*, revealed several epigenomic
390 patterns across these genes that consistently escape X-inactivation in the mouse hippocampus
391 (**Fig. 5A**). Namely, all three escapees have promoters that contain large CGIs (>500 nt) and
392 coincide with active histone marks (H3K4me2, H3K4me3, H3K27ac, H3K9ac) from publicly
393 available CNS data [82]. Further, the promoter region is almost entirely unmethylated in FCG
394 hippocampus (regardless of chromosomal or gonadal sex) and WT neurons (both males and

395 females) [83] (**Fig. 5A**). The escapee gene bodies each contained H3K36me3 marks in previously
396 published CNS data [82], although H3K36me3 peaks only cover 0.25% of the X-chromosome.
397 Each or the three escapee promoters are flanked by SINE-*Alu* repeats (+/- 5kb from TSS) and
398 are relatively depleted in intragenic LINE-L1 elements (<6% L1) compared to the whole X-
399 chromosome (~33% L1).

400 Within the X-chromosomal transcriptomic analysis, we identified histone H3-K4 and H3-K27
401 demethylation, as over-represented pathways in X-chromosomal sex differences. X-encoded
402 histone modifiers *Kdm6a* and *Kdm5c* demethylate H3K27me2/3 [84] and H3K4me2/3 [85],
403 respectively. The permutation of histone modifications delineates important gene regulatory
404 regions, including active promoters (H3K27ac, H3K9ac, H3K4me2, H3K4me3), weak/inactive
405 promoters (H3K9ac, H3K4me3, H3K4me2, H3K4me1), bivalent promoters (H3K27me3,
406 H3K4me3, H3K4me2, H3K4me1), and transcriptional regulation (H3K36me3). The publicly
407 available CNS histone modification data used for comparison was from pooled male and female
408 brains at postnatal day 0 [82] and serves as a mixed sex developmental baseline. We then use
409 differences in DNA methylation within the histone peaks to predict sex differences in the histone
410 modification patterns (which may be influenced by female-biased *Kdm6a* and *Kdm5c* activity).

411 Within marks of active promoters (H3K9ac, H3K4me2, H3K4me3, H3K27ac) there was higher
412 mCG in XX as opposed to XY genotypes, regardless of gonadal sex (**Fig. 5B**). Since promoter
413 hypermethylation is generally associated with gene inactivation [86], this difference is likely a
414 primary mechanism in maintenance of X-inactivation. As such, hypermethylation of XX active
415 promoters, is likely accompanied by a transition to an inactive promoter state which could involve
416 H3K4 demethylation by *Kdm5c*. Hypermethylation of gene body DNA coincides with H3K36me3
417 and is proposed to prevent cryptic transcription from non-canonical transcription start sites (TSSs)
418 [87]. Hypermethylation of H3K36me3 loci in XX genotypes compared to XY (**Fig. 5B**, Two-way
419 ANOVA, main effect sex chromosome complement, ***$p<0.001$) could indicate demarcation of X-
420 inactivation escape, as previously reported [88]. Repressive H3K4me1 and H3K27me3 are often
421 found at bivalent promoters along with active H3K4me3 [89]. Both H3K4me1 and H3K27me3
422 peaks showed higher methylation in XX over XY genotypes (**Fig. 5B**, Two-way ANOVA, main
423 effect sex chromosome complement, ***$p<0.001$). Since H3K4me1 and H3K27me3 are generally
424 repressive marks, we interpret the XX hypermethylation as indication that XX genotypes have
425 higher H3K4me1 and H3K27me3 within their promoter regions, a function of X-inactivation. As an
426 H3K27 demethylase, *Kdm6a* is likely responsible for liberating repressed chromatin to allow
427 escape from X-inactivation at specific genes.

428 To summarize, differences in DNA methylation within X-chromosomal histone modifications
429 established early in the brain [82] are regulated entirely by sex chromosome complement (XX v.
430 XY), with no effect of gonadal sex. The differences in mCG are most likely associated with
431 variance in histone modification between XX and XY, induced (in part) by imbalance in X-encoded
432 histone modifying enzymes.

433 In addition to genes that always escape X-inactivation in the mouse hippocampus (i.e. *Kdm6a*,
434 *Ddx3x*, *Eif2s3x*), there are also several genes that variably escape X-inactivation; potentially
435 depending on age, disease state, and interaction with gonadal hormones. To determine if genes
436 with similar epigenomic landscapes had similar escape expression patterns, we compiled a list of
437 32 X-chromosomal genes meeting the following criteria: 1) large CGI (>500 nt), 2) active promoter
438 (H3K27me2, H3K27me3, H3K9ac, H3K27ac), 3) H3K36me3 gene body methylation, 4) SINE-*Alu*
439 (+/- 5kb TSS), and 5) *L1* depleted in gene body (<10%) (**Fig**. **5C; Supplemental Table 4**).
440 However, unlike the escape genes which showed almost entirely unmethylated promoter regions
441 across all groups (with no difference by chromosomal or gonadal sex), the other 27 of the 29
442 identified genes had higher methylation in XX genotypes, as compared to XY genotypes (**Fig. 5D,**
443 Two-way ANOVA, Bonferonni MTC, $p<\alpha=0.0016$, main effect sex chromosome complement).
444 Two genes (*Rlim*, *Fam50a*) with the escape chromatin signature had no difference in promoter
445 mCG. However, the promoters mCG of *Rlim* (~28%) and *Fam50a* (~29%) were higher than the
446 consistent escape genes (~6%). Thus, it seems that protecting the Xi promoter from methylation
447 is necessary for consistent escape. In addition, the methylation levels of XXF/M (~32%) and
448 XYF/M (~8%) are indicative of potential shifting between active and poised chromatin.

449 To determine how the chromatin structure of 160 variably escaping genes (identified as X-
450 chromosomal DEG in previous WT [54-57] or present FCG studies) (**Supplemental Table 2-3**),
451 we compared the number of genes that met each of the five escape chromatin criteria
452 (**Supplemental Table 4)**. We found that only three variable escape genes (*Med14, Magt1,*
453 *BC065397*) shared the same chromatin signature as the common escape genes (*Kdm6a, Eif2s3x,*
454 and *Ddx3x*). However, the promoter regions of these genes (**Supplemental Table 4**), are
455 hypermethylated in XX genotypes compared to XY, suggesting that the epigenomic landscape
456 (including histone marks) are likely different between the active and inactive X.

457 Of the variable escape genes: 27% had large CGI promoters, 39% had active promoter histone
458 marks, 17% had gene body H3K36me3, 55% had SINE-*Alu* promoter flanks, and 49% had low
459 L1 gene body density (<10%) (**Fig. 5E**). Thus, it seems likely that the epigenomic regulation of
460 variably escaping genes is distinct from that of common escape genes. As previously suggested,

461 we believe that X-chromosomal DNA methylation could be modulated by gonadal hormone levels.
462 ATAC-Seq profiling of the female brain across the estrus cycle identified 238 genes closest to
463 estrus-responsive chromatin [90]. Intersecting the 238 estrus-responsive chromatin genes with
464 the 160 variable escapee genes and the consistent escape chromatin signature, identified 48
465 estrus-responsive genes with variable escape and a chromatin signature distinct from the
466 consistent escape genes (**Fig. 5F, Supplemental Table 4**). *Xist* was one of the estrus-responsive
467 DEGs and examination of the *Xist*/*Tsix* locus revealed estrus-responsive chromatin peaks in the
468 promoter of *Xist* and transcription end site of *Tsix*. Additionally, distribution of SINE-*Alu* repeats
469 mirrored that of TFBS (SP1, ESR2, JUN) [91] (**Fig. 5G**). Loss of *Xist* expression (and X-
470 inactivation) in female breast, ovarian, and cervical cancer cell lines [92] further support the
471 premise that hormonal mechanisms may contribute to *Xist* expression.

472 **Unbiased calling of X-chromosome differentially methylated regions (DMRs) from Whole**
473 **Genome Oxidative Bisulfite Sequencing (WGoxBS) in FCG hippocampi.**

474 To assess FCG X-chromosomal methylation patterning in an unbiased fashion, we called X-
475 chromosomal mCG DMRs with 1 kb non-overlapping windows and minimum average difference
476 of 10% between at least two groups (Chisq-test, sliding linear model (SLIM) $q<0.05$), followed by
477 a Two-way ANOVA to determine main effects of chromosomal and gonadal sex, as well as
478 potential interactions (Bonferroni correction for six pairwise comparisons, $p<\alpha=0.0083$). Using
479 these criteria, we identified 2552 DMRs: 2456 by sex chromosome (XX v. XY), 145 by gonadal
480 sex (M v. F), and 87 interactive effects (**Fig. 6A, Supplemental Table 5**) on the X-chromosome.
481 Consistent with our previous findings (**Fig. 3-5**), sex-chromosomally regulated DMRs were: 1)
482 enriched in gene regulatory features (gene body, promoter, TFBS, enhancer, CGI, CTCF) and
483 CNS histone marks for active promoters (H3K4me2, H3K4me3, H3K27ac, H3K9ac), poised
484 promoters (H3K4me1, H3K27me3) and transcriptional regulation (H3K36me3), and 2) depleted
485 in repetitive elements (LINEs, SINEs, LTRs) (Fisher's exact test, $p<0.05$) (**Fig. 6B**). Correlation of
486 Jaccard distances of the assessed genomic features with sex chromosomally-driven DMRs, show
487 strong correlation to active promoter regions, again suggesting strong sex chromosome
488 autonomous regulation of X-inactivation (**Fig. 6C**). Within unexpressed genes in the FCG
489 hippocampi there was a small but significant difference in promoter methylation between XX
490 (~68%) and XY (~64%) (**Fig. 6D**, Two-way ANOVA, main effect sex chromosome complement,
491 ***$p<0.001$), with no effect of gonadal sex. Within expressed gene promoters, there was a large
492 difference between XX (~40%) and XY (~17%) genotypes (**Fig. 6D**, Two-way ANOVA, main effect
493 sex chromosome complement, ***$p<0.001$), with no effect of gonadal sex. The incidence of CGI-

494 containing promoters was much higher within expressed genes (~61%) as compared to
495 unexpressed genes (~11%) (Chi-sq test, $p<0.05$) (**Fig. 6E**). There was a strong, negative
496 association between the difference in promoter mCG (XX-XY) and log(FC(XX/XY)) gene
497 expression (Pearson r, $p<0.05$) with no difference in slope or intercept of the linear fit between
498 gonadal males and females. X-chromosomal genes with XX-biased expression (XX>XY) had
499 smaller differences in promoter methylation (XX-XY), while genes with XY-biased genes had
500 larger differences in promoter methylation (XX-XY). These results are consistent with the escape
501 signature of *Kdm6a, Ddx3x*, and *Eif2s3x* (**Fig. 5A**).

502 In agreement with the predicate that gene expression anti-correlates with gene promoter
503 methylation, expression of DEGs *Xist* (**Fig. 6G**), *Flna* (**Fig. 6H**), *Arhgap6* (**Fig. 6I**), and *Hccs* (**Fig.**
504 **6J**) anticorrelated with gene body methylation of those genes.

505 Together, these epigenomic analyses suggest that X-chromosomal regulation of gene expression
506 is primarily controlled by sex chromosomal-autonomous mechanisms, reflecting patterns
507 consistent with X-inactivation and escape.

508 **Targeted bisulfite amplicon sequencing (BSAS) of X-chromosome gene promoters in FCG**
509 **hippocampal DNA**

510 Our WGoxBS data had 2-6X genome-wide coverage, which is sufficient to analyze methylation
511 values in windows and collapse certain genomic regions. In order to assess base-specific
512 methylation patterning, we performed targeted bisulfite amplicon sequencing (BSAS) within the
513 promoter region of X-chromosome genes, using custom primers (**Table 1**).

514 X-linked DEAD-box RNA helicase DDX3 (*Ddx3x*) plays an integral role in transcription and
515 translation, as well as splicing and RNA transport with loss-of-function mutations associated with
516 intellectual disability and developmental delays [93]. *Ddx3x* was more highly expressed in XX
517 genotypes (XXF/XXM) as compared to XY genotypes (XYF/XYM). We amplified a region of the
518 *Ddx3x* promoter, containing 4 CpG sites. Average mCG across the region was higher in XX
519 genotypes as compared to XY genotypes, regardless of gonadal sex (**Fig. 7A**), as well as each
520 individual CpG site (**Fig. 7B**). The site-specific methylation appeared to be strongly regulated by
521 sex chromosome complement, as evidenced by the consistent topography of mCG.

522 Following sex-chromosomally driven sex determination, development of the gonads and
523 production of gonadal hormones further drives dichotomization of sexual phenotypes.
524 Testosterone [94] is recognized by the androgen receptor (*Ar*), a hormone nuclear receptor and

525 transcription factor that has many biological functions, including male reproductive organ and
526 secondary sex characteristic development [95]. Androgens have been found to effect
527 hippocampal structure and function, as well as playing a role in hippocampal-dependent behavior,
528 long-term potentiation, and dendritic arborization [96]. *Ar* is an X-chromosomally encoded gene
529 and subject to X-chromosome inactivation. Although *Ar* was not differentially expressed by sex in
530 outside studies (**Supplemental table 2 (Union)**) or in the present study (neither by gonadal sex
531 (M v. F) or sex chromosome complement (XX v. XY)), we wanted to determine if gonadal sex had
532 any effect on *Ar* promoter methylation, as *Ar* was identified within estrus-responsive chromatin
533 (**Fig. 5F**). BSAS analysis of 22 CpGs in the *Ar* promoter region, showed very low (~0%) mCG in
534 XY genotypes with close to 40% average methylation in XX genotypes, regardless of gonadal sex
535 (**Fig. 7C**). Each CG-site within the amplified region of the *Ar* promoter had lower mCG (~0%) in
536 XY genotypes compared to XX genotypes (~10-60%), regardless of gonadal sex. The patterning
537 of *Ar* promoter mCG was well-conserved between XXF and XXM, suggesting tight regulation of
538 *Ar* promoter methylation by sex chromosome complement, with no effect of gonadal sex (**Fig.
539 7D**).

540 Toll-like receptor (*Tlr7*) is an X-encoded pattern recognition receptor (PRR), critical in innate
541 immunity. *Tlr7* is primarily expressed on microglia in the brain [97] and initiates a Type I interferon
542 (IFN) response to single-stranded viral RNA (ssRNA) [98]. *Tlr7* was differentially expressed by
543 sex in prior studies (**Supplemental table 2 (Union)**) and by sex chromosome complement in the
544 present study (**Fig. 2E**) with higher expression in XY (v. XX) genotypes. *Tlr7* was not found within
545 estrus-responsive chromatin (**Fig. 5F**). The average mCG in an amplified region of the *Tlr7*
546 promoter containing 4 CG sites is higher in XX genotypes over XY genotypes (**Fig. 7E**), and in
547 three of the four CG sites within the amplified region, with no differences by gonadal sex (**Fig.
548 7F**).

549 *Xist* was one X-encoded gene that was differentially expressed by sex in all outside studies
550 examined (**Supplemental table 2 (Intersect)**) and by sex chromosome complement in the
551 present study (**Fig. 2B, 2E**). As a critical regulator of X-inactivation and X-chromosome dosage
552 compensation, we analyzed mCG in an amplified region of the *Xist* promoter in FCG hippocampi.
553 The average mCG within the amplified region of the *Xist* promoter was higher in XY genotypes
554 than XX genotypes, regardless of their gonadal sex (**Fig. 7G**), despite the fact that *Xist* was
555 identified as a gene within estrus-responsive chromatin. The base-specific topography of CG
556 methylation is well conserved by sex chromosome complement (XX/XY), with no effect of gonadal
557 sex (**Fig. 7H**).

558 Angiotensin-converting enzyme 2 (*Ace2*) is surface receptor responsible for negative regulation
559 of the renin-angiotensin system to modulate blood pressure and fluid/electrolyte balance. *Ace2*
560 recently gained attention as the entry receptor for the novel SARS-coronavirus 2 (SARS-CoV-2)
561 [99]. *Ace2* was differentially expressed by sex in the prior studies we examined (**Supplemental**
562 **table 2 (Union)**) and by gonadal sex (M v. F) in the present study (**Fig. 2G**), as well as being
563 within close proximity to estrus-responsive chromatin (**Fig. 5F**). We assessed the mCG at a single
564 CpG site within the *Ace2* promoter and found higher mCG in XY genotypes as compared to XX
565 genotypes, irrespective of their gonadal sex (**Fig. 7I**).

566 In summary, targeted methylation analysis confirmed that X-chromosome methylation within the
567 analyzed regions is tightly regulated, in a base-specific fashion, by sex chromosome complement,
568 and not gonadal sex.

569 **Chromatin context of ChrX DMRs regulated by gonadal sex**

570 There were 145 ChrX DMRs by gonadal sex, including 67 DMRs that were also differentially
571 methylated by chromosomal sex, and 26 DMRs with significant interactive effects (**Fig. 6A,**
572 **Supplemental Table 5**). Gonadal sex regulated DMRs were: 1) enriched in gene regulatory
573 features (gene body, promoter, promoter flanking region, CGI, CTCF) and CNS histone marks for
574 active promoters (H3K4me2, H3K4me3, H3K27ac, H3K9ac), poised promoters (H3K4me1) and
575 heterochromatin (H3K9me3) and 2) depleted in LINE repetitive elements (Fisher's exact test,
576 $p<0.05$) (**Fig. 8A**). Correlation of Jaccard distances of the assessed genomic features with
577 gonadal sex-driven DMRs, show strong correlation to active promoter regions, CGIs, and estrus-
578 responsive chromatin (**Fig. 8B**).

579 There were 73 X-chromosomal genes that had a gonadal sex DMR within 4kb (+/-) of the gene
580 body. Intersecting these genes with the 160 variable escape genes (**Supplemental Table 2 &3**),
581 and 238 estrus-responsive genes (**Supplemental Table 4**) identified 9 genes (*Aff2, Morc4, Gpc4,*
582 *Gpc3, Dmd, Tab3, Stard8, Ammerc1, Tmsb4x*) whose escape from X-inactivation may be
583 regulated by sex hormonal mechanisms (**Fig. 8C**). Genome tracks of the *Morc4* promoter region
584 showed that the gonadal DMR (highlighted in yellow) was closely associated with the estrus-
585 responsive ATAC-seq peak [90] and JASPAR TFBS (SP1, JUN, ESR2) [91], was flanked by
586 SINE-*Alu* repeats, and corresponded to sex differential H3K27ac ChIP-Seq peaks (placenta v.
587 testis) [100] (**Fig. 8D**). Together these data suggest that *Morc4* variably escapes from X-
588 inactivation as a result of alterations in gonadal hormones. *Morc4* mCG within the DMR had higher
589 methylation in XX (v. XY) genotypes and higher methylation in gonadal females (v. males) with a

590 significant interaction effect (Two-way ANOVA, main effect sex chromosome complement
591 (***p=1.44E-08), main effect gonadal sex (#p= 0.0011), interaction (p= 0.0002)) (**Fig. 8E**).

592 **Transcriptomic analysis of autosomal differential expression from adult FCG hippocampi.**

593 After establishing that the sex chromosome transcriptome and methylome of FCG hippocampi
594 are primarily controlled by sex chromosome complement (XX v. XY) with some specific
595 interactions with gonadal sex (M v. F), we next examined regulation of autosomal sex differences.
596 We first intersected the previous hippocampal transcriptomic studies to determine steady-state
597 sex differences in the mouse hippocampus (**Fig. 9A**). Although there were no sex differences in
598 common between all studies (**Fig. 9A**, **Supplemental Table 6 (Intersection)**), there were 2896
599 sex differences identified in at least one study (**Supplemental Table 6 (Union)**). Age, sample
600 size, and estrus-cycle staging differences between these studies are summarized in **Table 2.** To
601 interrogate the discordance in sex differences across these studies, we performed pairwise
602 correlations (Pearson r) on fold change (M v. F) from DEGs expressed in across all studies.
603 Hierarchical clustering of the correlation matrix showed the strongest association between 3 mo
604 [101] and 4 mo [55] studies (**Fig. 9B**). The lack of correlation between other studies and early
605 developmental timepoints (1-2 mo [54]) suggests that hippocampal sex differences observed
606 during postnatal development are distinct from those seen in adulthood and with aging.

607 We next ran GO Biological Process, KEGG Pathway, and transcription factor over-representation
608 analysis (ORA) using WEB-based GEne SeT AnaLysis Toolkit (WebGestalt,
609 www.webgestalt.org) on autosomal genes that were differentially expressed by sex in at least one
610 outside study (**Supplemental Table 2 (Union)**) (**Fig. 9C**, **Supplemental Table 6**, hypergeometric
611 test, BHMTC, FDR<0.05). Enriched biological processes included lipid homeostasis, CNS neuron
612 differentiation, regulation of leukocyte activation, pattern specification process, and reproductive
613 system development, among others. Enriched transcription factors include immune regulators
614 (IRF1, SRF, and MEF2), metabolic regulators (FOXO4), and vesicular trafficking (AP4), among
615 others. Two significant KEGG pathways were over-represented in the hippocampal sex
616 differences: neuroactive ligand-receptor interaction and systemic lupus erythematosus. Together,
617 these data suggest that hippocampal sex differences alter neuronal differentiation/signaling and
618 immune-related processes, which both could be partially mediated by differences in metabolic
619 processes.

620 Of note is the fact that only one of the previous sex difference studies [54] mentioned estrus-cycle
621 staging females, with collection of 2 estrus, 2 metestrus, and 1 diestrus females from each age

622 group (1, 2, 4 mo). As such, this study [54] identified fewer estrus-dependent transcriptomic
623 changes in 2 mo (6 genes) and 4 mo (22 genes) compared to age-matched 2 mo [57] (78 genes)
624 and 4 mo [55] (90 genes) from other studies that did not estrus-cycle stage (**Fig. 9D, Table 2**).
625 The 24 mo group [56] had few estrus-responsive DEGs, while the 2 mo [57], 3 mo [101], and 4
626 mo [55] that were not estrus cycle staged showed the largest number of estrus-responsive DEGs
627 (**Fig. 9D**).

628 Next, we assessed autosomal sex differences in FCG hippocampus by sex chromosome
629 complement (XX v. XY) and gonadal sex (M v. F) using directional RNA-Seq. After aligning,
630 quantifying, and calling 212 differentially expressed genes: 62 genes differentially expressed by
631 sex chromosome complement alone (XX v. XY), 123 genes differentially expressed by gonadal
632 sex (M v. F), 26 genes differentially expressed by both sex chromosome complement and gonadal
633 sex, and 1 gene with a significant interaction of gonadal and chromosomal sex (**Fig. 9E**). Principal
634 component analysis of differentially expressed autosomal genes shows separation by gonadal
635 sex in component 1 (33.9%) and separation by sex chromosome complement in component 2
636 (20.2%) (**Fig. 9G**). Hierarchical clustering of autosomal-encoded DEG shows proper clustering of
637 samples by genotype (**Fig. 9H**). ORA of the 88 chromosomally-driven (XX v. XY) autosomal sex
638 differences in the FCG hippocampus revealed four enriched biological processes: antigen
639 processing and presentation, regulation of innate immune response, response to virus, and
640 response to protozoan (Hypergeometric test, BH FDR<0.05). ORA of the 149 gonadal sex-driven
641 (M v. F) autosomal sex differences in the FCG hippocampus revealed three enriched biological
642 processes: leukocyte mediated immunity, response to virus, and response to protozoan
643 (Hypergeometric test, BH FDR<0.05) (**Fig. 9I**).

644 Since we identified response to viruses and interferon-beta as pathways enriched in sex
645 differences in the FCG hippocampus, we further examined interferon-associated genes IRF-7 and
646 IFIT-3, both of which were differentially expressed by sex in other studies (**Supplemental Table**
647 **3 (Union)**). Interferon (IFN), as part of the innate immune system, triggers the expression of IFN-
648 stimulated genes (ISGs) in response to viral recognition. IFN-beta is a type I IFN that is activated
649 through PRRs [102], like *Tlr7*, is primarily in microglia [97]. In mouse models of AD, IFN was found
650 to activate microglia leading to neuroinflammation and synaptic degradation. Blocking IFN
651 signaling decreased microglia activation and concomitant synapse loss. Activation of IFN pathway
652 was also observed in human AD [103]. Transcription factor IRF-7 is considered a "master
653 regulator" in type-I IFN responses [104]. *Irf7* was differentially expressed in our study by sex
654 chromosome complement (XX v. XY) and gonadal sex (M v. F) in FCG hippocampus as

evidenced by RNA-Seq (**Supplemental Table 4**) and RT-qPCR confirmation (**Fig. 9J**). *Irf7* RT-qPCR also identified an interactive effect of gonadal and chromosomal sex (p=0.012). Interferon-induced protein with tetratricopeptide repeats 3 (IFIT3) is an antiviral RNA-binding protein which acts an intermediary in the activation of IRF-3 and upregulation of IFN-beta [105]. *Ifit3* was differentially expressed by sex chromosome complement (XX v. XY) and gonadal sex (M v. F) in FCG hippocampus as evidenced by RNA-Seq (**Supplemental Table 4**) and RT-qPCR confirmation (**Fig. 9K**).

Antigen processing and presentation pathways were also over-represented in our analysis of genes differentially expressed by chromosomal sex in the FCG hippocampus. Class I major histocompatibility (MHC-I) complexes function in innate viral antigen presentation and detection. Given that previous studies from our lab identified sexually divergent induction of MHC-I with aging in the mouse and rat hippocampus [106, 107], we examined expression of MHC-I components *B2m*, *H2-D1*, and *H2-K1*. Here we show differential expression of B2m by gonadal sex (**Fig. 9L**) and H2-D1/H2-K1 by sex chromosome complement and gonadal sex (**Fig. 9M-N**) in the FCG hippocampus (n=10-16/group, Two-Way ANOVA, main effect of sex chromosome complement (XX v. XY) *p<0.05, **p<0.01, ***p<0.001 and/or gonadal sex (M v. F) #p<0.05, ##p<0.01, ###p<0.001).

Based on the meta-analysis of previous studies, it appears that hippocampal autosomal sex differences are context-dependent and likely change throughout development and with aging. In the adult FCG hippocampus, sex differences were primarily enriched for in immune-related pathways and are regulated by both chromosomal and gonadal sex.

Autosomal chromosome levels of methylation in FCG hippocampus by WGoxBS

After analyzing autosomal sex differences in FCG hippocampal gene expression, we assessed autosomal methylation in CG and CH context by WGoxBS. Overall, there were no differences in total autosomal mCG (**Fig. 10A**), as well as when split into in repetitive (**Fig. 10B**) and non-repetitive (**Fig. 10C**) element autosomal mCG. No difference was found in average autosomal mCH (**Fig. 10D**), repetitive element mCH (**Fig. 10E**) or non-repetitive element mCH (**Fig. 10F**). There were also no apparent differences in autosomal mCG patterning across CGI, shores, and shelves (**Fig. 10G**), gene bodies/flanking regions (**Fig. 10H**), or CTCF-binding sites/flanking regions (**Fig. 10I**). These data are consistent with previous findings that sex differences in mouse hippocampal autosomal methylation are site-specific and are a mix of both hyper- and hypomethylation in females compared to males [108].

687 **Autosome differentially methylated regions (DMRs) by Whole Genome Oxidative Bisulfite**
688 **Sequencing (WGoxBS) in FCG hippocampi.**

689 CG methylation was examined in the context of autosomal: CNS-associated histone marks [82]
690 (H3K9ac, H3K4me2, H3K4me3, H3K27ac, H3K9me3, H3K36me3, H3K4me1, H3K27me3) (**Fig.**
691 **11A**), specific repetitive elements (SINE: Alu, B2, B4, MIR; LINE: L1, L2) (**Fig. 11B**), and proximal
692 gene regulatory regions (enhancer, promoter, CGI, gene body) (**Fig. 11C**). There were no main
693 effect differences by gonadal or chromosomal sex in average mCG across any of these genomic
694 regions. In LINE elements (L1 & L2) there was a significant interactive effect of gonadal and
695 chromosomal sex on autosomal LINE elements (L1, L2) mCG (Two-way ANOVA, $p<0.05$) but
696 with a minimal methylation difference (<1%). While there were no sex effects in average mCG
697 across these features, the levels of mCG varied among different features (i.e. Enhancers ~ 48%
698 and Promoters ~3%).

699 After exploring the overall levels and patterning of DNA methylation on the autosomes, autosomal
700 mCG DMRs were assessed using 1 kb non-overlapping windows (Chisq-test, sliding linear model
701 (SLIM) $q<0.05$) and *post-hoc* Two-way ANOVA with Bonferonni correction ($p<\alpha=0.0083$) to
702 assess main and interactive effects of chromosomal and gonadal sex. Using these criteria, we
703 identified 4505 DMRs by sex chromosome (XX v. XY), 1385 DMRs by gonadal sex (M v. F), and
704 487 significant interactive effects of gonadal and chromosomal sex (**Supplemental Table 7**). We
705 identified 2615 genic regions intersecting DMRs by chromosomal sex, 911 genic regions
706 intersecting DMRs by gonadal sex, and 332 genic regions intersecting DMRs with an interactive
707 effect of chromosomal and gonadal sex. These gene lists were assessed by GO Biological
708 process over-representation analysis to identify significant pathways (**Supplemental Table 7**,
709 hypergeometric test, BHMTC<0.2). ClusterProfiler [109] functional profiler assessment identified
710 enrichment in neuronal-specific pathways (synapse organization, dendrite development,
711 glutamatergic synaptic transmission) within the sex chromosomal and/or gonadal DMR- related
712 genes (**Fig. 11D**).

713 To determine if there was a relationship between autosomal gene expression and promoter
714 methylation, we correlated the difference in promoter methylation (mCG %) and differential gene
715 expression (log(FC)) by sex chromosome (**Fig. 11E**, XX v. XY) and gonadal sex (**Fig. 11F**, M v.
716 F). There was a weak negative correlation between differential gene expression and promoter
717 methylation among the XYF v. XYM comparison (**Fig. 11F,** Pearson $r=-0.167$, $^*p=0.045$). No other
718 significant correlations were identified.

719 Most (84%) of the autosomal FCG DEGs from **Fig. 9E** did not overlap with a DMR (**Fig. 11G**).
720 The autosomal DEGs that did overlap with DMRs appear to be primarily related to neuronal
721 functions (*Gabrb1*, *Syt2*, *Cacna1c*, *Kcnj6*). The 177 DEGs not overlapping with DMRs, were
722 enriched in immune-related genes (i.e. *Irf7*, *Ifit1/3*, *B2m*, *H2-D1*, *H2-K1*). Since immune cells, like
723 microglia, are minority populations compared to neurons, the epigenomic signatures of microglia
724 are not well represented in the bulk epigenomic data and require epigenomic analysis of these
725 specific cell types to reveal methylation differences not observed in whole tissue analyses [110].
726 Further cell type-specific epigenomic data will need to be collected from the FCG model to
727 determine the cell type-specific contributions to sex differential gene expression in the
728 hippocampus.

729 Although *Esr1* was not differentially expressed in the FCG hippocampus, it was identified as a
730 gene differentially expressed by sex in published mouse hippocampal data. Within the FCG mCG
731 data, we identified 3 DMRs within the *Esr1* gene body DMRs by chromosomal (DMRs 1 & 2) and
732 gonadal (DMR 3) sex (**Fig. 11H-I**). *Esr1* DMRs by chromosomal sex may suggest a sex differential
733 imprinting mechanism used to regulate *Esr1* expression before the induction of gonadal
734 hormones. The gonadal DMR indicates a potential feedback domain to modulate estrogen-
735 receptor expression in response to gonadal hormones. Examples of differential methylation within
736 differentially expressed genes was also shown for: GABA receptor *Gabrb1*, interferon response
737 gene *Oas2*, and methyl-CG dependent histone modifier *Setdb2* (**Fig. 11J)** demonstrating that
738 while some DEGs do not have a correspond methylation difference, in some genes like these
739 there is a corresponding methylation change.

740 Despite a strong immune-related transcriptomic signature, differential methylation appears to be
741 mostly involved in neuron-related pathways. This could be expected given that neurons are the
742 predominant cell type in the hippocampus. And while there is variable association of DMRs to
743 DEGs, the expression analysis is examining steady state gene expression and these DMRs may
744 cause differential gene expression in acute, stimulus-responsive situations. Future studies will
745 also need to specifically examine minority microglia cell population to uncover methylation-gene
746 expression relationships in these cells.

747 **Discussion**

748 The study of sex effects in brain health and disease have begun receiving needed experimental
749 attention in neuroscience studies. Not only do the sexual dimorphisms, differences, and
750 divergences [111] need to be characterized but also the regulatory mechanisms giving rise to
751 these sex effects. While hormonal mechanisms (both organizational and activational) have been

752 the most studied, the potential regulation of sex effects by sex chromosomes, either
753 independently or in concert with gonadal hormones, has received relatively limited attention.
754 Symptomology associated with human sex chromosome aneuploidies [39-41] and experimental
755 evidence obtained from FCG mouse studies [17, 31, 32, 48, 53] have provided critical insight into
756 the importance of sex chromosomes (independent of gonadal sex) to sex effects seen in
757 development, aging, and disease. Previous reports have established sex differences in the
758 hippocampal epigenome and transcriptome with brain aging [108, 125] and disease [57, 126,
759 127], further suggesting that the intersection of epigenetic alterations and sex effects requires
760 further investigation. Here we use the FCG mouse model to delineate the contributions of gonadal
761 and chromosomal sex to the epigenomic regulation of hippocampal gene expression in adult
762 mice.

763 We first validated the genetics of the FCG model, confirming prior imaging and PCR studies [53]
764 and providing a precise location of *Sry* insertion to an intergenic region of Chr3. While there are
765 ~13 copies of *Sry*, the insertion is not within an annotated gene. Since the concatemer of *Sry*
766 could disrupt the chromatin accessibility within and around the insertion site on chromosome 3,
767 we assayed for ectopic *Sry* expression and changes to gene expression genes adjacent to the
768 insertion site. However, we found no evidence of *Sry* expression in the hippocampus (as
769 expected) and no disruption of gene expression in adjacent genes. Additionally, tissue-specific
770 expression of Y-encoded genes (*Kdm5d*, *Eif2s3y*, *Ddx3y*, *Uty*) was maintained in the FCG,
771 despite deletion of *Sry*. Together these data provide confidence that the transgenic manipulations
772 used to generate the FCG are not confounding the analysis of sex differences in the hippocampus.

773 XCI, the random silencing of one X-chromosome (Xi) during female embryogenesis, is an
774 important mechanism for gene dosage compensation between males and females [112].
775 Maintenance of XCI occurs via intricate epigenomic mechanisms, including DNA
776 hypermethylation, lncRNA expression (i.e. *Xist*), and specific histone modifications [113].
777 However, Xi is not fully repressed and a subset of X-chromosome genes consistently escape XCI,
778 leading to higher expression in females [114, 115]. Escape from X-inactivation in females has
779 been implicated in the female bias in autoimmune diseases [116, 117] and AD [118]. X-
780 chromosomal paired transcriptomic and DNA methylation sequencing revealed that sex effects in
781 XCI and escape are principally driven by sex chromosome content, but may be “fine-tuned” by
782 gonadal sex. Contributions of gonadal sex XCI escape may explain why escape genes vary by
783 tissue [58]. We found that methylation of ChrX proximal gene regulatory features (gene body,
784 promoter, enhancer, CGI) was regulated autonomously by the sex chromosomes with patterning

785 consistent with XCI signatures previously reported in WT mice [55, 77]. Among ChrX DEGs,
786 promoter methylation showed a strong negative correlation to gene expression, suggesting an
787 important role of DNA methylation in modulating escape from XCI. We also propose a chromatin
788 signature for genes that always escape XCI, which is distinct from the chromatin context of
789 variable escape genes. This led us to hypothesize that variable XCI escape may result from sex
790 hormonal dependent mechanisms.

791 Repetitive elements (especially LINE-L1) have been implicated in XCI spreading, escape, and
792 maintenance [79, 119-121]. Specific L1 element expression is posited to facilitate propagation of
793 XCI [119]. In the FCG hippocampus, L1 elements were the only X-chromosomal genomic features
794 that showed lower mCG in XX (v. XY) genotypes. The hypomethylation of XX (v. XY) ChrX L1
795 elements could represent a sex chromosome autonomous mechanism of XCI. The only ChrX
796 genomic feature that displayed differential mCG by gonadal sex was SINE-Alu repeats, with
797 higher methylation in gonadal females than males. Using *Aff2* as an example, we propose an Alu-
798 repeat dependent mechanism for epigenomic modulation of gene expression by gonadal sex. The
799 idea of hormonal tuning of XCI is bolstered by ChrX chromatin accessibility alterations by estrus-
800 cycle stage [90]. Further hormone manipulation studies (i.e. ovariectomies) will need to be
801 conducted to confirm this hypothesis.

802 Autosome-encoded hippocampal gene expression and methylation sex differences are regulated
803 by both sex chromosomes and gonadal sex. Importantly, hippocampal changes induced with age
804 [56, 106-108] and female estrus-cycle stage [90, 122, 123] need to be considered in calling
805 consistent gene expression differences driven by gonadal sex. Despite the FCG chromosomal
806 and gonadal sex differential gene expression being strongly enriched in inflammatory pathways
807 (i.e. MHC-I, interferon-response), regions of differential methylation were strongly associated with
808 neuronal functions. Additionally, comparison of gene expression and promoter methylation within
809 DEGs did not show the strong, negative correlations normally seen with methylation-dependent
810 gene transcription. Since microglia are a minority cell population in the hippocampus, changes in
811 microglial methylation patterns are difficult to detect in bulk sequencing data. Thus, further studies
812 examining cell type-specific epigenomic regulation of sex differential gene expression are needed.

813 The mechanism for sex chromosome content directly regulating the autosomes may lie, in part,
814 in the X-chromosome encoded histone demethylases *Kdm6a* and *Kdm5c* and Y-encoded *Uty* and
815 *Kdm5d* since sex chromosome-regulated DEGs were enriched by H3-K27 and H3-K4
816 demethylation peaks. Recent reports have highlighted the importance of sex chromosome-
817 encoded histone modifiers in mouse models of autoimmunity [124, 125], adiposity [126], and AD

818 [32]. Further work will be needed to manipulate individual X- and Y- encoded histone modifiers to
819 determine their effect on the epigenomic landscape of both sex chromosomes and autosomes in
820 the context of brain aging and disease.

821 Of particular relevance to the present hippocampal study, Davis et al. (2020) used the FCG model
822 to establish that a second X-chromosome confers protection against AD [32] through X-linked H3-
823 K27 demethylase *Kdm6a*. They showed that hippocampal overexpression of *Kdm6a* in male mice
824 with a familial AD mutation (XY-hAPP-J20) attenuated AD-induced cognitive deficits when
825 compared to controls. This study provides critical insight into the sex-biased regulation of AD
826 pathogenesis and opens several new lines of investigation. Primarily, do alterations in H3-K27
827 methylation play a causal role in the neuroprotective effects of *Kdm6a*? If so, are alterations in
828 H3-K27 methylation localized to the X-chromosome or do sex chromosome-encoded histone
829 modifiers alter the autosomal epigenomic landscape? Do other cell types (e.g., microglia) rely on
830 *Kdm6a* for proper function in response to AD pathology? In the hAPP-J20 model used [30], the
831 humanized APP is inserted into a noncoding portion of Zinc finger protein *Zbtb20* gene (involved
832 in interferon response in macrophages [55]), causing decreased hippocampal *Zbtb20* expression
833 [56]. Since interferon response genes (e.g., *Tlr7, Irf7, Ifit3*) were identified in the present study as
834 being differentially regulated by both sex chromosome complement and gonadal sex, a different
835 mouse model of AD (in lieu of the hAPP-J20) may allow for further identification of sex differentially
836 regulated microglial inflammatory pathways contributing to AD.

837 Taken together these findings are consistent with the hypothesis that the sex chromosomes have
838 effects on the hippocampal epigenome and transcriptome independent of gonadal sex. This is
839 the first demonstration of the separable effects of hormones and sex chromosomes on the
840 epigenome and transcriptome in the FCG hippocampus. However, a number of questions remain
841 to be answered in future studies. These principally consist of further controlling for gonadal
842 hormone status but analyzing FCG mice that have been gonadectomized after development at
843 ~1-2 months of age. This will control for any activational hormonal differences between the
844 genotypes. It is worth noting that these studies were conducted in adult mice ~12 months of age.

845 Most importantly, analyses of specific cell types are needed for future studies, as transcriptomic
846 and epigenomic profiles differ between neuronal, glial, and other cell types of the CNS. Expanding
847 the research on the epigenetic and transcriptomic landscapes in specific cell populations of the
848 brain will help us more clearly delineate cellular contributions to sex differences in future molecular
849 studies. Further investigation is highly warranted given the significant effects of sex chromosome

850 regulation of gene expression and DNA modification patterns in cis of the X chromosome and in
851 trans of the autosomes.

852 **Methods**

853 **Animals**

854 All animal procedures were approved by the Institutional Animal Care and Use Committee at the
855 University of Alabama at Birmingham (UAB) under protocol 21506. Four Core Genotypes mice
856 on a C57Bl/6J background were obtained from the Jackson Laboratory (Stock #010905) where
857 they were revitalized from frozen embryo stocks. Breeder pairs were set up with a XX female and
858 a XY male, as described in the introduction. Pups were weaned into sex specific cages of 4-5
859 animals based on visual inspection of genitalia. Animals were maintained in an AAALAC approved
860 UAB animal facility at 21°C on a 12/12 light/dark cycle (lights on at 6:00am). Animals were
861 provided ad libitum water and standard mouse chow (NIH31) until time of tissue collection, ~12
862 months of age for both males and females. Euthanasia prior to tissue harvesting was carried out
863 by cervical dislocation followed by rapid decapitation. Genotyping was performed using the
864 primers: Sry (5′-AGC CCT ACA GCC ACA TGA TA-3′, 5′-GTC TTG CCT GTA TGT GAT GG-3′),
865 Ymt (Y chromosome-specific sequence, 5′-CTG GAG CTC TAC AGT GAT GA-3′, 5′-CAG TTA
866 CCA ATC AAC ACA TCA C-3′), and myogenin (5′-TTA CGT CCA TCG TGG ACA GCA T-3′, 5′-
867 TGG GCT GGG TGT TAG TCT TAT-3′) [53], following Jackson Laboratory's standard PCR assay
868 genotyping protocol #5590.

869 **High molecular weight (HWM) DNA isolation for pseudo long-read genomic sequencing**

870 Hippocampi were dissected from a FCG XYM mouse, snap frozen in microfuge tubes with liquid
871 nitrogen, and stored at -80ºC prior to DNA isolation. HMW DNA was extracted from fresh-frozen
872 tissue according to 10X Genomics sample preparation protocol
873 (https://support.10xgenomics.com/genome-exome/sample-prep/doc/demonstrated-protocol-
874 hmw-dna-extraction-from-fresh-frozen-tissue). Frozen tissue was thawed on ice and minced with
875 a razor blade. The tissue was gently Dounce homogenized in 500 µL of Nuclei Isolation Buffer
876 (Sigma Nuclei PURE Prep Kit: Lysis Buffer, 1 mM DTT, Sigma Nuclei PURE Prep Kit: 10% Triton
877 X-100). After a brief centrifugation, the supernatant was transferred using a wide-bore pipette tip
878 to a 2.0 mL round-bottom tube and centrifuged at 500 x g for 5 minutes. The supernatant was
879 discarded, and pelleted nuclei were then resuspended in 70 µL of ice-cold PBS. To digest the
880 nuclei, 10 µL of Proteinase K was added to the resuspended nuclei, followed by 70 µL ice-cold
881 Digestion Buffer (20 mM EDTA, pH 11, 2mM Tris-HCl, pH 8.3,10 mM N-Laurylsarcosine sodium

882 salt). Samples were rotated end-over-end for 2 hours at room temperature. To purify the DNA,
883 Tween-20 was added to the sample to a final concentration of 0.1% and then 1X SPRISelect
884 Reagent was added. The samples were rotated end-over end for 20 min. Tubes were placed in
885 the DynaMag-2 magnetic rack to allow bead capture. After removing and discarding the
886 supernatant, the beads were washed twice with 70% ethanol. The DNA was eluted from the beads
887 with 50 µL Sample Elution Buffer (Qiagen AE Buffer, 0.1% Tween-20). Qubit dsDNA BR kit was
888 used to quantify the DNA.

889 **10X Linked-Read Library Preparation**

890 Linked-read genomic libraries Chromium were constructed from 1 ng of HMW DNA from an XYM
891 using Chromium Genome Library Prep Kit (#PN-120229, 10X Genomics, Pleasanton, CA),
892 according to manufacturer's instructions. Briefly, following HMW gDNA extraction 1 ng of HMW
893 DNA was loaded onto a Chromium Genome Chip Kit (#PN-120216, 10X Genomics) for Gel Bead-
894 in-Emulsions (GEM) generation and barcoding. After SPRISelect bead cleanup and library
895 construction, libraries were normalized to 4 nM, pooled, and sequenced NextSeq500 (High
896 PE150) in the OMRF Clinical Genomics Center (CGC). Sequencing data was aligned to the mm10
897 genome using the LongRanger pipeline (10X Genomics) and visualized in the Loupe browser.

898 **Isolation of DNA/RNA from FCG hippocampi**

899 Hippocampi were dissected from XXF, XXM, XYF, and XYM FCG mice (n=10-16/group), snap
900 frozen in microfuge tubes with liquid nitrogen, and stored at -80ºC prior to DNA isolation. Nucleic
901 acids (DNA/RNA) were isolated from flash-frozen tissues using the All Prep DNA/RNA Mini Kit
902 (Qiagen, Germantown, MD) as previously described [127-129]. Briefly, 600 µL of Buffer RLT with
903 beta-mercaptoethanol was added to the tube containing the frozen hippocampi. A steel bead was
904 added to the tube and homogenized for 30 s at 30 Hz using a Tissue Lyser II (Qiagen).
905 Homogenate was loaded onto a DNA spin column and the flow through supplemented with
906 ethanol was loaded onto an RNA spin column. Columns were washed and nucleic acids eluted
907 by centrifugation. Total DNA/RNA were quantified by Nanodrop (Thermofisher Scientific,
908 Madison, USA). Quality of DNA and RNA were assessed by genomic and RNA screentapes,
909 respectively, on a Tapestation 2200 (Agilent Technologies, Frankfurt, Germany). Only samples
910 with RNA and DNA integrity numbers > 7 were used for subsequent experiments.

911 **Digital PCR (dPCR) *Sry* copy number assay**

912 Custom *Sry* fluorogenic copy number assays were designed and purchased from Integrated DNA
913 Technologies (Coralville, IA) with primers (5'-GTC ACA GAG GAG TGG CAT TT-3', 5'-AGT CTT
914 GCC TGT ATG TGA TGG-3') and probe (5'-/56-FAM/CAACCTTCT/ZEN/GCAGTGGGACAG
915 GAA/3IABkFQ/-3'). Mouse *Tert* fluorogenic copy number assay was used as a single copy gDNA
916 control as reference (#4403316, Life Technologies). DNA from FCG hippocampi (n=3/group) was
917 used for dPCR, as previously [129], using the QuantStudio 3D Digital PCR kit (#A26361,
918 ThermoFisher Scientific), according to manufacturer's instructions. After combining DNA with the
919 Quantstudio 3D mastermix and *Sry* or *Tert* fluorogenic assay, reactions were loaded onto a
920 Quantstudio 3D PCR chip with a Quantstudio 3D chip loader (#4482592, Thermofisher Scientific)
921 and cycled on a GeneAmp PCR system 9700 with a flatblock attachment. Chips were read by the
922 Quantstudio 3D chip reader (#4489084, Thermofisher Scientific) and analyzed using Quantstudio
923 3D AnalysisSuite cloud software V3.1.

924 **Quantitative PCR (qPCR)**

925 Confirmation of gene expression levels was performed with qPCR as previously described [55,
926 130, 131]. cDNA was synthesized with the ABI High-Capacity cDNA Reverse Transcription Kit
927 (Applied Biosystems Inc., Foster City, CA) from 25ng of purified RNA. qPCR was performed with
928 gene-specific primer probe fluorogenic exonuclease assays (TaqMan, Life Technologies,
929 Waltham, MA, **Supplemental table 5**) and the QuantStudio 12K Flex Real-Time PCR System
930 (Applied Biosystems). Relative gene expression (RQ) was calculated with Expression Suite v
931 1.0.3 software using the $2^{-\Delta\Delta}$Ct analysis method with GAPDH as an endogenous control.
932 Statistical analysis of the qPCR data was performed using GraphPad Prism 8 (San Diego, CA).
933 Two-way ANOVA analyses were performed followed by the Tukey's multiple comparison test
934 ($p<0.05$).

935 **Library construction and RNA sequencing (RNA-seq)**

936 Illumina's TruSeq Stranded mRNA Library Prep Kit (#20020594, Illumina) was used on 500 ng of
937 total RNA for the preparation of strand-specific sequencing libraries according to manufacturer's
938 guidelines. As previously described [56], rRNA depletion was performed prior to library
939 construction.

940 RNA was isolated from fresh-frozen hippocampal tissue of 12 mo FCG mice (n=5-6/group), using
941 Qiagen AllPrep DNA/RNA Mini Kit. After verifying RNA integrity numbers (RIN) with TapeStation
942 (Agilent) and quantifying RNA with Qubit dsDNA Broad Range Assay kit (Invitrogen), 1 ug of RNA
943 was used to construct RNA-Seq libraries using the Illumina TruSeq Stranded RNA Library Prep

944 Kit, following the manufacturer's guidelines. cDNA libraries were sized by TapeStation (Agilent)
945 and quantified by qPCR (KAPA Biosystems). Libraries were then normalized to 4 nM, pooled,
946 denatured, and diluted for sequencing on Illumina Hiseq2500 in a 2x100 bp fashion.

947 **RNA-Seq Data Analysis**

948 Following sequencing, reads were trimmed, aligned, differential expression statistics and
949 correlation analyses were performed in Strand NGS software package (Agilent), as previously
950 described [55]. Reads were aligned against the Mm10 build of the mouse genome (2014.11.26).
951 Alignment and filtering criteria included: adapter trimming, fixed 2bp trim from 5' and 6bp from 3'
952 ends, a maximum number of one novel splice allowed per read, a minimum of 90% identity with
953 the reference sequence, a maximum of 5% gap, trimming of 3' end with Q<30. Alignment was
954 performed directionally with Read 1 aligned in reverse and Read 2 in forward orientation. Reads
955 were filtered based on the mapping status and only those reads that aligned normally (in the
956 appropriate direction) were retained. Normalization was performed with the DESeq algorithm
957 [132]. Transcripts with an average read count value >20 in at least 100% of the samples in at
958 least one group were considered expressed at a level sufficient for quantitation per tissue. Those
959 transcripts below this level were considered not detected/not expressed and excluded, as these
960 low levels of reads are close to background and are highly variable. A fold change >|1.25| cutoff
961 was used to eliminate those genes which were unlikely to be biologically significant and
962 orthogonally confirmable due to their very small magnitude of change. For statistical analysis of
963 differential expression, a two-way ANOVA with the factors of sex chromosome complement and
964 gonadal sex and a Benjamini-Hochberg Multiple Testing Correction (BHMTC) with an FDR of 0.1.
965 Visualizations of hierarchical clustering and principal components analysis were performed in
966 Strand Next Generation Analysis Software (NGS) (Version 3.1, Bangalore, India). The entirety of
967 the sequencing data is available for download in FASTQ format from NCBI Gene Expression
968 Omnibus (GEO) under accession number GSE184098.

969 **Bisulfite amplicon sequencing (BSAS)**

970 BSAS for specific gene promoters was performed as previously described [110, 128]. Briefly, FCG
971 hippocampal DNA (200 ng) was bisulfite converted with the EZ DNA Methylation-Lightning Kit
972 (#D5030T; Zymo Research, Irvine, CA), according to the manufacturer's guidelines. Bisulfite-PCR
973 was conducted using primer sets (Integrated DNA Technologies; **Table 1**) designed against
974 specific genomic regions with Methyl Primer Express v1.0 software (Thermofisher Scientific).
975 PCR amplicons were cleaned with AmpureXP beads (#A63882; Beckman Coulter Life Sciences,

976 Indianapolis, IN) using size selection with 0.7x bead ratio. Following clean-up, the amplicons were
977 quantified using QubitTM dsDNA HS assay kit (#Q32851; Thermofisher Scientific) and pooled.
978 One ng of the pooled amplicons was used for library construction with the Nextera XT DNA library
979 preparation kit (#FC-131–1096; Illumina, San Diego, CA), according to the manufacturer's
980 instructions. Libraries were quantified with Qubit dsDNA HS assay kit and TapeStation HD1000,
981 normalized to 1 nM or 4 nM, and pooled for sequencing. Pooled libraries were then sequenced
982 on iSeq or MiSeq (Illumina) at loading concentrations 35 pM or 8 pM, respectively. Fastq files
983 were aligned to amplicon sequences in CLC Genomics Workbench 11.0 (Qiagen) using the "Map
984 Bisulfite Reads to Reference" feature. Site-specific CpG (CG) and CH methylation percentages
985 were extracted for downstream analysis.

986 **Library construction and oxidative bisulfite sequencing (WGoxBS-seq)**

987 DNA was isolated from fresh-frozen hippocampal tissue of 12 mo FCG mice (n=3/group), using
988 Qiagen AllPrep DNA/RNA Mini Kit. Whole genome oxidative bisulfite sequencing libraries were
989 prepared according to manufacturer's guidelines (Ovation Ultralow Methyl-Seq Library System,
990 Tecan Genomics, Inc., Redwood City, CA) as previously described [55, 110]. Briefly, 1 µg of
991 gDNA in 50 µl 1X low-EDTA TE buffer was sheared with a Covaris E220 sonicator (Covaris, Inc.,
992 Woburn, MA) to an average of 200 base pairs. Sheared products were sized by capillary
993 electrophoresis (DNA HSD1000, Agilent) and cleaned using an Agencourt bead-based
994 purification protocol. After quantifying (Qubit dsDNA, Thermofisher Scientific) the cleaned DNA,
995 200 ng gDNA fragments were prepared in a 12 µl volume to which 1µl of spike-in control DNA
996 (0.08 ng/ul) with known levels of specific mC, hmC, and fC at individual sites was added. End
997 repair, ligation of methylated adaptors (#L2V11DR-BC 1-96 adaptor plate, Tecan Genomics) and
998 final repair were performed according to manufacturer's instructions. Normalized DNA was
999 oxidized and then bisulfite- converted with the True Methyl oxBS module (NuGEN) with
1000 desulfonation and purification. 22 µl of libraries were eluted from the magnetic beads. qPCR was
1001 used to determine the number (N) of PCR cycles required for library amplification. Oxidative
1002 bisulfite-converted samples were amplified for 13 cycles [95° C- 2 min, N (95°C-15 s, 60°C-1 min,
1003 72° C-30s)]. Amplified libraries were purified with Agencourt beads and eluted in low-EDTA TE
1004 buffer. Capillary electrophoresis (TapeStation HSD1000, Agilent) was used to validate and
1005 quantify libraries. Amplified libraries were normalized to a concentration of 4 nM and pooled,
1006 denatured, and diluted to 12 pM for sequencing on NovaSeq 6000 (Illumina) according to
1007 manufacturer's guidelines with the exception of a custom sequencing primer (MetSeq Primer) that
1008 was spiked in with the Illumina Read 1 primer to a final concentration of 0.5 µM.

1009 **OxBS-seq data analysis**

1010 Global levels of mCG, hmCG, and mCH were analyzed as previously described [55],[110] Before
1011 aligning, paired-end reads were adaptor-trimmed and filtered using Trimmomatic [133] 0.35. End-
1012 trimming removed leading and trailing bases with Q-score<25, cropped 4 bases from the start of
1013 the read, dropped reads less than 25 bases long, and dropped reads with average Q-score<25.
1014 Unpaired reads after trimming were not considered for alignment. Alignment of trimmed OxBS-
1015 converted sequences was carried out using Bismark [134] 0.16.3 with Bowtie 2 [135] against the
1016 mouse reference genome (GRCm38/mm10). Bams were de-duplicated using Bismark.
1017 Methylation call percentages for each CpG and non-CpG (CH) site within the genome were
1018 calculated by dividing the methylated counts over the total counts for that site in the oxidative
1019 bisulfite - converted libraries (OXBS). Genome-wide CpG and CH methylation levels were
1020 calculated separately. BAM files generated during alignment were run through methylKit in R [136]
1021 to generate context-specific (CpG/CH) coverage text files. Bisulfite conversion efficiency for C,
1022 mC, and hmC was estimated using CEGX spike-in control sequences. Untrimmed fastq files were
1023 run through CEGX QC v0.2, which output a fastqc_data.txt file containing the conversion mean
1024 for C, mC, and hmC. The entirety of the sequencing data is available for download in FASTQ
1025 format from NCBI Gene Expression Omnibus (GEO) under accession number GSE184013.

1026 **DMR Analysis**

1027 CpG text files were read into methylKit [136] and converted to an object. The mouse genome was
1028 tiled in 1000 nt non-overlapping windows. Each window was filtered for a minimum count of 10.
1029 Samples were then united and compared for windows covered in at least two samples per group.
1030 Differentially methylated regions (DMRs) were called using default parameters. DMRs were
1031 filtered to differences that were >10% different between at least two groups and had a SLIM-
1032 generated q-value less than 0.05. The methylDiff object was intersected with the methylBase
1033 object to calculate the % methylation for each window that passed the described filtering. *Post-*
1034 *hoc* assessment of main and interactive effects of chromosomal and gonadal sex was conducted
1035 using a Two-way ANOVA with Bonferonni correction for six pairwise comparisons ($p<\alpha=0.0083$).

1036 **Software usage for tertiary analysis of transcriptomic and epigenomic data**

1037 Over-representation analysis (ORA) for GO Biological processes, transcription factor networks,
1038 and KEGG pathways was conducted using WEB-based GEne SeT AnaLysis Toolkit (WebGestalt,
1039 www.webgestalt.org) [137]. EnrichedHeatmap [138] in R was used to visualize DNA methylation
1040 levels across ChrX and autosomal CGI, Gene body/promoter, and CTCF binding sites. Bed files

1041 for genomic features were downloaded from the UCSC table browser [139] and visualized with
1042 custom tracks using the UCSC genome browser (http://genome.ucsc.edu) [140]. BEDtools [141]
1043 was used to intersect mCG/CH text files with specific genomic features. TrawlerWeb [142] was
1044 used to identify over-represented motifs from BED files. STRING protein-protein association
1045 networks [81] were used to determine potential protein interactors with SP1. Venny [143] and
1046 BioVenn [144] were used to compare gene lists and make Venn diagrams. BedSect [145] was
1047 used to create Jaccard distance matrices comparing genomic features to differentially methylated
1048 and expressed regions. ggplot2 [146] and clusterProfiler [147] were used to generate dotplots of
1049 GO biological processes.

Declarations

Funding

This work was supported by grants from the National Institutes of Health (NIH) P30AG050911, R01AG059430, R56AG067754, T32AG052363, F31AG064861, P30EY021725, P30AG050886, R21AG058811, R01AG057434, R01AG070035, R01AG069742, Oklahoma Center for Adult Stem Cell Research (OCASCR), a program of the Oklahoma Tobacco Settlement Endowment Trust, BrightFocus Foundation (M2020207), and Presbyterian Health Foundation. This work was also supported in part by the MERIT award I01BX003906 and a Shared Equipment Evaluation Program (ShEEP) award ISIBX004797 from the United States (U.S.) Department of Veterans Affairs, Biomedical Laboratory Research and Development Service.

Conflicts of Interest/Competing Interest

The authors have no conflicts of interest to declare that are relevant to the content of this article.

Availability of data and material

The datasets generated during and/or analyzed during the current study are available in the NCBI Gene Expression Omnibus (GEO) repository and Sequence Read Archive (SRA) with accession numbers: GSE83931, GSE135752, GSE76567, GSE184098, and PRJNA523985. All other data are available from the corresponding author on reasonable request

Code availability

All data were analyzed with commercially available software packages and open-source web applications and R packages, as indicated in the text.

Author contributions

Sarah R. Ocañas: first author, design of the study, execution of experiments, data acquisition, analysis, and interpretation, figure generation, manuscript writing and preparation.

Victor A. Ansere: execution of experiments, data acquisition, analysis, and interpretation, figure generation, manuscript preparation.

Kyla B. Tooley: execution of experiments, data acquisition, analysis, and interpretation, figure generation.

Niran Hadad: data analysis and interpretation, figure generation, manuscript writing and preparation.

Ana J. Chucair-Elliott: design of the study, data interpretation, manuscript writing and preparation.

David R. Stanford: design of the study, data analysis and interpretation.

Shannon Rice: execution of experiments, data acquisition, analysis, and interpretation.

Benjamin Wronowski: execution of experiments, data acquisition, analysis, and interpretation, figure generation.

Kevin D. Pham: data analysis and interpretation, manuscript writing and preparation.

Jessica M. Hoffman: design of the study, execution of experiments, data analysis and interpretation, manuscript writing and preparation.

Steven N. Austad: design of the study, data analysis and interpretation, manuscript writing and preparation.

Michael B. Stout: design of the study, execution of experiments, data acquisition, analysis, and interpretation, manuscript writing and preparation.

Willard M. Freeman: Corresponding author, design of the study, data analysis and interpretation, figure generation, manuscript writing, preparation, and submission.

Ethics approval

Not applicable

Consent to participate

Not applicable

Consent for publication

Not applicable

References

1. Ferretti, M.T., et al., *Sex differences in Alzheimer disease - the gateway to precision medicine.* Nat Rev Neurol, 2018. **14**(8): p. 457-469.
2. Dumitrescu, L., et al., *Sex differences in the genetic predictors of Alzheimer's pathology.* Brain, 2019. **142**(9): p. 2581-2589.
3. Voskuhl, R.R., et al., *Sex differences in brain atrophy in multiple sclerosis.* Biology of Sex Differences, 2020. **11**(1): p. 49.
4. Jobin, C., et al., *Gender Issues in Multiple Sclerosis: An Update.* Women's Health, 2010. **6**(6): p. 797-820.
5. Werling, D.M. and D.H. Geschwind, *Sex differences in autism spectrum disorders.* Current opinion in neurology, 2013. **26**(2): p. 146-153.
6. Arnett, A.B., et al., *Sex differences in ADHD symptom severity.* Journal of child psychology and psychiatry, and allied disciplines, 2015. **56**(6): p. 632-639.
7. Eid, R.S., A.R. Gobinath, and L.A.M. Galea, *Sex differences in depression: Insights from clinical and preclinical studies.* Progress in Neurobiology, 2019. **176**: p. 86-102.
8. Burke, S.L., et al., *Sex differences in the development of mild cognitive impairment and probable Alzheimer's disease as predicted by hippocampal volume or white matter hyperintensities.* J Women Aging, 2019. **31**(2): p. 140-164.
9. Gur, R.E. and R.C. Gur, *Gender differences in aging: cognition, emotions, and neuroimaging studies.* Dialogues in clinical neuroscience, 2002. **4**(2): p. 197-210.
10. Anand, K.S. and V. Dhikav, *Hippocampus in health and disease: An overview.* Annals of Indian Academy of Neurology, 2012. **15**(4): p. 239-246.
11. Yagi, S. and L.A.M. Galea, *Sex differences in hippocampal cognition and neurogenesis.* Neuropsychopharmacology, 2019. **44**(1): p. 200-213.
12. Purves D, A.G., Fitzpatrick D, et al., editors., *Neuroscience*. 2nd edition ed. 2001, Sunderland (MA): Sinauer Associates.
13. Fechner, P.Y., *The role of SRY in mammalian sex determination.* Acta Paediatr Jpn, 1996. **38**(4): p. 380-9.
14. Mauvais-Jarvis, F., et al., *Sex and gender: modifiers of health, disease, and medicine.* Lancet, 2020. **396**(10250): p. 565-582.
15. Eggers, S. and A. Sinclair, *Mammalian sex determination-insights from humans and mice.* Chromosome Res, 2012. **20**(1): p. 215-38.
16. Phoenix, C.H., et al., *Organizing action of prenatally administered testosterone propionate on the tissues mediating mating behavior in the female guinea pig.* Endocrinology, 1959. **65**: p. 369-82.
17. Arnold, A.P., *Conceptual frameworks and mouse models for studying sex differences in physiology and disease: why compensation changes the game.* Exp Neurol, 2014. **259**: p. 2-9.
18. Zárate, S., T. Stevnsner, and R. Gredilla, *Role of Estrogen and Other Sex Hormones in Brain Aging. Neuroprotection and DNA Repair.* Frontiers in aging neuroscience, 2017. **9**: p. 430-430.
19. Russell, J.K., C.K. Jones, and P.A. Newhouse, *The Role of Estrogen in Brain and Cognitive Aging.* Neurotherapeutics, 2019. **16**(3): p. 649-665.
20. Martel, M.M., et al., *Potential hormonal mechanisms of attention-deficit/hyperactivity disorder and major depressive disorder: a new perspective.* Hormones and behavior, 2009. **55**(4): p. 465-479.
21. Wang, L.-J., et al., *Potential role of pre- and postnatal testosterone levels in attention-deficit/hyperactivity disorder: is there a sex difference?* Neuropsychiatric disease and treatment, 2017. **13**: p. 1331-1339.

1147 22. Lv, W., et al., *Low Testosterone Level and Risk of Alzheimer's Disease in the Elderly Men: a*
1148 *Systematic Review and Meta-Analysis.* Mol Neurobiol, 2016. **53**(4): p. 2679-84.
1149 23. Maki, P.M., L.M. Girard, and J.E. Manson, *Menopausal hormone therapy and cognition.* Bmj,
1150 2019. **364**: p. l877.
1151 24. Savolainen-Peltonen, H., et al., *Use of postmenopausal hormone therapy and risk of Alzheimer's*
1152 *disease in Finland: nationwide case-control study.* BMJ, 2019. **364**: p. l665.
1153 25. Imtiaz, B., et al., *Postmenopausal hormone therapy and Alzheimer disease: A prospective cohort*
1154 *study.* Neurology, 2017. **88**(11): p. 1062-1068.
1155 26. Fournier, A., et al., *Risks of Endometrial Cancer Associated With Different Hormone Replacement*
1156 *Therapies in the E3N Cohort, 1992–2008.* American Journal of Epidemiology, 2014. **180**(5): p.
1157 508-517.
1158 27. Beral, V., et al., *Use of HRT and the subsequent risk of cancer.* J Epidemiol Biostat, 1999. **4**(3): p.
1159 191-210; discussion 210-5.
1160 28. Arnold, A.P., E.F. Rissman, and G.J. De Vries, *Two perspectives on the origin of sex differences in*
1161 *the brain.* Ann N Y Acad Sci, 2003. **1007**: p. 176-88.
1162 29. Arnold, A.P., *Genetically Triggered Sexual Differentiation of Brain and Behavior.* Hormones and
1163 Behavior, 1996. **30**(4): p. 495-505.
1164 30. Smith-Bouvier, D.L., et al., *A role for sex chromosome complement in the female bias in*
1165 *autoimmune disease.* J Exp Med, 2008. **205**(5): p. 1099-108.
1166 31. Davis, E.J., I. Lobach, and D.B. Dubal, *Female XX sex chromosomes increase survival and extend*
1167 *lifespan in aging mice.* Aging cell, 2019. **18**(1): p. e12871-e12871.
1168 32. Davis, E.J., et al., *A second X chromosome contributes to resilience in a mouse model of*
1169 *Alzheimer's disease.* Sci Transl Med, 2020. **12**(558).
1170 33. Maan, A.A., et al., *The Y chromosome: a blueprint for men's health?* European Journal of Human
1171 Genetics, 2017. **25**(11): p. 1181-1188.
1172 34. Forsberg, L.A., et al., *Mosaic loss of chromosome Y in peripheral blood is associated with shorter*
1173 *survival and higher risk of cancer.* Nature Genetics, 2014. **46**(6): p. 624-628.
1174 35. Dumanski, J.P., et al., *Mosaic Loss of Chromosome Y in Blood Is Associated with Alzheimer*
1175 *Disease.* The American Journal of Human Genetics, 2016. **98**(6): p. 1208-1219.
1176 36. Fang, H., C.M. Disteche, and J.B. Berletch, *X Inactivation and Escape: Epigenetic and Structural*
1177 *Features.* Front Cell Dev Biol, 2019. **7**: p. 219.
1178 37. Wise, A.L., L. Gyi, and T.A. Manolio, *eXclusion: toward integrating the X chromosome in genome-*
1179 *wide association analyses.* American journal of human genetics, 2013. **92**(5): p. 643-647.
1180 38. Martin, J., et al., *Examining Sex-Differentiated Genetic Effects Across Neuropsychiatric and*
1181 *Behavioral Traits.* Biological Psychiatry, 2021. **89**(12): p. 1127-1137.
1182 39. Knickmeyer, R.C. and M. Davenport, *Turner syndrome and sexual differentiation of the brain:*
1183 *implications for understanding male-biased neurodevelopmental disorders.* J Neurodev Disord,
1184 2011. **3**(4): p. 293-306.
1185 40. Otter, M., C.T.R.M. Schrander-Stumpel, and L.M.G. Curfs, *Triple X syndrome: a review of the*
1186 *literature.* European journal of human genetics : EJHG, 2010. **18**(3): p. 265-271.
1187 41. Harris, V.M., et al., *Klinefelter's syndrome (47,XXY) is in excess among men with Sjogren's*
1188 *syndrome.* Clin Immunol, 2016. **168**: p. 25-29.
1189 42. Arnold, A.P., *Mouse models for evaluating sex chromosome effects that cause sex differences in*
1190 *non-gonadal tissues.* J Neuroendocrinol, 2009. **21**(4): p. 377-86.
1191 43. De Vries, G.J., et al., *A model system for study of sex chromosome effects on sexually dimorphic*
1192 *neural and behavioral traits.* J Neurosci, 2002. **22**(20): p. 9005-14.
1193 44. Lovell-Badge, R. and E. Robertson, *XY female mice resulting from a heritable mutation in the*
1194 *primary testis-determining gene, Tdy.* Development, 1990. **109**(3): p. 635-46.

1195 45. Mahadevaiah, S.K., et al., *Mouse homologues of the human AZF candidate gene RBM are*
1196 *expressed in spermatogonia and spermatids, and map to a Y chromosome deletion interval*
1197 *associated with a high incidence of sperm abnormalities.* Hum Mol Genet, 1998. **7**(4): p. 715-27.
1198 46. Markham, J.A., et al., *Sex differences in mouse cortical thickness are independent of the*
1199 *complement of sex chromosomes.* Neuroscience, 2003. **116**(1): p. 71-5.
1200 47. Wagner, C.K., et al., *Neonatal mice possessing an Sry transgene show a masculinized pattern of*
1201 *progesterone receptor expression in the brain independent of sex chromosome status.*
1202 Endocrinology, 2004. **145**(3): p. 1046-9.
1203 48. Arnold, A.P. and X. Chen, *What does the "four core genotypes" mouse model tell us about sex*
1204 *differences in the brain and other tissues?* Front Neuroendocrinol, 2009. **30**(1): p. 1-9.
1205 49. Carruth, L.L., I. Reisert, and A.P. Arnold, *Sex chromosome genes directly affect brain sexual*
1206 *differentiation.* Nat Neurosci, 2002. **5**(10): p. 933-4.
1207 50. Gioiosa, L., et al., *Sex chromosome complement affects nociception in tests of acute and chronic*
1208 *exposure to morphine in mice.* Horm Behav, 2008. **53**(1): p. 124-30.
1209 51. Chen, X., et al., *Sex difference in neural tube defects in p53-null mice is caused by differences in*
1210 *the complement of X not Y genes.* Dev Neurobiol, 2008. **68**(2): p. 265-73.
1211 52. Kashimada, K. and P. Koopman, *Sry: the master switch in mammalian sex*
1212 *determination.* Development, 2010. **137**(23): p. 3921-3930.
1213 53. Itoh, Y., et al., *Four core genotypes mouse model: localization of the Sry transgene and bioassay*
1214 *for testicular hormone levels.* BMC Res Notes, 2015. **8**: p. 69.
1215 54. Bundy, J.L., C. Vied, and R.S. Nowakowski, *Sex differences in the molecular signature of the*
1216 *developing mouse hippocampus.* BMC Genomics, 2017. **18**(1): p. 237.
1217 55. Chucair-Elliott, A.J., et al., *Tamoxifen induction of Cre recombinase does not cause long-lasting or*
1218 *sexually divergent responses in the CNS epigenome or transcriptome: implications for the design*
1219 *of aging studies.* Geroscience, 2019.
1220 56. Hadad, N., et al., *Early-life DNA methylation profiles are indicative of age-related transcriptome*
1221 *changes.* Epigenetics Chromatin, 2019. **12**(1): p. 58.
1222 57. Vied, C., et al., *Transcriptomic analysis of the hippocampus from six inbred strains of mice*
1223 *suggests a basis for sex-specific susceptibility and severity of neurological disorders.* J Comp
1224 Neurol, 2016. **524**(13): p. 2696-710.
1225 58. Berletch, J.B., et al., *Escape from X Inactivation Varies in Mouse Tissues.* PLOS Genetics, 2015.
1226 **11**(3): p. e1005079.
1227 59. Cerase, A., et al., *Xist localization and function: new insights from multiple levels.* Genome
1228 Biology, 2015. **16**(1): p. 166.
1229 60. Mizukami, H., et al., *KDM5D-mediated H3K4 demethylation is required for sexually dimorphic*
1230 *gene expression in mouse embryonic fibroblasts.* J Biochem, 2019. **165**(4): p. 335-342.
1231 61. Ramathal, C., et al., *DDX3Y gene rescue of a Y chromosome AZFa deletion restores germ cell*
1232 *formation and transcriptional programs.* Scientific Reports, 2015. **5**(1): p. 15041.
1233 62. Chu, H.-P., et al., *PAR-TERRA directs homologous sex chromosome pairing.* Nature structural &
1234 molecular biology, 2017. **24**(8): p. 620-631.
1235 63. Marks, H., et al., *High-resolution analysis of epigenetic changes associated with X inactivation.*
1236 Genome research, 2009. **19**(8): p. 1361-1373.
1237 64. Tate, P.H. and A.P. Bird, *Effects of DNA methylation on DNA-binding proteins and gene*
1238 *expression.* Curr Opin Genet Dev, 1993. **3**(2): p. 226-31.
1239 65. Jones, P.L., et al., *Methylated DNA and MeCP2 recruit histone deacetylase to repress*
1240 *transcription.* Nat Genet, 1998. **19**(2): p. 187-91.

1241 66. Watanabe, S., et al., *Methylated DNA-binding domain 1 and methylpurine-DNA glycosylase link*
1242 *transcriptional repression and DNA repair in chromatin.* Proceedings of the National Academy of
1243 Sciences of the United States of America, 2003. **100**(22): p. 12859-12864.
1244 67. Fujita, N., et al., *Methyl-CpG binding domain 1 (MBD1) interacts with the Suv39h1-HP1*
1245 *heterochromatic complex for DNA methylation-based transcriptional repression.* J Biol Chem,
1246 2003. **278**(26): p. 24132-8.
1247 68. Brackertz, M., et al., *Two highly related p66 proteins comprise a new family of potent*
1248 *transcriptional repressors interacting with MBD2 and MBD3.* J Biol Chem, 2002. **277**(43): p.
1249 40958-66.
1250 69. Razin, A. and H. Cedar, *DNA methylation and genomic imprinting.* Cell, 1994. **77**(4): p. 473-6.
1251 70. Wolf, S.F., et al., *Methylation of the hypoxanthine phosphoribosyltransferase locus on the human*
1252 *X chromosome: implications for X-chromosome inactivation.* Proceedings of the National
1253 Academy of Sciences, 1984. **81**(9): p. 2806-2810.
1254 71. Pfeifer, G.P., et al., *Polymerase Chain Reaction-Aided Genomic Sequencing of an X Chromosome-*
1255 *Linked CpG Island: Methylation Patterns Suggest Clonal Inheritance, CpG Site Autonomy, and an*
1256 *Explanation of Activity State Stability.* Proceedings of the National Academy of Sciences of the
1257 United States of America, 1990. **87**(21): p. 8252-8256.
1258 72. Bartlett, M.H., et al., *DNA methylation of two X chromosome genes in female somatic and*
1259 *embryonal carcinoma cells.* Somatic Cell and Molecular Genetics, 1991. **17**(1): p. 35-47.
1260 73. Angrisano, T., et al., *TACC3 mediates the association of MBD2 with histone acetyltransferases*
1261 *and relieves transcriptional repression of methylated promoters.* Nucleic acids research, 2006.
1262 **34**(1): p. 364-372.
1263 74. Sharp, A.J., et al., *DNA methylation profiles of human active and inactive X chromosomes.*
1264 Genome Res, 2011. **21**(10): p. 1592-600.
1265 75. Chucair-Elliott, A.J., et al., *Tamoxifen induction of Cre recombinase does not cause long-lasting or*
1266 *sexually divergent responses in the CNS epigenome or transcriptome: implications for the design*
1267 *of aging studies.* Geroscience, 2019. **41**(5): p. 691-708.
1268 76. Jeziorska, D.M., et al., *DNA methylation of intragenic CpG islands depends on their*
1269 *transcriptional activity during differentiation and disease.* Proceedings of the National Academy
1270 of Sciences, 2017. **114**(36): p. E7526-E7535.
1271 77. Duncan, C.G., et al., *Dosage compensation and DNA methylation landscape of the X*
1272 *chromosome in mouse liver.* Scientific Reports, 2018. **8**(1): p. 10138.
1273 78. Kung, J.T., et al., *Locus-specific targeting to the X chromosome revealed by the RNA interactome*
1274 *of CTCF.* Mol Cell, 2015. **57**(2): p. 361-75.
1275 79. Lyon, M.F., *X-chromosome inactivation: a repeat hypothesis.* Cytogenet Cell Genet, 1998. **80**(1-
1276 4): p. 133-7.
1277 80. Diehl, A.G., N. Ouyang, and A.P. Boyle, *Transposable elements contribute to cell and species-*
1278 *specific chromatin looping and gene regulation in mammalian genomes.* Nature
1279 Communications, 2020. **11**(1): p. 1796.
1280 81. von Mering, C., et al., *STRING: known and predicted protein-protein associations, integrated and*
1281 *transferred across organisms.* Nucleic Acids Res, 2005. **33**(Database issue): p. D433-7.
1282 82. Gorkin, D.U., et al., *An atlas of dynamic chromatin landscapes in mouse fetal development.*
1283 Nature, 2020. **583**(7818): p. 744-751.
1284 83. Lister, R., et al., *Global epigenomic reconfiguration during mammalian brain development.*
1285 Science, 2013. **341**(6146): p. 1237905.
1286 84. Tran, N., A. Broun, and K. Ge, *Lysine Demethylase KDM6A in Differentiation, Development, and*
1287 *Cancer.* Mol Cell Biol, 2020. **40**(20).

1288 85. Outchkourov, Nikolay S., et al., *Balancing of Histone H3K4 Methylation States by the*
1289 *Kdm5c/SMCX Histone Demethylase Modulates Promoter and Enhancer Function.* Cell Reports,
1290 2013. **3**(4): p. 1071-1079.
1291 86. Maurano, Matthew T., et al., *Role of DNA Methylation in Modulating Transcription Factor*
1292 *Occupancy.* Cell Reports, 2015. **12**(7): p. 1184-1195.
1293 87. Teissandier, A. and D. Bourc'his, *Gene body DNA methylation conspires with H3K36me3 to*
1294 *preclude aberrant transcription.* Embo j, 2017. **36**(11): p. 1471-1473.
1295 88. Barros de Andrade E Sousa, L., et al., *Kinetics of Xist-induced gene silencing can be predicted*
1296 *from combinations of epigenetic and genomic features.* Genome research, 2019. **29**(7): p. 1087-
1297 1099.
1298 89. Bae, S. and B.J. Lesch, *H3K4me1 Distribution Predicts Transcription State and Poising at*
1299 *Promoters.* Frontiers in Cell and Developmental Biology, 2020. **8**.
1300 90. Jaric, I., et al., *Chromatin organization in the female mouse brain fluctuates across the oestrous*
1301 *cycle.* Nature Communications, 2019. **10**(1): p. 2851.
1302 91. Castro-Mondragon, J.A., et al., *JASPAR 2022: the 9th release of the open-access database of*
1303 *transcription factor binding profiles.* Nucleic Acids Research, 2022. **50**(D1): p. D165-D173.
1304 92. Weakley, S.M., et al., *Expression and function of a large non-coding RNA gene XIST in human*
1305 *cancer.* World journal of surgery, 2011. **35**(8): p. 1751-1756.
1306 93. Snijders Blok, L., et al., *Mutations in DDX3X Are a Common Cause of Unexplained Intellectual*
1307 *Disability with Gender-Specific Effects on Wnt Signaling.* American journal of human genetics,
1308 2015. **97**(2): p. 343-352.
1309 94. Cortes, L.R., C.D. Cisternas, and N.G. Forger, *Does Gender Leave an Epigenetic Imprint on the*
1310 *Brain?* Frontiers in Neuroscience, 2019. **13**(173).
1311 95. Davey, R.A. and M. Grossmann, *Androgen Receptor Structure, Function and Biology: From Bench*
1312 *to Bedside.* The Clinical biochemist. Reviews, 2016. **37**(1): p. 3-15.
1313 96. Atwi, S., et al., *Androgen Modulation of Hippocampal Structure and Function.* The Neuroscientist
1314 : a review journal bringing neurobiology, neurology and psychiatry, 2016. **22**(1): p. 46-60.
1315 97. Zhang, Y., et al., *An RNA-Sequencing Transcriptome and Splicing Database of Glia, Neurons, and*
1316 *Vascular Cells of the Cerebral Cortex.* The Journal of Neuroscience, 2014. **34**(36): p. 11929.
1317 98. Kawasaki, T. and T. Kawai, *Toll-like receptor signaling pathways.* Front Immunol, 2014. **5**: p. 461.
1318 99. Hikmet, F., et al., *The protein expression profile of ACE2 in human tissues.* Molecular Systems
1319 Biology, 2020. **16**(7): p. e9610.
1320 100. Moore, J.E., et al., *Expanded encyclopaedias of DNA elements in the human and mouse*
1321 *genomes.* Nature, 2020. **583**(7818): p. 699-710.
1322 101. Hadad, N., et al., *Absence of genomic hypomethylation or regulation of cytosine-modifying*
1323 *enzymes with aging in male and female mice.* Epigenetics Chromatin, 2016. **9**: p. 30.
1324 102. Blank, T. and M. Prinz, *Type I interferon pathway in CNS homeostasis and neurological disorders.*
1325 Glia, 2017. **65**(9): p. 1397-1406.
1326 103. Roy, E.R., et al., *Type I interferon response drives neuroinflammation and synapse loss in*
1327 *Alzheimer disease.* The Journal of Clinical Investigation, 2020. **130**(4): p. 1912-1930.
1328 104. Honda, K., et al., *IRF-7 is the master regulator of type-I interferon-dependent immune responses.*
1329 Nature, 2005. **434**(7034): p. 772-777.
1330 105. Liu, X.-Y., et al., *IFN-Induced TPR Protein IFIT3 Potentiates Antiviral Signaling by Bridging MAVS*
1331 *and TBK1.* The Journal of Immunology, 2011. **187**(5): p. 2559.
1332 106. VanGuilder Starkey, H.D., et al., *Neuroglial expression of the MHCI pathway and PirB receptor is*
1333 *upregulated in the hippocampus with advanced aging.* Journal of molecular neuroscience : MN,
1334 2012. **48**(1): p. 111-126.

1335 107. Mangold, C.A., et al., *CNS-wide Sexually Dimorphic Induction of the Major Histocompatibility*
1336 *Complex 1 Pathway With Aging.* J Gerontol A Biol Sci Med Sci, 2017. **72**(1): p. 16-29.
1337 108. Masser, D.R., et al., *Sexually divergent DNA methylation patterns with hippocampal aging.* Aging
1338 Cell, 2017. **16**(6): p. 1342-1352.
1339 109. Wu, T., et al., *clusterProfiler 4.0: A universal enrichment tool for interpreting omics data.* The
1340 Innovation, 2021. **2**(3).
1341 110. Chucair-Elliott, A.J., et al., *Inducible cell-specific mouse models for paired epigenetic and*
1342 *transcriptomic studies of microglia and astroglia.* Communications Biology, 2020. **3**(1): p. 693.
1343 111. McCarthy, M.M., et al., *Sex differences in the brain: the not so inconvenient truth.* J Neurosci,
1344 2012. **32**(7): p. 2241-7.
1345 112. Panning, B., *X-chromosome inactivation: the molecular basis of silencing.* Journal of Biology,
1346 2008. **7**(8): p. 30.
1347 113. Fang, H., C.M. Disteche, and J.B. Berletch, *X Inactivation and Escape: Epigenetic and Structural*
1348 *Features.* Frontiers in cell and developmental biology, 2019. **7**: p. 219-219.
1349 114. Carrel, L. and H.F. Willard, *X-inactivation profile reveals extensive variability in X-linked gene*
1350 *expression in females.* Nature, 2005. **434**(7031): p. 400-404.
1351 115. Berletch, J.B., et al., *Genes that escape from X inactivation.* Human Genetics, 2011. **130**(2): p.
1352 237-245.
1353 116. Mousavi, M.J., M. Mahmoudi, and S. Ghotloo, *Escape from X chromosome inactivation and*
1354 *female bias of autoimmune diseases.* Molecular Medicine, 2020. **26**(1): p. 127.
1355 117. Youness, A., C.-H. Miquel, and J.-C. Guéry, *Escape from X Chromosome Inactivation and the*
1356 *Female Predominance in Autoimmune Diseases.* International journal of molecular sciences,
1357 2021. **22**(3): p. 1114.
1358 118. Bajic, V.P., et al., *The X Files: "The Mystery of X Chromosome Instability in Alzheimer's Disease".*
1359 Frontiers in genetics, 2020. **10**: p. 1368-1368.
1360 119. Chow, J.C., et al., *LINE-1 Activity in Facultative Heterochromatin Formation during X*
1361 *Chromosome Inactivation.* Cell, 2010. **141**(6): p. 956-969.
1362 120. Bailey, J.A., et al., *Molecular evidence for a relationship between LINE-1 elements and X*
1363 *chromosome inactivation: The Lyon repeat hypothesis.* Proceedings of the National Academy of
1364 Sciences, 2000. **97**(12): p. 6634.
1365 121. Cotton, A.M., et al., *Spread of X-chromosome inactivation into autosomal sequences: role for*
1366 *DNA elements, chromatin features and chromosomal domains.* Hum Mol Genet, 2014. **23**(5): p.
1367 1211-23.
1368 122. Kato, A., et al., *Female hippocampal estrogens have a significant correlation with cyclic*
1369 *fluctuation of hippocampal spines.* Frontiers in Neural Circuits, 2013. **7**.
1370 123. DiCarlo, L.M., C. Vied, and R.S. Nowakowski, *The stability of the transcriptome during the estrous*
1371 *cycle in four regions of the mouse brain.* J Comp Neurol, 2017. **525**(15): p. 3360-3387.
1372 124. Itoh, Y., et al., *The X-linked histone demethylase Kdm6a in CD4+ T lymphocytes modulates*
1373 *autoimmunity.* The Journal of clinical investigation, 2019. **129**(9): p. 3852-3863.
1374 125. Doss, P.M.I.A., et al., *Male sex chromosomal complement exacerbates the pathogenicity of Th17*
1375 *cells in a chronic model of central nervous system autoimmunity.* Cell Reports, 2021. **34**(10).
1376 126. Link, J.C., et al., *X chromosome dosage of histone demethylase KDM5C determines sex*
1377 *differences in adiposity.* J Clin Invest, 2020. **130**(11): p. 5688-5702.
1378 127. Ansere, V.A., et al., *Cellular hallmarks of aging emerge in the ovary prior to primordial follicle*
1379 *depletion.* Mech Ageing Dev, 2021. **194**: p. 111425.
1380 128. Masser, D.R., A.S. Berg, and W.M. Freeman, *Focused, high accuracy 5-methylcytosine*
1381 *quantitation with base resolution by benchtop next-generation sequencing.* Epigenetics &
1382 chromatin, 2013. **6**(1): p. 33-33.

1383 129. Masser, D.R., et al., *Loss of the antioxidant enzyme CuZnSOD (Sod1) mimics an age-related*
1384 *increase in absolute mitochondrial DNA copy number in the skeletal muscle.* Age (Dordrecht,
1385 Netherlands), 2016. **38**(4): p. 323-333.
1386 130. Simpson, J.T., et al., *Detecting DNA cytosine methylation using nanopore sequencing.* Nature
1387 Methods, 2017. **14**: p. 407.
1388 131. Masser, D.R., et al., *Hippocampal subregions exhibit both distinct and shared transcriptomic*
1389 *responses to aging and nonneurodegenerative cognitive decline.* J Gerontol A Biol Sci Med Sci,
1390 2014. **69**(11): p. 1311-24.
1391 132. Anders, S. and W. Huber, *Differential expression analysis for sequence count data.* Genome Biol,
1392 2010. **11**(10): p. R106.
1393 133. Bolger, A.M., M. Lohse, and B. Usadel, *Trimmomatic: a flexible trimmer for Illumina sequence*
1394 *data.* Bioinformatics, 2014. **30**(15): p. 2114-20.
1395 134. Krueger, F. and S.R. Andrews, *Bismark: a flexible aligner and methylation caller for Bisulfite-Seq*
1396 *applications.* Bioinformatics, 2011. **27**(11): p. 1571-2.
1397 135. Langmead, B. and S.L. Salzberg, *Fast gapped-read alignment with Bowtie 2.* Nat Methods, 2012.
1398 **9**(4): p. 357-9.
1399 136. Akalin, A., et al., *methylKit: a comprehensive R package for the analysis of genome-wide DNA*
1400 *methylation profiles.* Genome Biol, 2012. **13**(10): p. R87.
1401 137. Liao, Y., et al., *WebGestalt 2019: gene set analysis toolkit with revamped UIs and APIs.* Nucleic
1402 Acids Res, 2019. **47**(W1): p. W199-w205.
1403 138. Gu, Z., et al., *EnrichedHeatmap: an R/Bioconductor package for comprehensive visualization of*
1404 *genomic signal associations.* BMC Genomics, 2018. **19**(1): p. 234.
1405 139. Karolchik, D., et al., *The UCSC Table Browser data retrieval tool.* Nucleic Acids Res, 2004.
1406 **32**(Database issue): p. D493-6.
1407 140. Lee, B.T., et al., *The UCSC Genome Browser database: 2022 update.* Nucleic Acids Research,
1408 2022. **50**(D1): p. D1115-D1122.
1409 141. Quinlan, A.R. and I.M. Hall, *BEDTools: a flexible suite of utilities for comparing genomic features.*
1410 Bioinformatics, 2010. **26**(6): p. 841-842.
1411 142. Dang, L.T., et al., *TrawlerWeb: an online de novo motif discovery tool for next-generation*
1412 *sequencing datasets.* BMC Genomics, 2018. **19**(1): p. 238.
1413 143. Oliveros, J.C., *VENNY. An interactive tool for comparing lists with Venn Diagrams.* 2007.
1414 144. Hulsen, T., *BioVenn – an R and Python package for the comparison and visualization of*
1415 *biological lists using area-proportional Venn diagrams.* Data Science, 2021. **4**: p. 51-61.
1416 145. Mishra, G.P., et al., *BedSect: An Integrated Web Server Application to Perform Intersection,*
1417 *Visualization, and Functional Annotation of Genomic Regions From Multiple Datasets.* Frontiers
1418 in Genetics, 2020. **11**.
1419 146. Wickman, H., *ggplot2: Elegant Graphics for Data Analysis*. 2016: Springer-Verlag New York.
1420 147. Wu, T., et al., *clusterProfiler 4.0: A universal enrichment tool for interpreting omics data.* The
1421 Innovation, 2021. **2**(3): p. 100141.

1422

1423

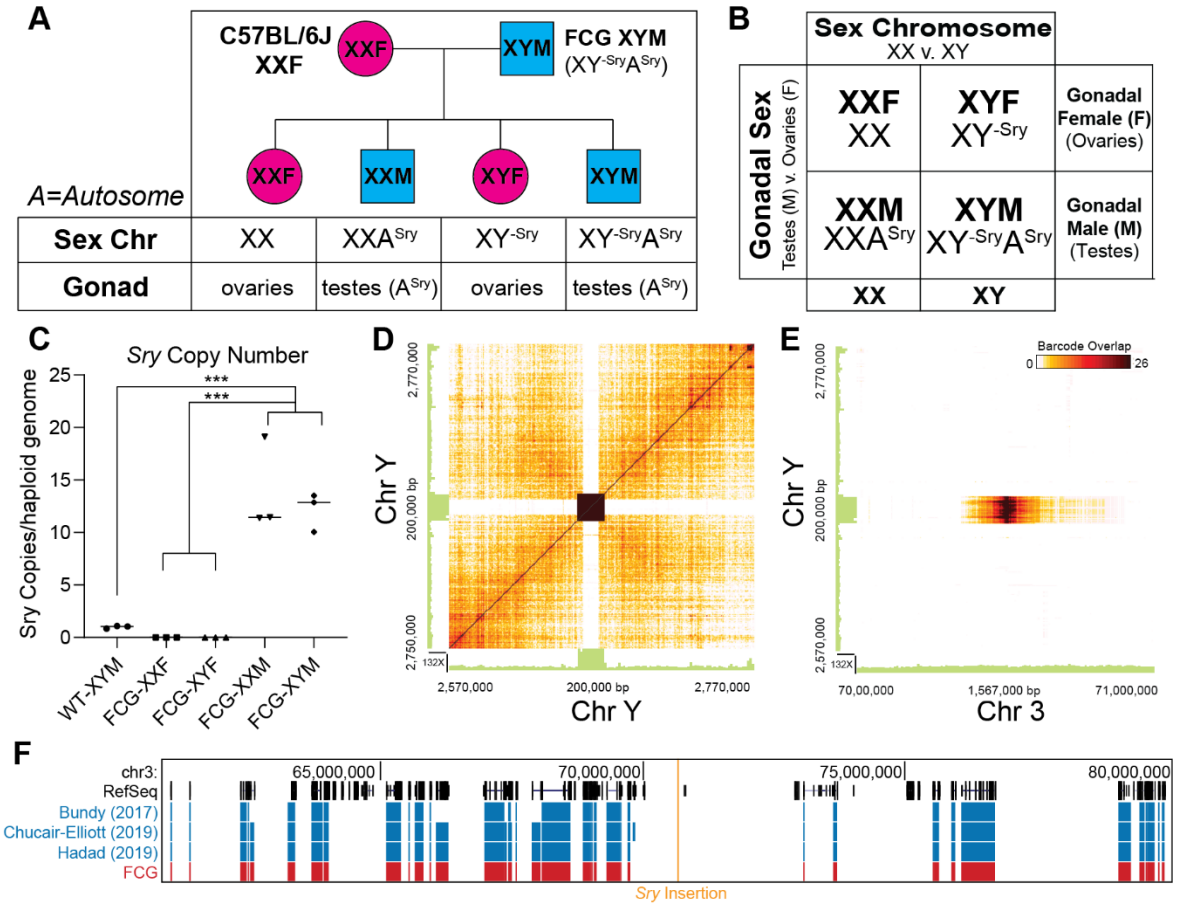

Fig. 1 *Sry* copy number and localization in FCG hippocampi

A) Breeding strategy used to generate the Four Core Genotypes (FCG). **B**) FCG mouse model two-way design to study gonadal sex and sex chromosomal contributions to sex effects. DNA isolated from FCG and wild type hippocampi (n=3/group) was used for digital PCR *Sry* copy number and 10X genomics linked read sequencing. **C**) Wildtype (WT) C57BL/6J mice have one copy of the testis-determining *Sry* gene, while FCG males (both XX and XY) have 12-14 copies of *Sry. Sry* was not detected in the FCG females. **D**) Linked read sequencing of FCG XYM, shows strong linkage of the *Sry* gene to itself, but not to adjacent regions of the Y-chromosome (ChrY) indicating *Sry* is no longer on ChrY. **E**) *Sry* gene shows strong linkage to an intergenic region on Chromosome 3 (Chr3). **F)** Adult mouse (3-4 months old) hippocampal gene expression from previously published studies [Bundy et al., 2017 (GSE83931), Chucair-Elliott et al., 2019 (GSE135752); and Hadad et al., 2019 (PRJNA523985)] were compared to FCG hippocampal gene expression in the present study, to determine potential alterations in gene expression adjacent (+/- 10 Mbp) to the *Sry* insertion site on Chr3 in the FCG XXM/XYM. Tracks represent genes that are detected as expressed in previously published datasets (blue) and the present FCG study (red).

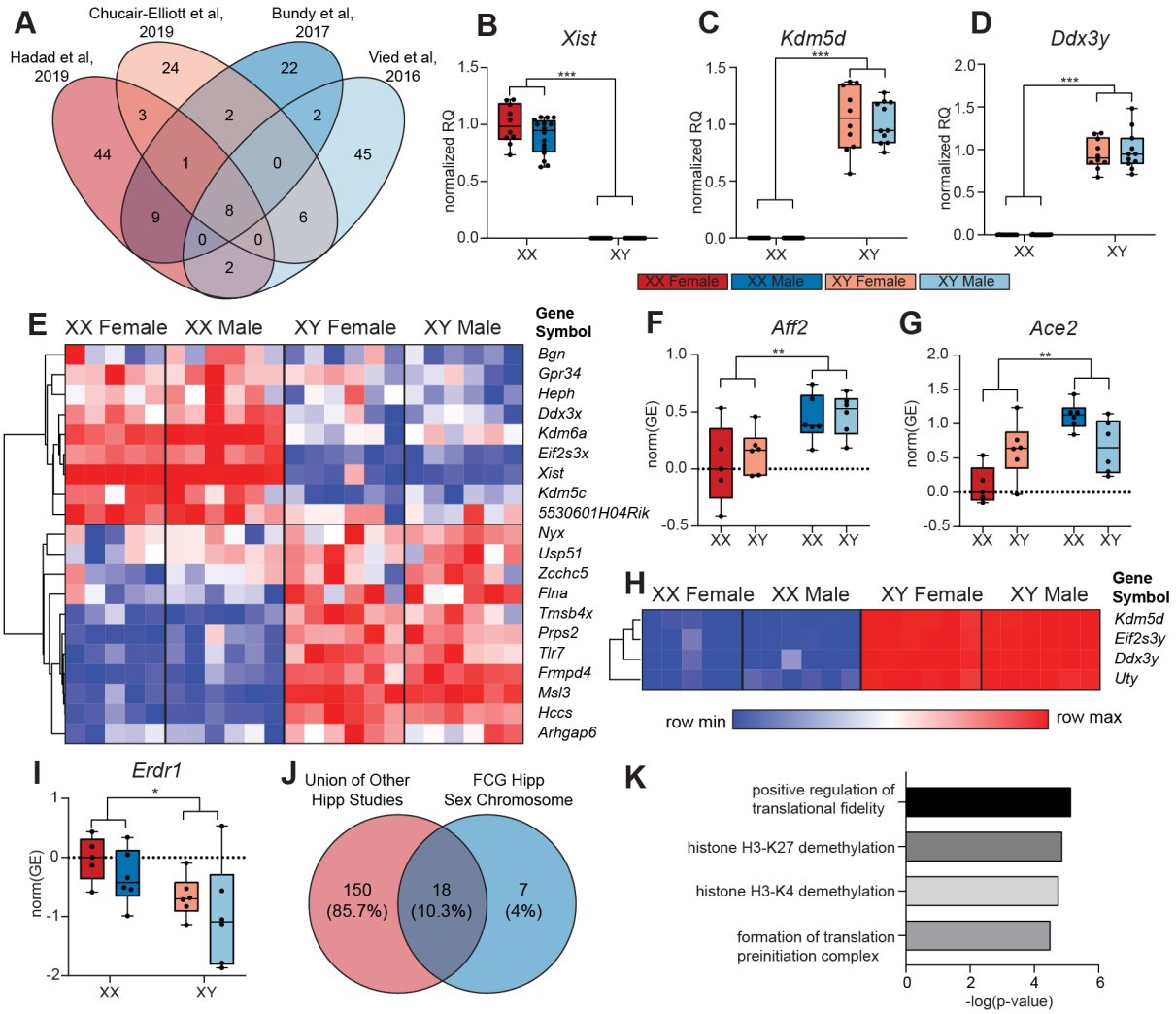

Fig. 2 Transcriptomic analysis of differential expression in sex chromosome-encoded (X/Y) genes in adult FCG hippocampi

DNA and RNA were isolated from FCG hippocampi (n=10-16/group). mRNA expression was assessed by RT-qPCR (n=10-16/group) and stranded RNA-Seq (n=6/group). Results were compared to previously published hippocampal transcriptomic sex differences. **Boxplots** represent median, interquartile range, and minimum/maximum normalized gene expression. **A**) Comparison of four previous hippocampal transcriptomic studies, showed 168 sex chromosome-encoded sex differences in wild-type mice across studies with eight genes common between all studies (*Xist Ddx3x, Kdm6a, Eif2s3x, Kdm5d, Eif2s3y, Uty, Ddx3y)* **B**) In the FCG hippocampus, RT-qPCR of X-chromosome encoded gene *Xist* confirms differential expression by sex chromosome (XX vs. XY) but not gonadal sex (M v. F) (Two-way ANOVA, main effect of sex-chromosome complement (XX v. XY), ***p<0.001) . **C-D**) RT-qPCR of Y-chromosome encoded genes shows similar levels of expression of (C) *Kdm5d* and (D) *Ddx3y* in XYM and XYF, and no detectable expression in XXM or XXF (Two-way ANOVA, main effect of sex chromosome complement (XX v. XY), ***p<0.001). **E**) RNA-Seq analysis of X-chromosome encoded genes showed 20 genes that are differentially expressed by sex chromosome (XX vs. XY) but not by gonadal sex (M v. F). **F-G**) RNA-seq analysis of X chromosome genes revealed only two genes

(*Aff2, Ace2*) differentially expressed by gonadal sex (M v. F) and not by sex chromosome complement. Both (**F**) *Aff2* and (**G**) *Ace2* had higher expression in gonadal males than females regardless of their sex chromosome (Two-way ANOVA, main effect of gonadal sex (M v. F), **p<0.01). **H-I**) RNA-Seq analysis of Y-chromosome encoded genes identified 5 differentially expressed genes by sex chromosome (XX vs. XY) but not by gonadal sex (M v. F). There were no Y-chromosome genes that were differentially expressed by gonadal sex (M v. F). **H**) Four of the genes (*Kdm5d, Eif2s3y, Ddx3y, Uty*) show no expression in XX genotypes. **I**) Located in the pseudo autosomal region (PAR) of the X/Y-chromosomes, *Erdr1* shows higher expression in XX genotype. **J**) Comparing the union of previous hippocampal studies described in (**A**) to the FCG sex chromosome genes differentially expressed between XX and XY genotypes, yields 18 common genes. **K**) GO Ontology analysis of the 18 genes from (**J**), identified four significantly enriched biological pathways

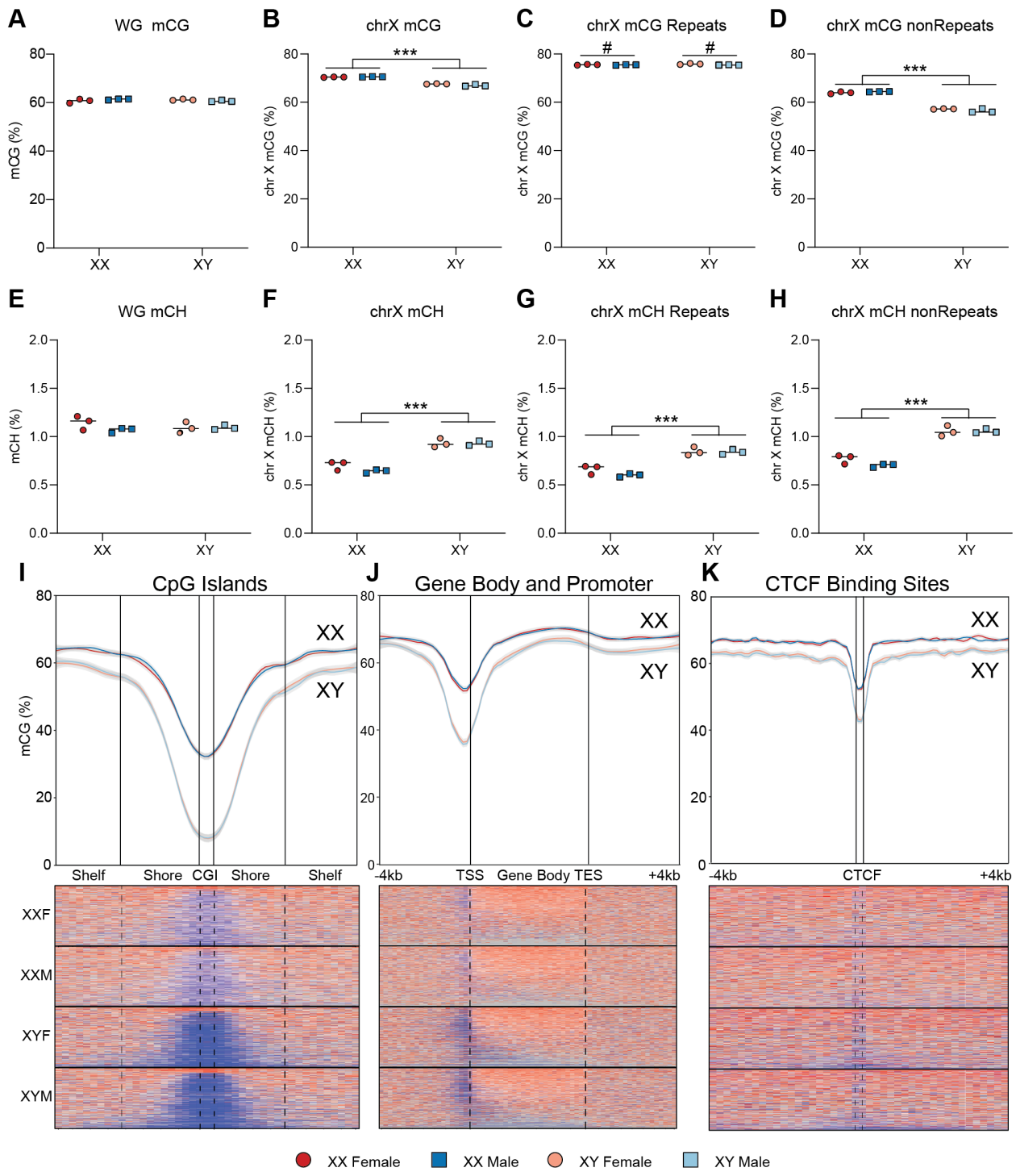

Fig. 3 X-chromosome DNA methylation landscape in FCG hippocampus by WGoxBS

DNA was isolated from FCG hippocampi (n=3/group). Methylation in CpG (CG) and non-CpG (CH) contexts was assessed by WGoxBS (n=3/group). **A)** There was no main effect difference or interaction in overall whole genome (WG) levels of methylation in CG context (mCG) (Two-way ANOVA). **B)** XX mice had higher levels of X-chromosome mCG than XY mice regardless of gonadal sex (M v. F) (Two-way ANOVA, main effect sex chromosome complement, ***p<0.001).

There was also a significant interaction of gonadal and chromosomal sex (p=0.02). **C**) Within repetitive elements of the X-chromosome there was higher mCG in gonadal females than males, with no effect of sex chromosome (Two-way ANOVA, main effect gonadal sex, #p<0.05) and no interaction. **D**) Within non-repetitive elements of the X-chromosome, there was higher mCG in XX genotypes as compared to XY, regardless of gonadal sex (Two-way ANOVA, main effect sex chromosome complement, ***p<0.001) with no significant interaction between gonadal and chromosomal sex. **E)** There was no main effect difference or interaction in genome-wide methylation in non-CpG context (mCH) (Two-way ANOVA). **F)** XX mice had lower mCH than XY mice specifically on the X-chromosome (Two-way ANOVA, main effect sex chromosome complement, ***p<0.001), regardless of their gonadal sex and with no significant interactive effect. The differences in X-chromosome mCH are seen in both (**G**) repetitive and (**F**) non-repetitive elements of the genome. mCG levels were calculated with respect to genic regions by binning 200 nucleotides in flanking regions and region-size dependent bins within the genic region (CGI, gene body, and CTCF) as to maintain the same number of bins for each feature. The average for all (**I**) CGI, (**J**) Gene Body, and (**K**) CTCF were assessed for each of the FCG (XXF, XXM, XYF, XYM) and plotted as averages with 95% CI. **I)** X-chromosome CpG Islands (CGI), shores, and shelves have higher levels of mCG in XX genotypes as compared to XY. The greatest difference in mCG is in the CGI. **J)** X-chromosome gene bodies and flanking regions (+/- 4 Kb) have higher levels of mCG in XX genotypes as compared to XY. The greatest difference in mCG is upstream of TSS (i.e. promoter region). **K)** X-chromosome CTCF binding sites have higher levels of mCG in XX genotypes as compared to XY. The difference in mCG (XX-XY) is greater within the CTCF binding site than in flanking regions (+/- 4 Kb).

1501

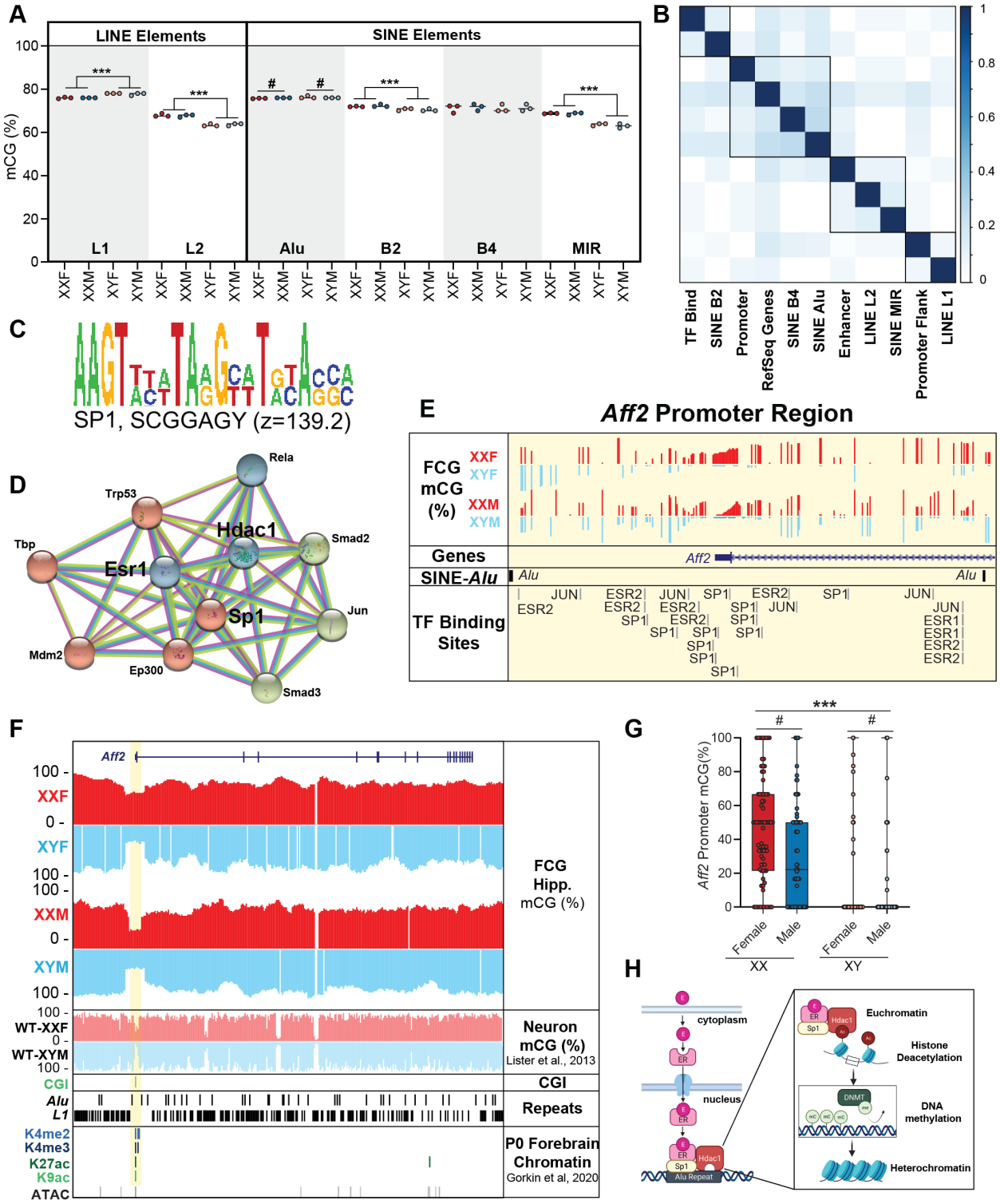

1503 **Fig. 4 X-chromosome repetitive element DNA methylation in adult FCG hippocampus**

1504 FCG DNA methylation levels in X-chromosomal repetitive elements were assessed by WGoxBS
1505 (n=3/group). **A)** Average mCG in common X-chromosomal LINE (L1, L2) and SINE (Alu, B2, B4,

1506 MIR) repetitive elements were compared between FCG groups for main effects of chromosomal
1507 and gonadal sex, as well as interactive effects of gonadal and chromosomal sex. LINE-L1
1508 elements had higher mCG in XY genotypes as compared to XX, regardless of gonadal sex (Two-
1509 way ANOVA, main effect sex chromosome complement, ***p<0.001). LINE-L2, SINE-B2, and
1510 SINE-MIR repetitive elements had higher mCG levels in XX genotypes as compared to their XY
1511 counterparts, regardless of gonadal sex (Two-way ANOVA, main effect sex chromosome
1512 complement, ***p<0.001). SINE-Alu repetitive elements had higher methylation in gonadal
1513 females than in gonadal males (Two-way ANOVA, main effect gonadal sex, #p<0.05), and a
1514 significant interactive effect of gonadal and chromosomal sex (p=0.0231). There was no
1515 difference in mCG in SINE-B4 elements. **B)** X-chromosomal browser extensible data (BED) files
1516 for common gene regulatory regions and repetitive elements were correlated by Jaccard distance
1517 using the BedSect application (Mishra et al., 2020). **C)** TrawlerWeb motif analysis (Dang et al.,
1518 2018) on X-chromosomal SINE-*Alu* repeat elements identified SP1 as a potential transcription
1519 factor interactor. **D)** STRING protein network analysis (von Mering et al., 2005) of SP1 identified
1520 a network of proteins that interact with SP1, including estrogen receptor 1 (ESR1) and histone
1521 deacetylase 1 (HDAC1). **E)** *Aff2* (DEG by gonadal sex in **Fig.** 2F) promoter genome tracks
1522 including representative mCG from FCG hippocampus (present study) compared to SINE-*Alu* and
1523 transcription factor binding sites (SP1, ESR1, ESR2, JUN) distribution. **F)** *Aff2* gene body genome
1524 tracks including representative mCG from FCG hippocampus (present study) compared to
1525 genomic features (CGI, SINE-Alu, LINE-L1), previously published DNA methylation from male
1526 and female neurons (Lister et al., 2013), and previously published chromatin data from P0
1527 forebrain (Gorkin et al., 2020). **G)** DNA methylation at individual CG sites within the promoter
1528 region of *Aff2* bound by the flanking SINE-Alu repeats (highlighted yellow in **Fig. 4E-F**) were
1529 compared between FCG groups. *Aff2* promoter methylation was higher in XX genotypes
1530 compared to XY (Two-way ANOVA, main effect sex chromosome complement, ***p<0.001) and
1531 higher in females than males (main effect gonadal sex, *#p<0.001), as well as an interactive effect
1532 of gonadal and chromosomal sex (p=0.001). **H)** Working model for gonadal effect on X-
1533 chromosomal methylome. We hypothesize that circulating estradiol binds to ESR1, which then
1534 enters the nucleus. The estrogen receptor forms interactions with SP1 and HDAC1, which then
1535 binds to X-chromosomal SINE-Alu repeats. The HDAC1 then removes active histone acetylation
1536 marks and recruits DNA methyltransferases to hypermethylate the region and compact the
1537 chromatin. Created with BioRender.com.

1538

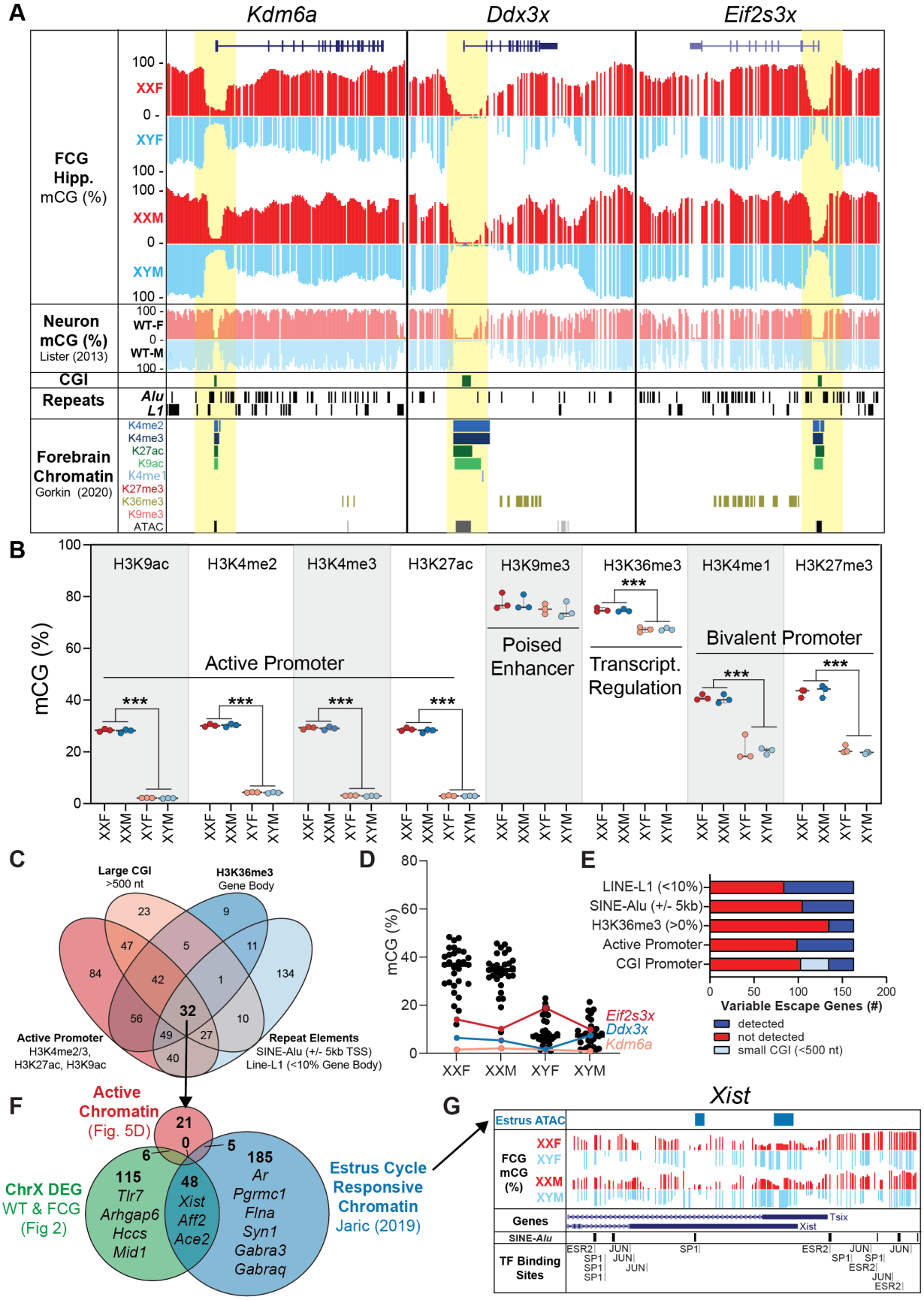
A
Kdm6a
Ddx3x
Eif2s3x
FCG Hipp. mCG (%)
XXF
XYF
XXM
XYM
Neuron mCG (%) Lister (2013)
WT-F
WT-M
CGI
Repeats
Alu
L1
Forebrain Chromatin Gorkin (2020)
K4me2
K4me3
K27ac
K9ac
K4me1
K27me3
K36me3
K9me3
ATAC
B
mCG (%)
H3K9ac
H3K4me2
H3K4me3
H3K27ac
H3K9me3
H3K36me3
H3K4me1
H3K27me3
Active Promoter
Poised Enhancer
Transcript. Regulation
Bivalent Promoter
***
C
Large CGI >500 nt
H3K36me3 Gene Body
Active Promoter H3K4me2/3, H3K27ac, H3K9ac
Repeat Elements SINE-Alu (+/- 5kb TSS) Line-L1 (<10% Gene Body)
D
mCG (%)
Eif2s3x
Ddx3x
Kdm6a
XXF XXM XYF XYM
E
LINE-L1 (<10%)
SINE-Alu (+/- 5kb)
H3K36me3 (>0%)
Active Promoter
CGI Promoter
Variable Escape Genes (#)
detected
not detected
small CGI (<500 nt)
F
Active Chromatin (Fig. 5D)
ChrX DEG WT & FCG (Fig 2)
Estrus Cycle Responsive Chromatin Jaric (2019)
115 Tlr7 Arhgap6 Hccs Mid1
48 Xist Aff2 Ace2
185 Ar Pgrmc1 Flna Syn1 Gabra3 Gabraq
G
Xist
Estrus ATAC
FCG mCG (%)
Genes
Tsix
Xist
SINE-Alu
TF Binding Sites
ESR2
JUN
SP1

1540 **Fig. 5 Epigenomic signatures of genes that escape X-inactivation**

1541 FCG hippocampal DNA methylation levels within different genomic contexts were compared for
1542 genes that escape X-inactivation. **A)** *Kdm6a*, *Ddx3x*, and *Eif2s3x* were found to consistently
1543 escape X-inactivation in mouse hippocampus from the previous studies examined in **Fig. 2a** and
1544 FCG (present study). Genome tracks for *Kdm6a*, *Ddx3x*, and *Eif2s3x* compared FCG mCG
1545 patterning to genomic features (CGI, Repeats) and previously published CNS mCG (Lister et al.,
1546 2013) and chromatin (Gorkin et al., 2020) patterns. **B)** Average methylation across published CNS
1547 X-chromosomal histone modification peaks (Gorkin et al., 2020), showed higher methylation in
1548 XX genotypes as compared to XY genotypes in H3K9ac, H3K4me2, H3K4me3, H3K27ac,
1549 H3K36me3, H3K4me1, and H3K27me3 regardless of gonadal sex, with no interactive effect (Two-
1550 way ANOVA, main effect sex chromosome complement, ***p<0.001). There was no detected
1551 difference in mCG in H3K9me3 peaks. **C)** Commonalities between the chromatin structure in
1552 genes that consistently escape X-inactivation include: 1) Large CGIs (>500 nt) within the
1553 promoter, 2) Active promoter histone marks (H3K4me2, H3K4me3, H3K27ac, H3K9ac), 3)
1554 H3K36me3 gene body peaks, 4) SINE-*Alu* flanks (+/- 5kb from TSS), and 5) low LINE-L1 gene
1555 body (<10%). There were 32 genes which had the same chromatin signature as the common
1556 escape genes (**Supplemental Table X**). **D)** Promoter mCG (%) for the 32 genes with the same
1557 chromatin signature as the escape genes. All genes, except *Eif2s3x, Ddx3x,* and *Kdm6a*
1558 (common escape), had higher mCG in XX genotypes compared to XY genotypes (Two-way
1559 ANOVA, main effect sex chromosome complement, ***p<0.001), regardless of gonadal sex with
1560 no interaction. **E)** There were 169 X-chromosomal genes that show variable escape from X-
1561 inactivation (i.e. differentially expressed in mouse hippocampus by gonadal and/or chromosomal
1562 sex in the previous studies examined in **Fig. 2A** and/or the present FCG study). These 169
1563 variable escape genes were examined for their concordance with the five signatures of consistent
1564 escape gene chromatin. The majority of variable escape genes did not have chromatin signatures
1565 consistent with the consistent escape genes. **F)** Comparison of 32 genes that share the active
1566 chromatin signature from **Fig. 5C**, the 169 sex differentially expressed genes from **Fig. 5E,** and
1567 238 genes with estrus cycle-responsive chromatin (Jaric et al., 2019), identified 48 differentially
1568 expressed genes that have estrus-responsive chromatin. **G)** *Xist/Tsix* locus genome tracks
1569 showing overlap with estrus-responsive chromatin (Jaric et al., 2019), SINE-*Alu* repeats and SP1,
1570 ESR2, and JUN transcription factor binding sites.

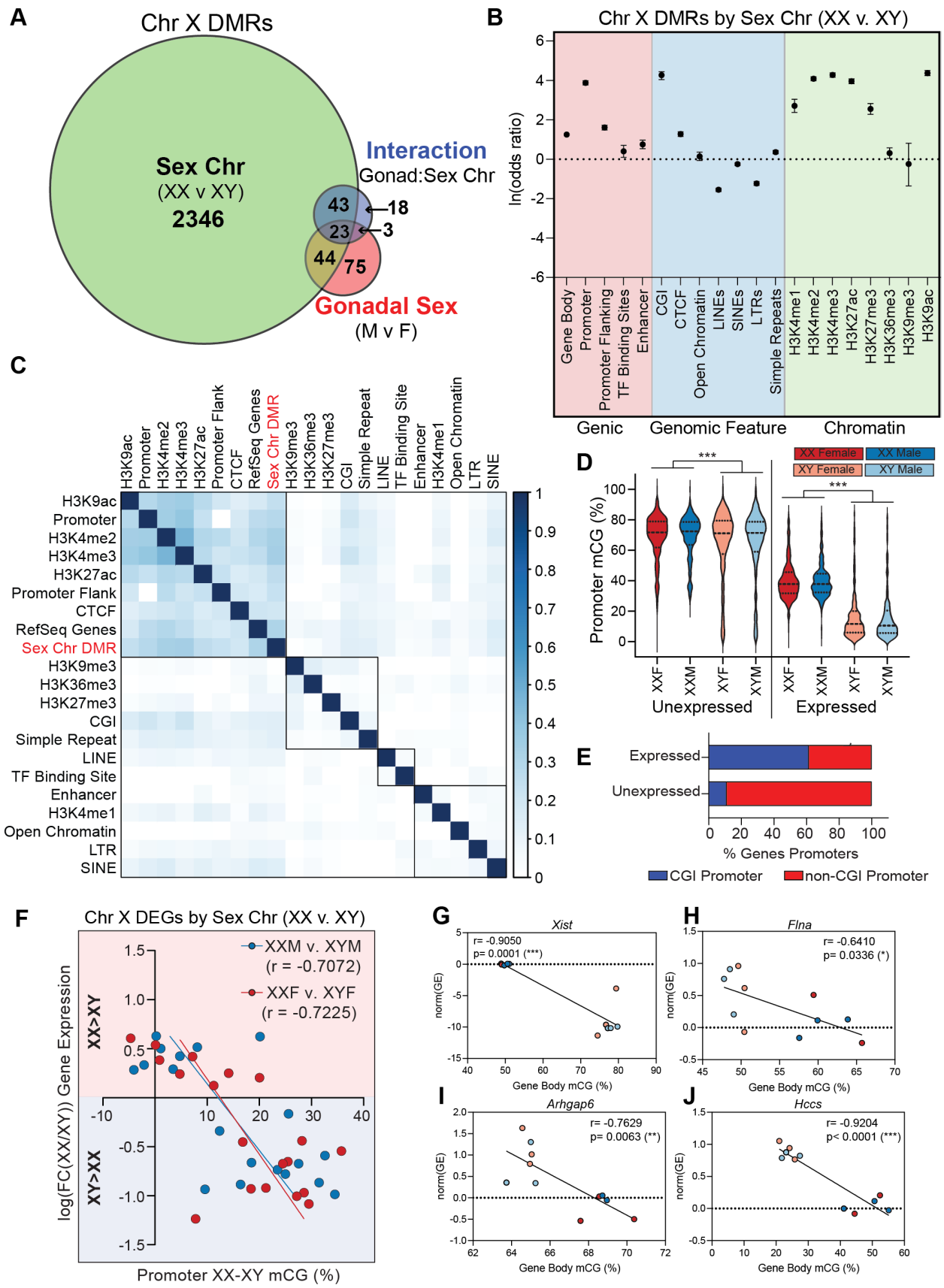
A
Chr X DMRs
Sex Chr
(XX v XY)
2346
Interaction
Gonad:Sex Chr
43
18
23
3
44
75
Gonadal Sex
(M v F)
B
Chr X DMRs by Sex Chr (XX v. XY)
ln(odds ratio)
Gene Body
Promoter
Promoter Flanking
TF Binding Sites
Enhancer
CGI
CTCF
Open Chromatin
LINEs
SINEs
LTRs
Simple Repeats
H3K4me1
H3K4me2
H3K4me3
H3K27ac
H3K27me3
H3K36me3
H3K9me3
H3K9ac
Genic
Genomic Feature
Chromatin
C
H3K9ac
Promoter
H3K4me2
H3K4me3
H3K27ac
Promoter Flank
CTCF
RefSeq Genes
Sex Chr DMR
H3K9me3
H3K36me3
H3K27me3
CGI
Simple Repeat
LINE
TF Binding Site
Enhancer
H3K4me1
Open Chromatin
LTR
SINE
D
XX Female
XX Male
XY Female
XY Male
Promoter mCG (%)
XXF
XXM
XYF
XYM
Unexpressed
Expressed
E
Expressed
Unexpressed
% Genes Promoters
CGI Promoter
non-CGI Promoter
F
Chr X DEGs by Sex Chr (XX v. XY)
XXM v. XYM
(r = -0.7072)
XXF v. XYF
(r = -0.7225)
XX>XY
XY>XX
log(FC(XX/XY)) Gene Expression
Promoter XX-XY mCG (%)
G
Xist
r= -0.9050
p= 0.0001 (***)
norm(GE)
Gene Body mCG (%)
H
Flna
r= -0.6410
p= 0.0336 (*)
norm(GE)
Gene Body mCG (%)
I
Arhgap6
r= -0.7629
p= 0.0063 (**)
norm(GE)
Gene Body mCG (%)
J
Hccs
r= -0.9204
p< 0.0001 (***)
norm(GE)
Gene Body mCG (%)

1572 **Fig. 6 Epigenomic analysis of X-chromosomal differentially methylated regions (DMRs)**
1573 **from adult FCG hippocampi**

1574 DNA was isolated from FCG hippocampi (n=3/group). Methylation in CG context was assessed
1575 by WGoxBS (n=3/group) and analyzed in methylKit to identify ChrX DMRs (w=1000). ChrX DMRs
1576 with minimum mCG difference of 10% between at least two groups (Chisq-test, sliding linear
1577 model (SLIM) q<0.05) were assessed for main effects of sex chromosome (XX v. XY) and gonadal
1578 sex (M v. F) (2-way ANOVA, Bonferonni α<0.0083). **A)** Venn diagram of DMRs by sex
1579 chromosome (XX v. XY), gonadal sex (M v. F), and interactive effect of gonadal and chromosomal
1580 sex. **B)** Relative enrichment and depletion of ChrX DMRs by sex chromosome (XX v. XY) within
1581 various genomic features. **C)** BedSect (Mishra et al., 2020) correlation plot of ChrX genomic
1582 regulatory features (Ward hierarchical clustering, Jaccard similarity index). **D)** Distribution of
1583 unexpressed and expressed gene promoter mCG (%). Unexpressed gene promoters (+/- 2kb
1584 from TSS) had higher mCG in XX genotypes (68%) as compared to XY genotypes (54%),
1585 regardless of gonadal sex. Expressed gene promoters had higher mCG in XX genotypes (40%)
1586 as compared to XY genotypes (17%), regardless of gonadal sex (2-way ANOVA, main effect sex
1587 chromosome complement, ***p<0.001). **E)** Only 11% of unexpressed ChrX gene promoters
1588 contain CGIs, as compared to 61% of expressed ChrX gene promoters. **F)** Correlation of log(FC)
1589 gene expression (XX/XY) and difference in gene promoter mCG (XX-XY) for 19 ChrX DEGs
1590 identified in **Fig. 2E** (Pearson r, p<0.05). *Xist* was excluded from the correlation since lack of
1591 expression in XY genotypes inflates the fold-change values used for analysis. **G-J)** Intersection
1592 of DMRs within gene bodies with differentially expressed genes by sex chromosome (XX v. XY)
1593 identified four genes: (F) *Xist,* (G) *Flna*, (H) *Arhgap6*, and (I) *Hccs*, all of which have a significant
1594 negative correlation between gene body methylation and gene expression (Pearson r, *p<0.05,
1595 **p<0.01, ***p<0.001).

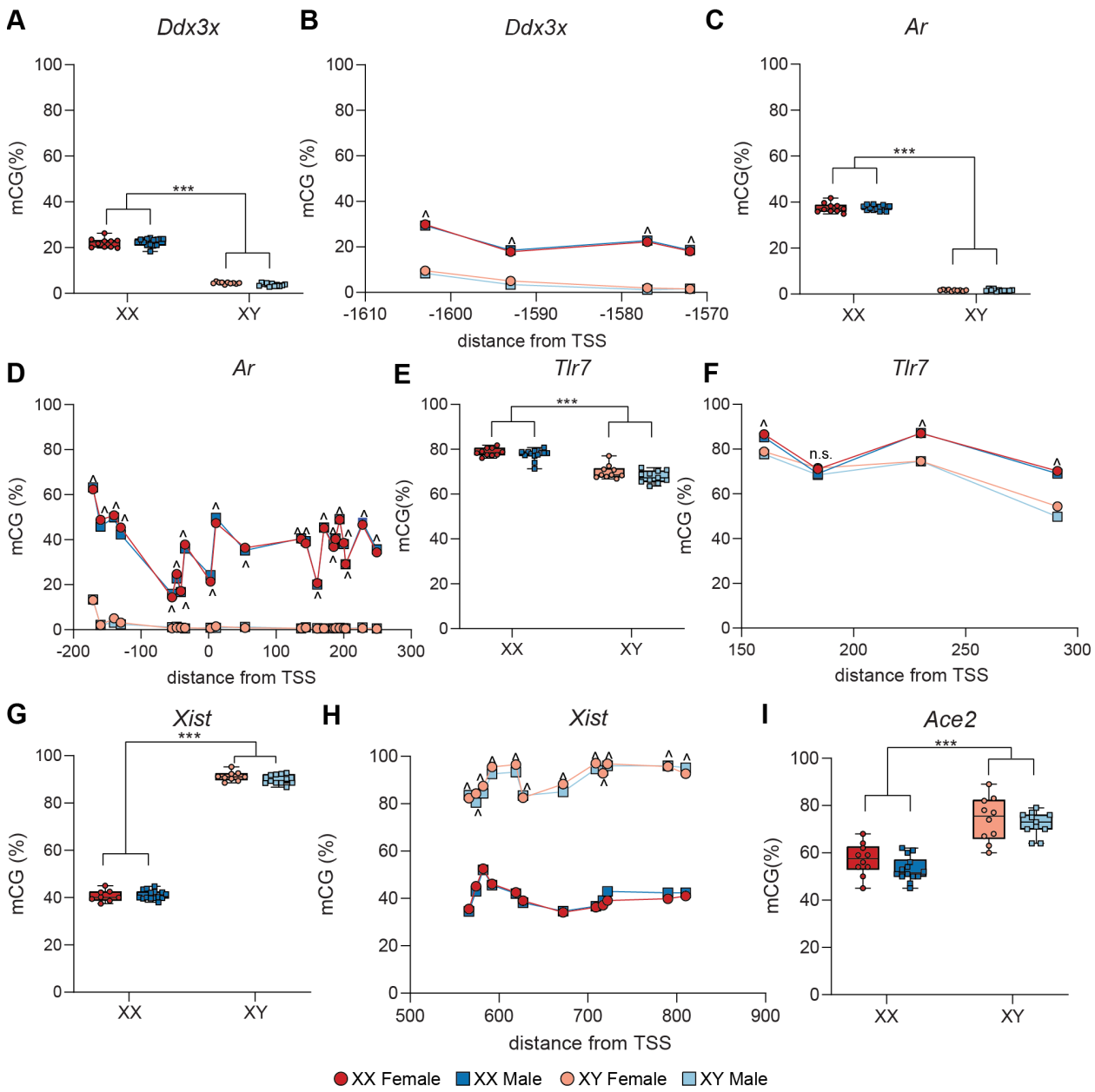

Fig. 7 Targeted bisulfite amplicon sequencing (BSAS) of X-chromosome gene promoters in FCG hippocampus

DNA isolated from FCG hippocampi (n=10-16/group) was bisulfite-converted and DNA methylation in gene promoters (+/- 2kb from TSS) was assessed by BSAS. (A) Average *Ddx3x* promoter mCG is lower in XY genotypes (XYF/XYM) as compared to XX genotypes (XXF/XXM), regardless of gonadal sex. (B) The topography, or patterning, of mCG across the amplified region of the *Ddx3x* promoter shows base-specific regulation of mCG by sex chromosome complement (XX v. XY), with higher mCG in XX genotypes than XY genotypes at each CG site in the region. (C) Average *Ar* promoter mCG is lower in XY genotypes (XYF/XYM) as compared to XX genotypes (XXF/XXM), regardless of gonadal sex. (D) The topography of mCG across the amplified region of the *Ar* promoter shows base-specific regulation of mCG by sex chromosome

complement (XX v. XY), with higher mCG in XX genotypes than XY genotypes at each CG site in the region. (E) Average *Tlr7* promoter mCG is lower in XY genotypes (XYF/XYM) as compared to XX genotypes (XXF/XXM), regardless of gonadal sex. (F) The topography of mCG across the amplified region of the *Tlr7* promoter shows base-specific regulation of mCG by sex chromosome complement (XX v. XY), with higher mCG in XX genotypes than XY genotypes at three of the four CG sites in the region. (G) Average *Xist* promoter mCG is higher in XY genotypes (XYF/XYM) as compared to XX genotypes (XXF/XXM), regardless of gonadal sex. (H) The topography of mCG across the amplified region of the *Xist* promoter shows base-specific regulation of mCG by sex chromosome complement (XX v. XY), with higher mCG in XY genotypes than XX genotypes at each CG site in the region. (I) Average *Ace2* promoter mCG is higher in XY genotypes (XYF/XYM) as compared to XX genotypes (XXF/XXM), regardless of gonadal sex.

Boxplots represent median, interquartile range, and minimum/maximum mCG (%) averaged over all CG sites within the amplified region of the respective gene promoter. (2way ANOVA, main effect of sex chromosome complement (XX v. XY), ***$p<0.001$) (2way ANOVA, Tukey's *post-hoc*, ^$p<0.05$ for all four XX v XY comparisons: XXF v XYF, XXF v. XYM, XXM v. XYM, XXM v. XYF)

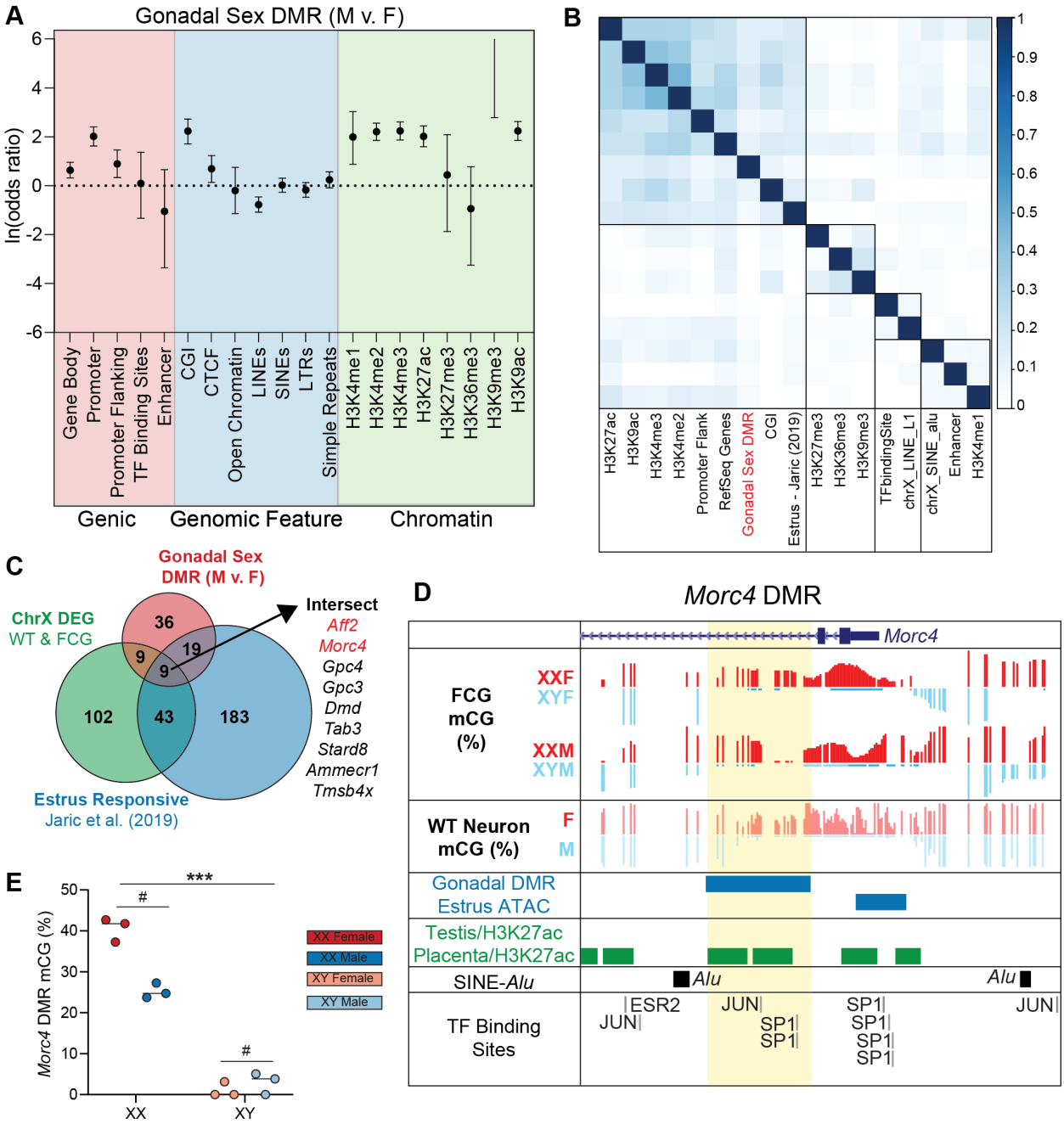

Fig. 8 Comparison of DMRs X-chromosome differentially regulated by gonadal sex (M v. F) to chromatin context and gene expression

A) Relative enrichment and depletion of ChrX DMRs by gonadal sex (M v. F) within various genomic features. **B)** BedSect (Mishra et al., 2020) correlation plot of ChrX genomic regulatory features (Ward hierarchical clustering, Jaccard similarity index) with gonadal sex DMRs and estrus-responsive chromatin (Jaric et al., 2019). **C)** Comparison of 145 gonadal sex DMRs, 169 sex differentially expressed genes from **Fig. 5E,** and 238 genes with estrus cycle-responsive chromatin (Jaric et al., 2019), identified 9 DMRs with variable escape from X-inactivation and estrus-responsive chromatin. **D)** Genome tracks of *Morc4* promoter region with gonadal DMR region (highlighted yellow), FCG mCG, WT male and female neuronal mCG (Lister et al., 2013),

1635 estrus-cycle differential ATAC-seq peaks (Jaric et al., 2019), male (testis) and female (placenta)
1636 specific H3K27ac peaks, SINE-*Alu* repeats, and JASPAR 2022 TFBSs (SP1, JUN, ESR2)
1637 (Castro-Mondragon et al., 2022). **E)** *Morc4* DMR mCG (%) is higher in XX vs XY genotypes and
1638 higher in M v F, with an interaction between chromosomal and gonadal sex (Two-way ANOVA,
1639 main effect sex chromosome complement (***p=1.44E-08), main effect gonadal sex (#p= 0.0011),
1640 interaction (p= 0.0002)).

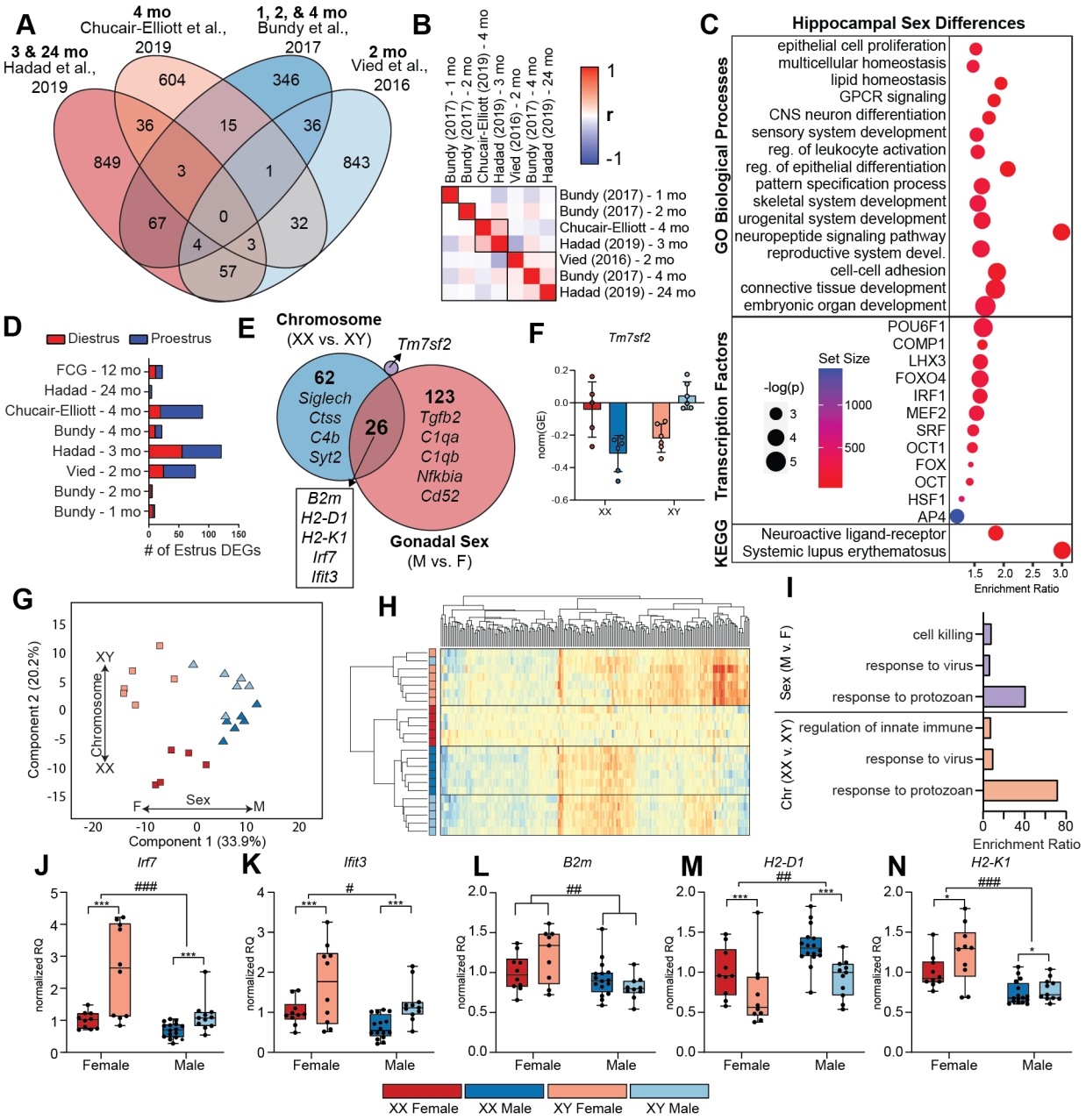

Fig. 9 Transcriptomic analysis of autosomal differential expression from adult FCG hippocampi

DNA and RNA were isolated from FCG hippocampi (n=10-16/group). mRNA expression was assessed by stranded RNA-Seq (n=5-6/group) and RT-qPCR (n=10-16/group). Results were compared to previously published hippocampal transcriptomic sex differences. **Boxplots** represent median, interquartile range, and minimum/maximum normalized RQ. **A**) Comparison of four previous hippocampal transcriptomic studies (**Supplemental Table 4n**), shows 2896 autosomal-encoded sex differences in wild-type mice across all studies with no genes in common between all studies. **B**) Pairwise correlations of the fold-change (M v. F) for the 2896 autosomal DEGs were conducted for genes that were expressed in all studies. Hierarchical clustering of the correlation coefficients (Pearson r) shows grouping of studies. **C)** WebGestalt over-representation

analysis of the 2896 autosomal-encoded sex differences in WT hippocampus identified KEGG pathways, transcription factors, and GO biological processes enriched in hippocampal sex difference genes (hypergeometric test, BHMTC, FDR<0.05). **D)** Previously identified estrus-cycle responsive genes (Jaric et al., 2019) were compared to hippocampal sex differences identified in previous WT (**Fig. 9A**) and the present FCG study. The number of estrus-responsive genes (diestrus female v. male – red, proestrus female v. male – blue) were plotted for each dataset. **E)** Differential expression analysis of FCG hippocampal RNA-Seq libraries identified 212 differentially expressed autosomal genes, 62 had a main effect of chromosome only (XX v. XY), 123 had a main effect of gonadal sex only (M v. F) and 26 genes had main effects of chromosome and gonadal sex. There was only one gene (*Tm7sf2*) which had an interactive effect of chromosomal and gonadal sex (Two-way ANOVA, BHMTC, FC>=1.25, FDR<0.1). **F)** Normalized gene expression of *Tm7sf2* by RNA-Seq (Two-way ANOVA, BHMTC, FC>=1.25, FDR<0.1, interactive effect). Bar chart is mean +/- SEM. **G)** Principal component analysis of differentially expressed autosomal genes showed separation of gonadal sex (M v. F) in the first component (33.9%) and separation of the chromosome (XX v. XY) in the second component (20.2%). **H)** Hierarchical clustering of differentially expressed autosomal genes shows separation of genotypes by gonadal sex and sex chromosome complement. **I)** ORA of the autosomal sex differences identified in the FCG hippocampus revealed biological differentially regulated by sex chromosome complement and/or gonadal sex. **J-N)** Differential expression of select genes was confirmed by RT-qPCR (n=10-16/group, Two-Way ANOVA, main effect of sex chromosome complement (XX v. XY) *p<0.05, **p<0.01, and ***p<0.001 or gonadal sex (M v. F) #p<0.05, ##p<0.01, and ###p<0.001). Only *Irf7* had a significant interaction between gonadal and chromosomal sex (p=0.012).

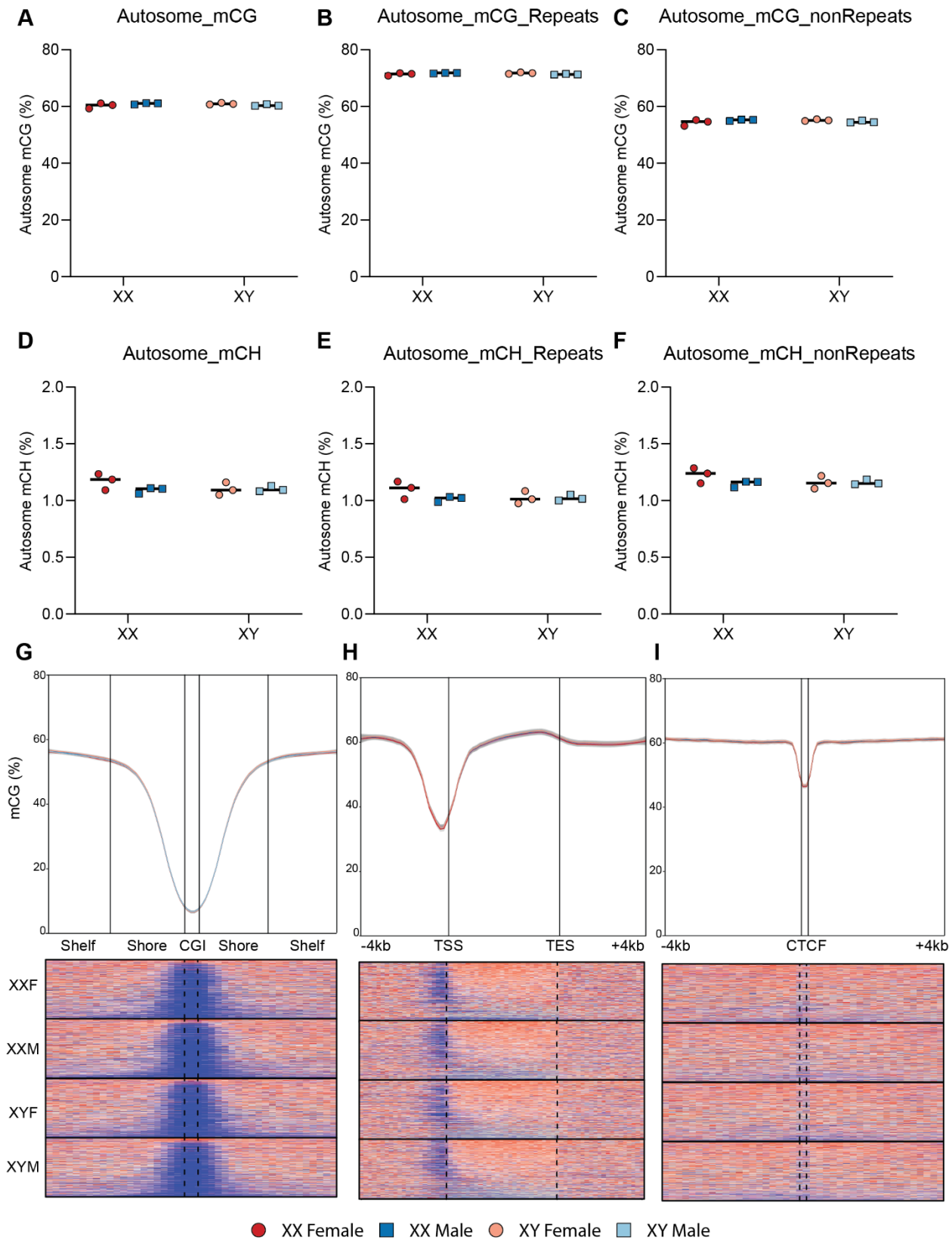

1677 **Fig. 10 Autosomal levels of DNA methylation in FCG hippocampus by WGoxBS**

1678 DNA and RNA were isolated from FCG hippocampi (n=10-16/group). Autosomal methylation in
1679 CpG (CG) and non-CpG (CH) contexts were assessed by WGoxBS (n=3/group). A) There is no
1680 difference in overall mCG on autosomes, in either (B) Repetitive or (C) Non-repetitive elements.
1681 D) There is no difference in overall mCH on autosomes in either (E) Repetitive or (F) Non-
1682 repetitive elements (Two-way ANOVA). G-I) There is no difference in autosomal mCG in: (G) CpG
1683 Islands (CGI), shores, and shelves; (H) gene bodies and flanking regions (+/- 4 kb); or (I) CTCF
1684 binding sites and flanking regions (+/- 4 kb).

1685

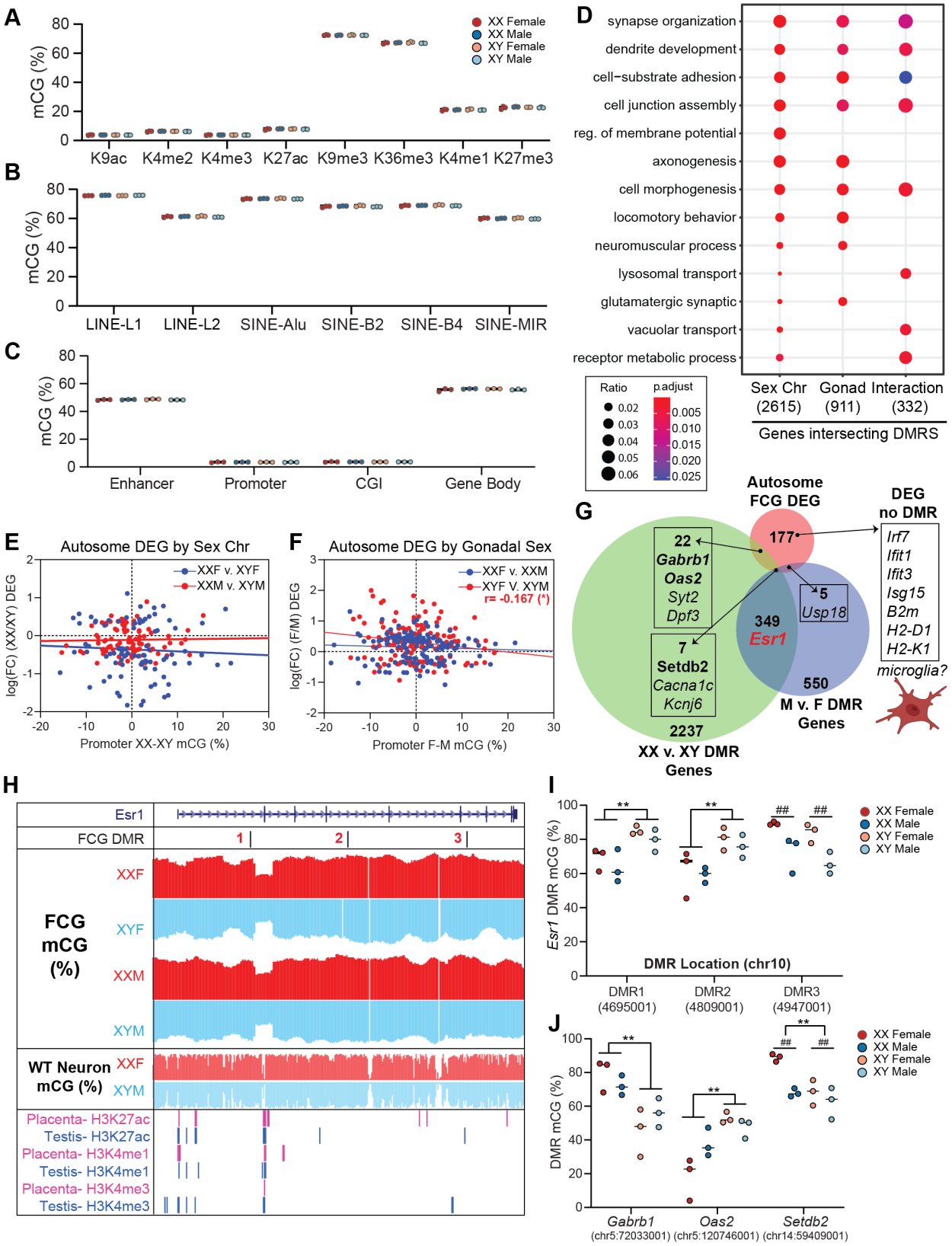

1687 **Fig. 11 Epigenomic analyses of autosomal differentially methylated regions (DMRs) from**
1688 **adult FCG hippocampi**

Autosomal methylation in CpG (CG) context was assessed by WGoxBS (n=3/group). First, average mCG levels in various genome contexts across autosomes were compared and no overall significant sex effects (gonadal or chromosomal) in mCG within: (**A**) autosomal P0 forebrain histone modification foci, (**B**) repetitive elements (LINE-L1, LINE-L2, SINE-Alu, SINE-B2, SINE-B4, SINE-MIR) or (**C**) autosomal proximal gene regulatory regions (Enhancer, promoter, CGI, Gene Body) (Two-way ANOVA). Differentially methylated regions (DMRs) (w=1000 bp) were called in methylKit (*post-hoc* Two-Way ANOVA with Bonferonni correction $p<\alpha=0.0083$). **D)** GO Biological process over-representation analysis of autosomal genes (+/- 2kb) containing DMRs by sex chromosome, gonadal sex, or an interaction of gonadal and chromosomal sex. **E)** Correlation of promoter mCG (-2kb from TSS (XX-XY) and gene expression (log(FC)(XX/XY)) in autosomal DEGs by sex chromosome (XX v. XY) was not significant in XXF v. XYF or XXM v. XYM comparisons (Pearson r, $p>0.05$). **F)** Correlation of promoter mCG (-2kb from TSS (XX-XY)) and gene expression (log(FC)(XX/XY)) (Pearson r) in autosomal DEGs by sex chromosome (XX v. XY). Promoter methylation and gene expression were negatively correlated in XYF v. XYM comparison (Pearson r=-0.167, *p=0.045) but this was not observed in the XXF v. XXM comparison. **G)** Genes closest to autosomal DMRs (+/- 2kb gene body) with main effects of sex chromosome (XX v. XY) and/or gonadal sex (M v. F) were intersected with FCG autosomal DEGs (**Fig. 9E**). The majority (177/211=84%) of DEGs did not coincide with differentially methylated regions. **H)** Genome tracks of *Esr1* gene body (chr10) with FCG DMRs by chromosomal (1 & 2) and gonadal (3) sex, FCG mCG (%), WT male and female neuronal mCG (Lister et al., 2013), and male (testis) and female (placenta) specific histone peaks (H3K27ac, H3K4me1, H3K4me3) (The ENCODE Project Consortium et al. 2020). **I)** *Esr1* DMR (1, 2, & 3) mCG. DMRs 1 & 2 were differentially methylated by chromosomal sex (XX v. XY), while DMR 3 was differentially methylated by gonadal sex (M v. F) (Two-way ANOVA, main effect of sex chromosome **$p<0.01$, main effect gonadal sex, ##$p<0.01$). No significant interactions between gonadal and chromosomal sex were observed. **J)** DMR mCG levels within select autosomal FCG DEGs (*Gabrb1, Oas2*, *Setbd2*). DMRs within *Gabrb1* and *Oas2* were differentially methylated by sex chromosome complement (Two-way ANOVA, main effect sex chromosome complement, **$p<0.01$). The DMR within the *Setdb2* gene body was differentially methylated by chromosomal and gonadal sex (Two-way ANOVA, main effect sex chromosome complement, **$p<0.01$, main effect of gonadal sex, ##$p<0.01$). No interactive effect of gonadal and chromosomal sex was observed.

Gene-Primer#	Forward	Reverse	# CpG Sites
Sry dPCR Copy #	GTCACAGAGGAGTGGCATTT	AGTCTTGCCTGTATGTGATGG	N/A
Sry Probe	/56-FAM/ CAACCTTCT/ZEN/ GCAGTGGGACAGGAA		
Ddx3x-2	GGTAGTAGAAGGTTTTTGGTGG	CTTACCTCAAACCTCTCTCTCC	4
Ar-1	GAAGAGGGGTTTTTAAAGGTTA	CTCCCAACAAACTAACTCCTAA	10
Ar-2	AGGAGTTAGTTTGTTGGGAGAA	TCCTTACTTCCTCTAAATCTCCC	12
Tlr7-2	TTTTTTGTTGTTTTTTTTTTGTT	CTCCAAAAAACTATTTCCAATC	4
Xist-3	GGGTTGTGGATATTTGTTTTTATT	TAAACCATAAATTCACTCACACAA	13
Ace2-2	TTTTATGGAGTGGAGAAGAGTTT	CACCACAACCACCTAACTAAAT	1

1722

1723 **Table 1. Digital PCR copy number and BSAS primers (5'->3') for targeted methylation**
1724 **analysis.**

1725

Author/Year	**Bundy et al., 2017**	**Vied et al., 2016**	**Chucair-Elliott et al., 2019**	**Hadad et al., 2019**
PMID	**PMID: 28302071**	**PMID: 26917114**	**PMID: 31493147**	**PMID: 31594536**
Data Availability	**GEO Accession: GSE83931**	**GEO Accession: GSE76567**	**GEO Accession: GSE135752**	**SRA bioProject: PRJNA523985**
Age (Group 1)	1 mo	2 mo	4 mo	3 mo
Age (Group 2)	2 mo	-	-	24 mo
Age (Group 3)	4 mo	-	-	-
n	5	5	3	6
Estrus staging	**1 mo –** no staging **2 mo –** vaginal cytology; 2 estrus, 2 metestrus, 1 diestrus	No mention	No mention	No mention

1726

1727 **Table 2. Age, sample size, and estrus staging for previous hippocampal transcriptomic**
1728 **studies.**

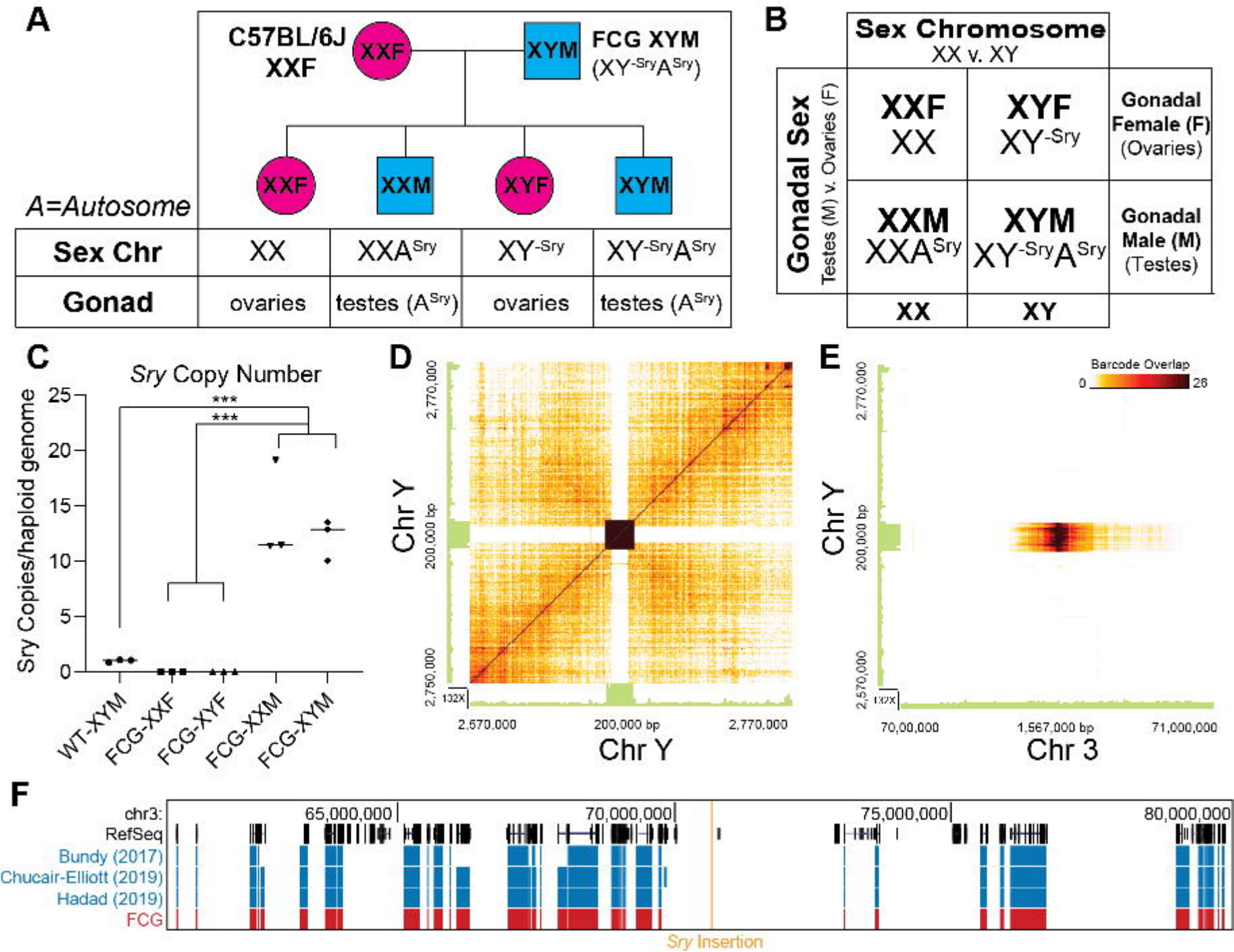
A
C57BL/6J
XXF
XXF
XYM
FCG XYM
(XY-SryASry)
XXF
XXM
XYF
XYM
A=Autosome
Sex Chr
XX
XXASry
XY-Sry
XY-SryASry
Gonad
ovaries
testes (ASry)
ovaries
testes (ASry)
B
Sex Chromosome
XX v. XY
Gonadal Sex
Testes (M) v. Ovaries (F)
XXF
XX
XYF
XY-Sry
Gonadal Female (F)
(Ovaries)
XXM
XXASry
XYM
XY-SryASry
Gonadal Male (M)
(Testes)
XX
XY
C
Sry Copy Number
Sry Copies/haploid genome
25
20
15
10
5
0
***
***
WT-XYM
FCG-XXF
FCG-XYF
FCG-XXM
FCG-XYM
D
Chr Y
2,770,000
200,000 bp
2,750,000
132X
2,570,000
200,000 bp
2,770,000
Chr Y
E
Barcode Overlap
0
26
Chr Y
2,770,000
200,000 bp
2,570,000
132X
70,000,000
1,567,000 bp
71,000,000
Chr 3
F
chr3:
65,000,000
70,000,000
75,000,000
80,000,000
RefSeq
Bundy (2017)
Chucair-Elliott (2019)
Hadad (2019)
FCG
Sry Insertion

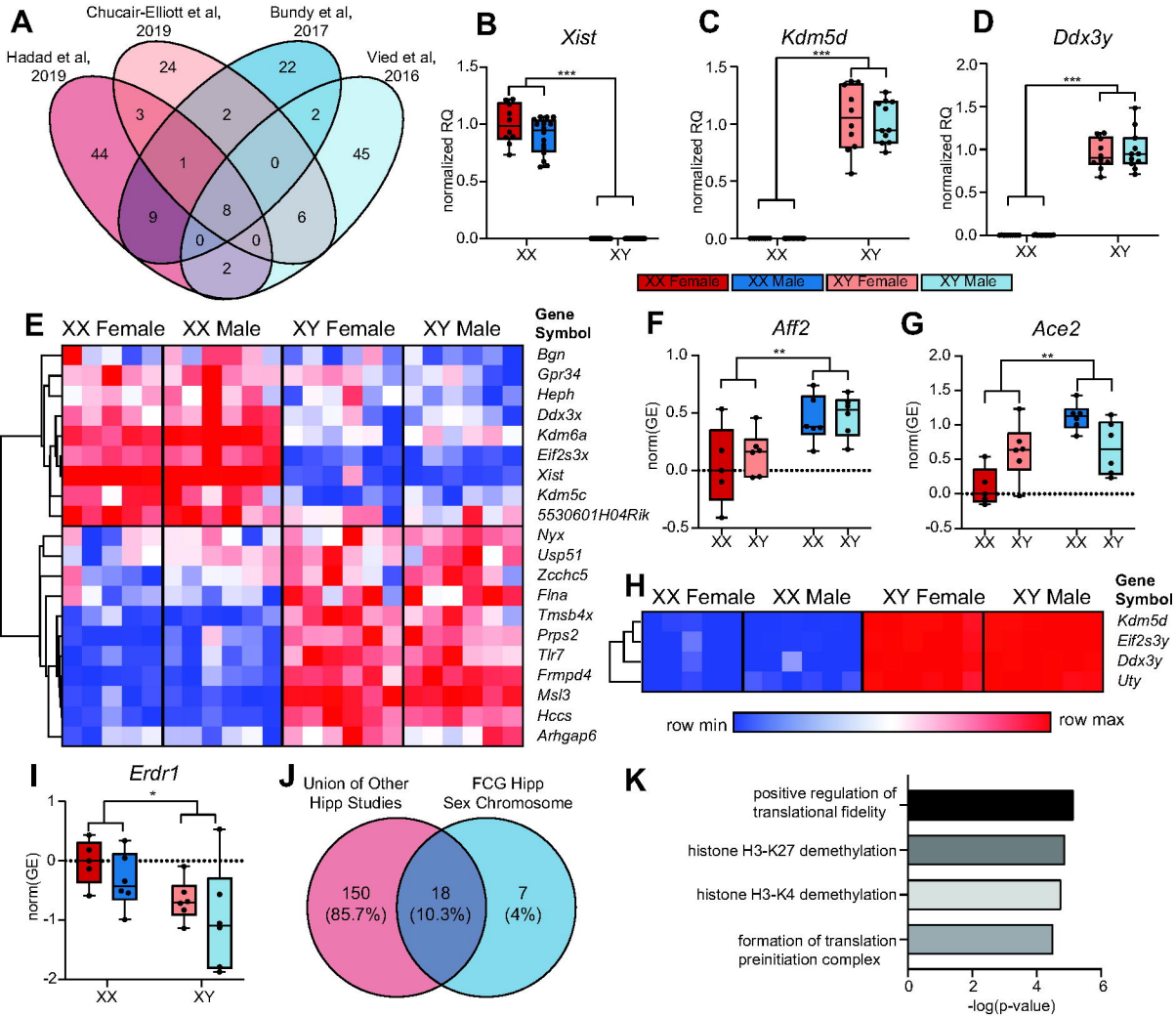
A
Chucair-Elliott et al, 2019
Bundy et al, 2017
Hadad et al, 2019
Vied et al, 2016
24
22
3
2
2
44
1
0
45
9
8
6
0
0
2
B
Xist
C
Kdm5d
D
Ddx3y
normalized RQ
XX
XY
XX Female
XX Male
XY Female
XY Male
E
XX Female
XX Male
XY Female
XY Male
Gene Symbol
Bgn
Gpr34
Heph
Ddx3x
Kdm6a
Eif2s3x
Xist
Kdm5c
5530601H04Rik
Nyx
Usp51
Zcchc5
Flna
Tmsb4x
Prps2
Tlr7
Frmpd4
Msl3
Hccs
Arhgap6
F
Aff2
G
Ace2
norm(GE)
H
Kdm5d
Eif2s3y
Ddx3y
Uty
row min
row max
I
Erdr1
J
Union of Other Hipp Studies
FCG Hipp Sex Chromosome
150 (85.7%)
18 (10.3%)
7 (4%)
K
positive regulation of translational fidelity
histone H3-K27 demethylation
histone H3-K4 demethylation
formation of translation preinitiation complex
-log(p-value)

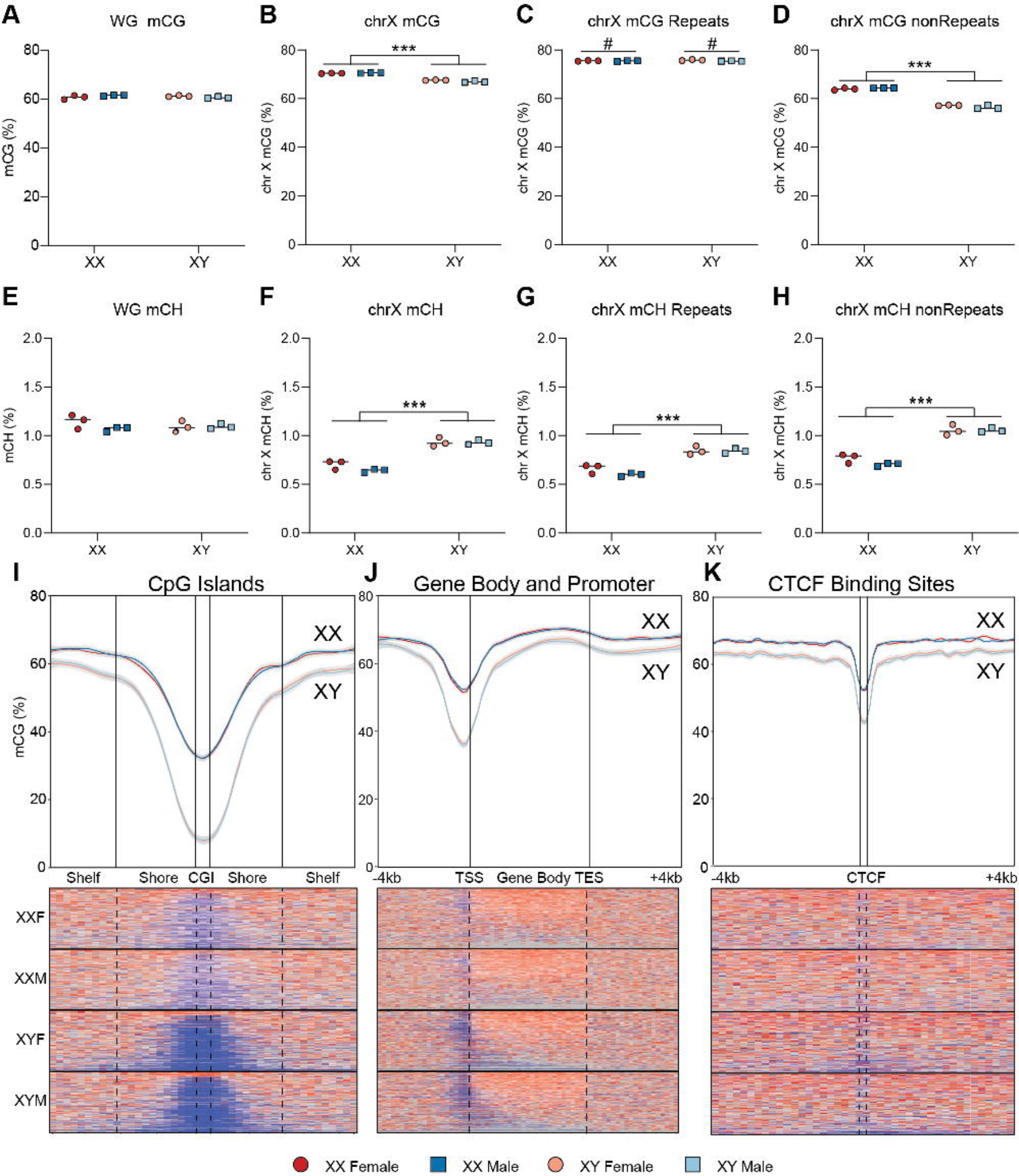
A
WG mCG
mCG (%)
B
chrX mCG
chr X mCG (%)
***
C
chrX mCG Repeats
#
#
D
chrX mCG nonRepeats
E
WG mCH
mCH (%)
F
chrX mCH
chr X mCH (%)
G
chrX mCH Repeats
H
chrX mCH nonRepeats
XX
XY
I
CpG Islands
Shelf
Shore
CGI
Shore
Shelf
J
Gene Body and Promoter
-4kb
TSS
Gene Body
TES
+4kb
K
CTCF Binding Sites
CTCF
XXF
XXM
XYF
XYM
XX Female
XX Male
XY Female
XY Male

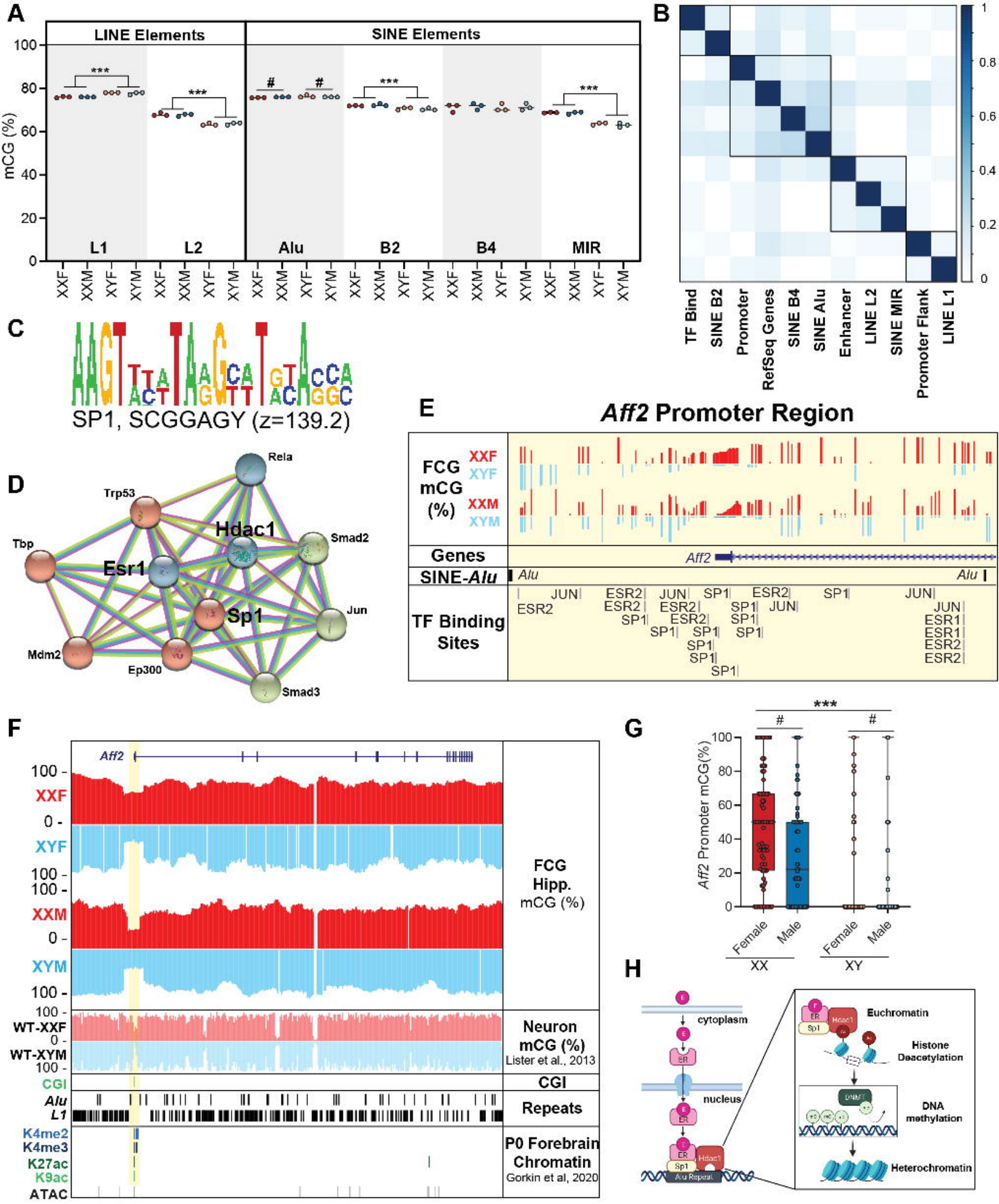
A
LINE Elements
SINE Elements
mCG (%)
L1
L2
Alu
B2
B4
MIR
XXF
XXM
XYF
XYM
B
TF Bind
SINE B2
Promoter
RefSeq Genes
SINE B4
SINE Alu
Enhancer
LINE L2
SINE MIR
Promoter Flank
LINE L1
C
SP1, SCGGAGY (z=139.2)
D
Rela
Trp53
Hdac1
Smad2
Tbp
Esr1
Sp1
Jun
Mdm2
Ep300
Smad3
E
Aff2 Promoter Region
FCG mCG (%)
XXF
XYF
XXM
XYM
Genes
Aff2
SINE-Alu
Alu
TF Binding Sites
F
Aff2
FCG Hipp. mCG (%)
WT-XXF
WT-XYM
Neuron mCG (%)
Lister et al., 2013
CGI
Alu
L1
Repeats
K4me2
K4me3
K27ac
K9ac
ATAC
P0 Forebrain Chromatin
Gorkin et al, 2020
G
Aff2 Promoter mCG(%)
Female
Male
XX
XY
H
cytoplasm
nucleus
ER
Sp1
Hdac1
Alu Repeat
Euchromatin
Histone Deacetylation
DNA methylation
Heterochromatin

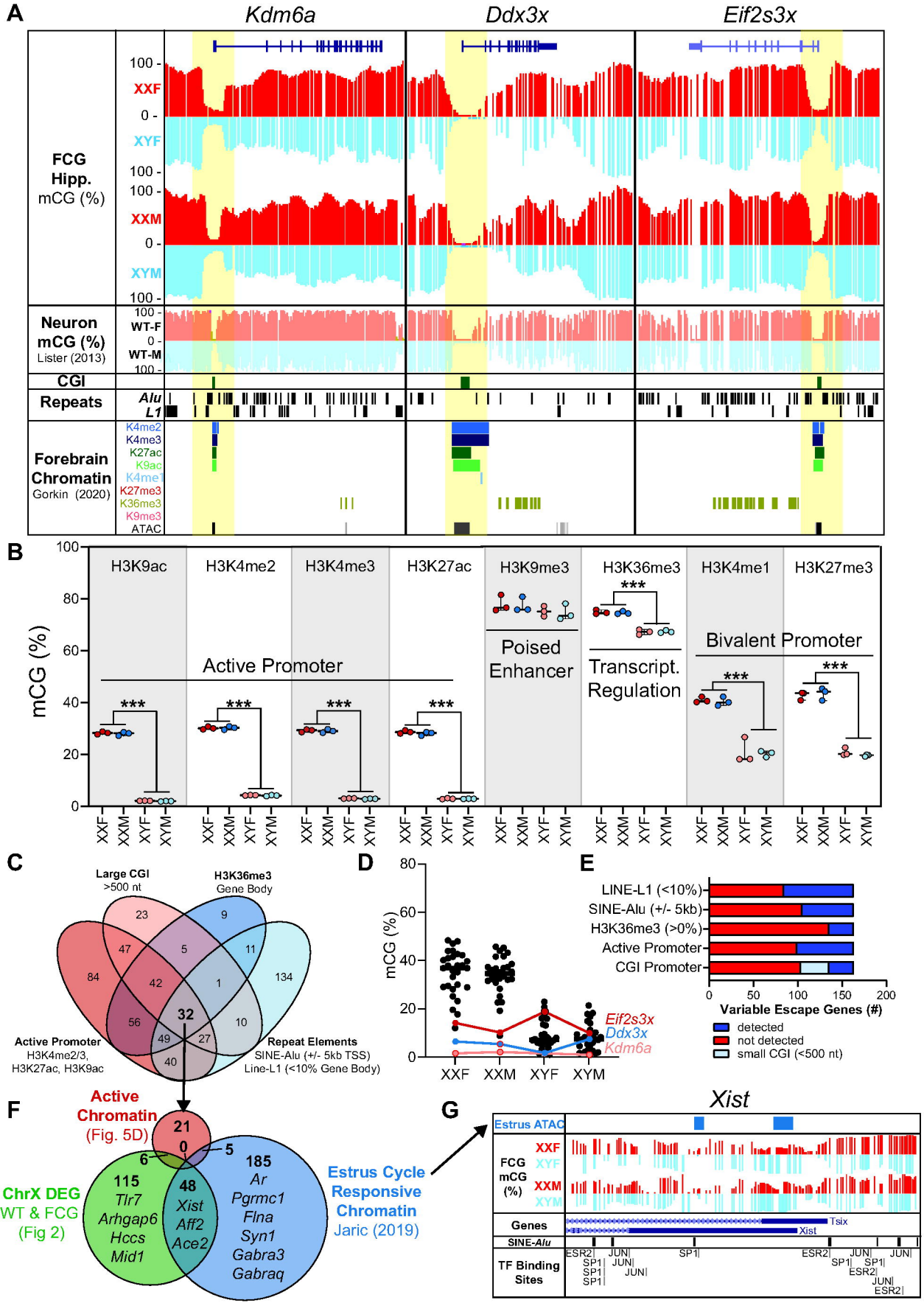
A
Kdm6a
Ddx3x
Eif2s3x
FCG Hipp. mCG (%)
XXF
XYF
XXM
XYM
Neuron mCG (%) Lister (2013)
WT-F
WT-M
CGI
Repeats
Alu
L1
Forebrain Chromatin Gorkin (2020)
K4me2
K4me3
K27ac
K9ac
K4me1
K27me3
K36me3
K9me3
ATAC
B
mCG (%)
H3K9ac
H3K4me2
H3K4me3
H3K27ac
H3K9me3
H3K36me3
H3K4me1
H3K27me3
Active Promoter
Poised Enhancer
Transcript. Regulation
Bivalent Promoter
***
XXF
XXM
XYF
XYM
C
Large CGI >500 nt
H3K36me3 Gene Body
Active Promoter H3K4me2/3, H3K27ac, H3K9ac
Repeat Elements SINE-Alu (+/- 5kb TSS) Line-L1 (<10% Gene Body)
D
mCG (%)
Eif2s3x
Ddx3x
Kdm6a
E
LINE-L1 (<10%)
SINE-Alu (+/- 5kb)
H3K36me3 (>0%)
Active Promoter
CGI Promoter
Variable Escape Genes (#)
detected
not detected
small CGI (<500 nt)
F
Active Chromatin (Fig. 5D)
ChrX DEG WT & FCG (Fig 2)
Estrus Cycle Responsive Chromatin Jaric (2019)
115 Tlr7 Arhgapa6 Hccs Mid1
48 Xist Aff2 Ace2
185 Ar Pgrmc1 Flna Syn1 Gabra3 Gabraq
G
Xist
Estrus ATAC
FCG mCG (%)
Genes
Tsix
Xist
SINE-Alu
TF Binding Sites
ESR2
SP1
JUN

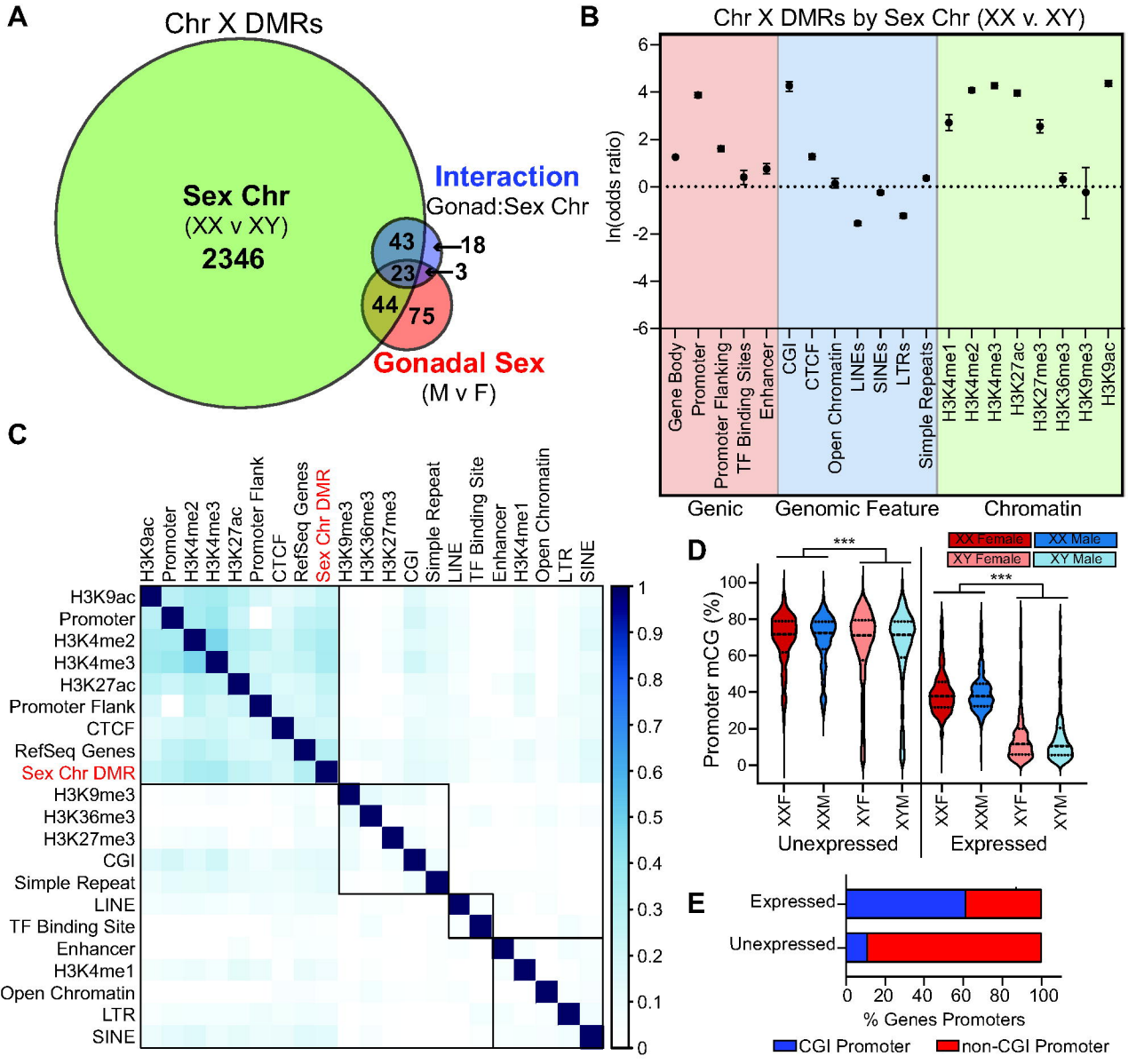
A
Chr X DMRs
Sex Chr
(XX v XY)
2346
Interaction
Gonad:Sex Chr
43
18
23
3
44
75
Gonadal Sex
(M v F)
B
Chr X DMRs by Sex Chr (XX v. XY)
ln(odds ratio)
Gene Body
Promoter
Promoter Flanking
TF Binding Sites
Enhancer
CGI
CTCF
Open Chromatin
LINEs
SINEs
LTRs
Simple Repeats
H3K4me1
H3K4me2
H3K4me3
H3K27ac
H3K27me3
H3K36me3
H3K9me3
H3K9ac
Genic
Genomic Feature
Chromatin
C
H3K9ac
Promoter
H3K4me2
H3K4me3
H3K27ac
Promoter Flank
CTCF
RefSeq Genes
Sex Chr DMR
H3K9me3
H3K36me3
H3K27me3
CGI
Simple Repeat
LINE
TF Binding Site
Enhancer
H3K4me1
Open Chromatin
LTR
SINE
D
XX Female
XX Male
XY Female
XY Male
Promoter mCG (%)
XXF
XXM
XYF
XYM
Unexpressed
Expressed
E
Expressed
Unexpressed
% Genes Promoters
CGI Promoter
non-CGI Promoter
F
Chr X DEGs by Sex Chr (XX v. XY)
XXM v. XYM
(r = -0.7072)
XXF v. XYF
(r = -0.7225)
XX>XY
XY>XX
log(FC(XX/XY)) Gene Expression
Promoter XX-XY mCG (%)
G
Xist
r= -0.9050
p= 0.0001 (***)
norm(GE)
Gene Body mCG (%)
H
Flna
r= -0.6410
p= 0.0336 (*)
I
Arhgap6
r= -0.7629
p= 0.0063 (**)
J
Hccs
r= -0.9204
p< 0.0001 (***)

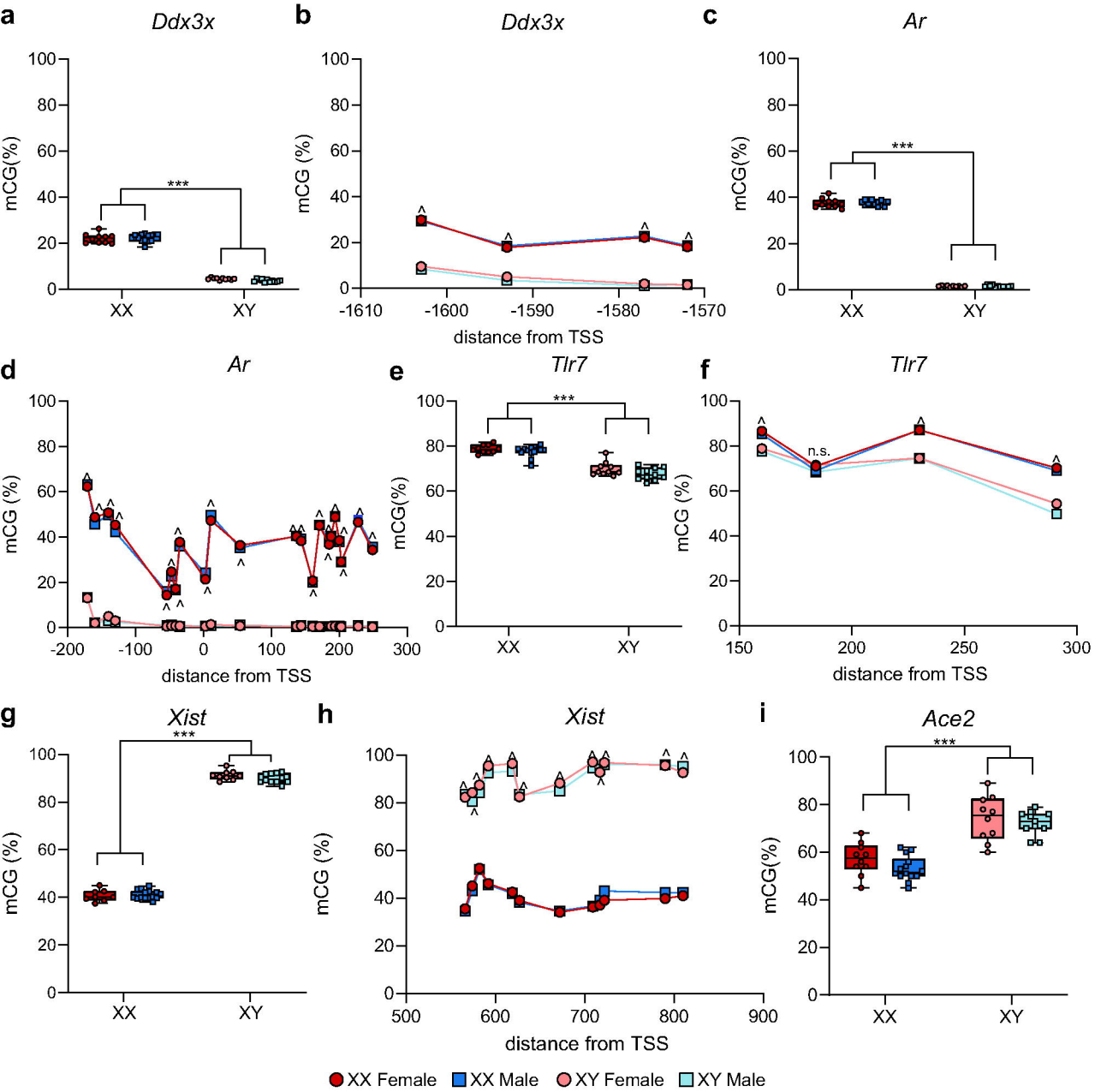
a
Ddx3x
mCG(%)
***
XX
XY
b
Ddx3x
mCG (%)
distance from TSS
c
Ar
mCG(%)
***
XX
XY
d
Ar
mCG (%)
distance from TSS
e
Tlr7
mCG(%)
***
XX
XY
f
Tlr7
mCG (%)
n.s.
distance from TSS
g
Xist
mCG (%)
***
XX
XY
h
Xist
mCG (%)
distance from TSS
i
Ace2
mCG(%)
***
XX
XY
XX Female
XX Male
XY Female
XY Male

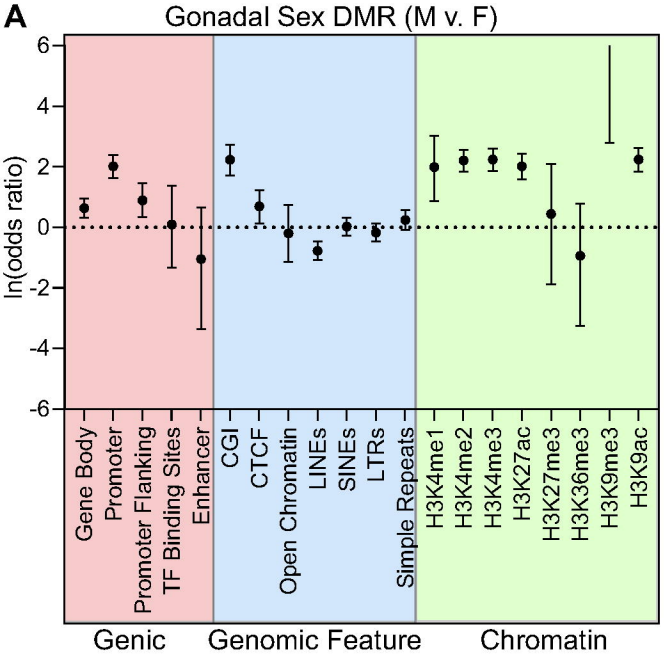
A
Gonadal Sex DMR (M v. F)
ln(odds ratio)
6
4
2
0
-2
-4
-6
Gene Body
Promoter
Promoter Flanking
TF Binding Sites
Enhancer
CGI
CTCF
Open Chromatin
LINEs
SINEs
LTRs
Simple Repeats
H3K4me1
H3K4me2
H3K4me3
H3K27ac
H3K27me3
H3K36me3
H3K9me3
H3K9ac
Genic
Genomic Feature
Chromatin

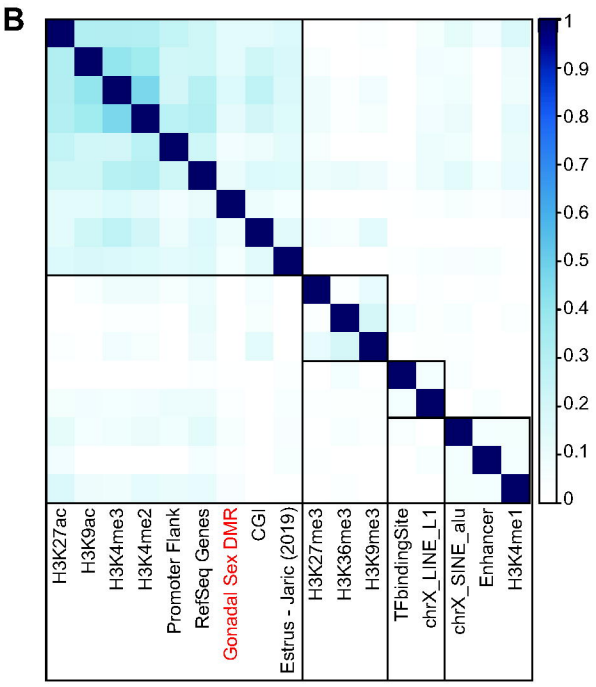
B
1
0.9
0.8
0.7
0.6
0.5
0.4
0.3
0.2
0.1
0
H3K27ac
H3K9ac
H3K4me3
H3K4me2
Promoter Flank
RefSeq Genes
Gonadal Sex DMR
CGI
Estrus - Jaric (2019)
H3K27me3
H3K36me3
H3K9me3
TFbindingSite
chrX_LINE_L1
chrX_SINE_alu
Enhancer
H3K4me1

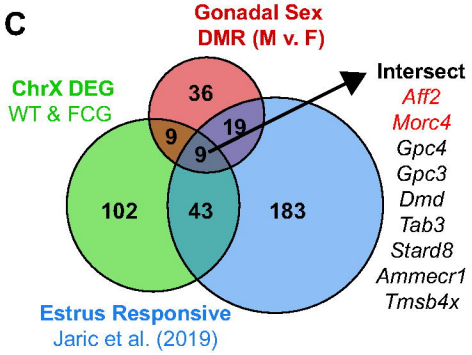
C
Gonadal Sex DMR (M v. F)
ChrX DEG
WT & FCG
36
9
19
9
102
43
183
Intersect
Aff2
Morc4
Gpc4
Gpc3
Dmd
Tab3
Stard8
Ammecr1
Tmsb4x
Estrus Responsive
Jaric et al. (2019)

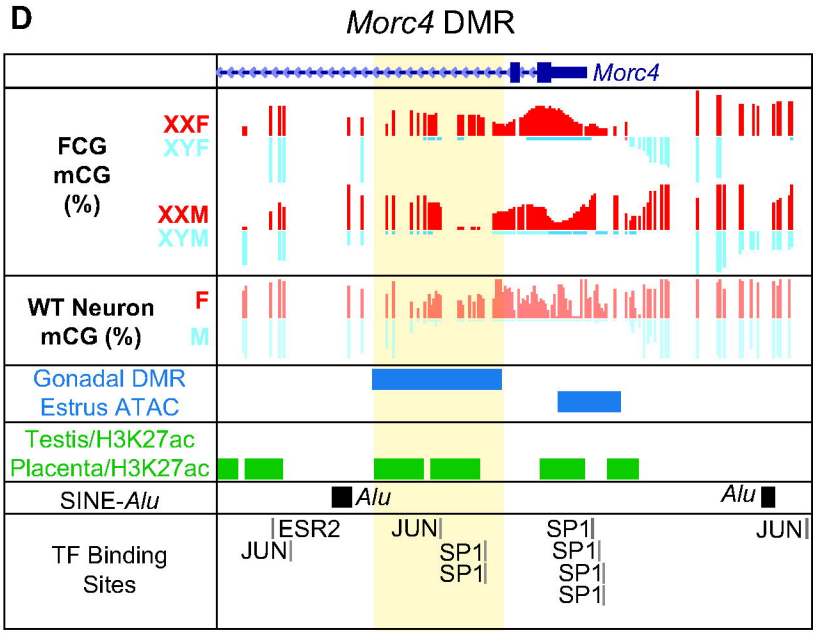
D
Morc4 DMR
Morc4
FCG mCG (%)
XXF
XYF
XXM
XYM
WT Neuron mCG (%)
F
M
Gonadal DMR
Estrus ATAC
Testis/H3K27ac
Placenta/H3K27ac
SINE-Alu
Alu
Alu
TF Binding Sites
ESR2
JUN
JUN
SP1
SP1
SP1
SP1
SP1
SP1
JUN

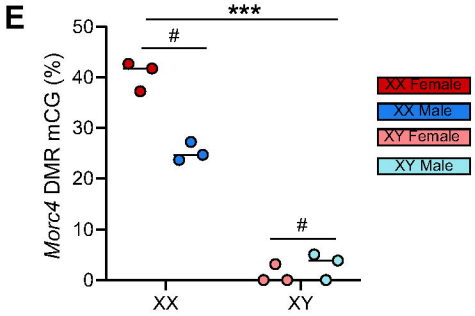
E
***
#
#
Morc4 DMR mCG (%)
50
40
30
20
10
0
XX
XY
XX Female
XX Male
XY Female
XY Male

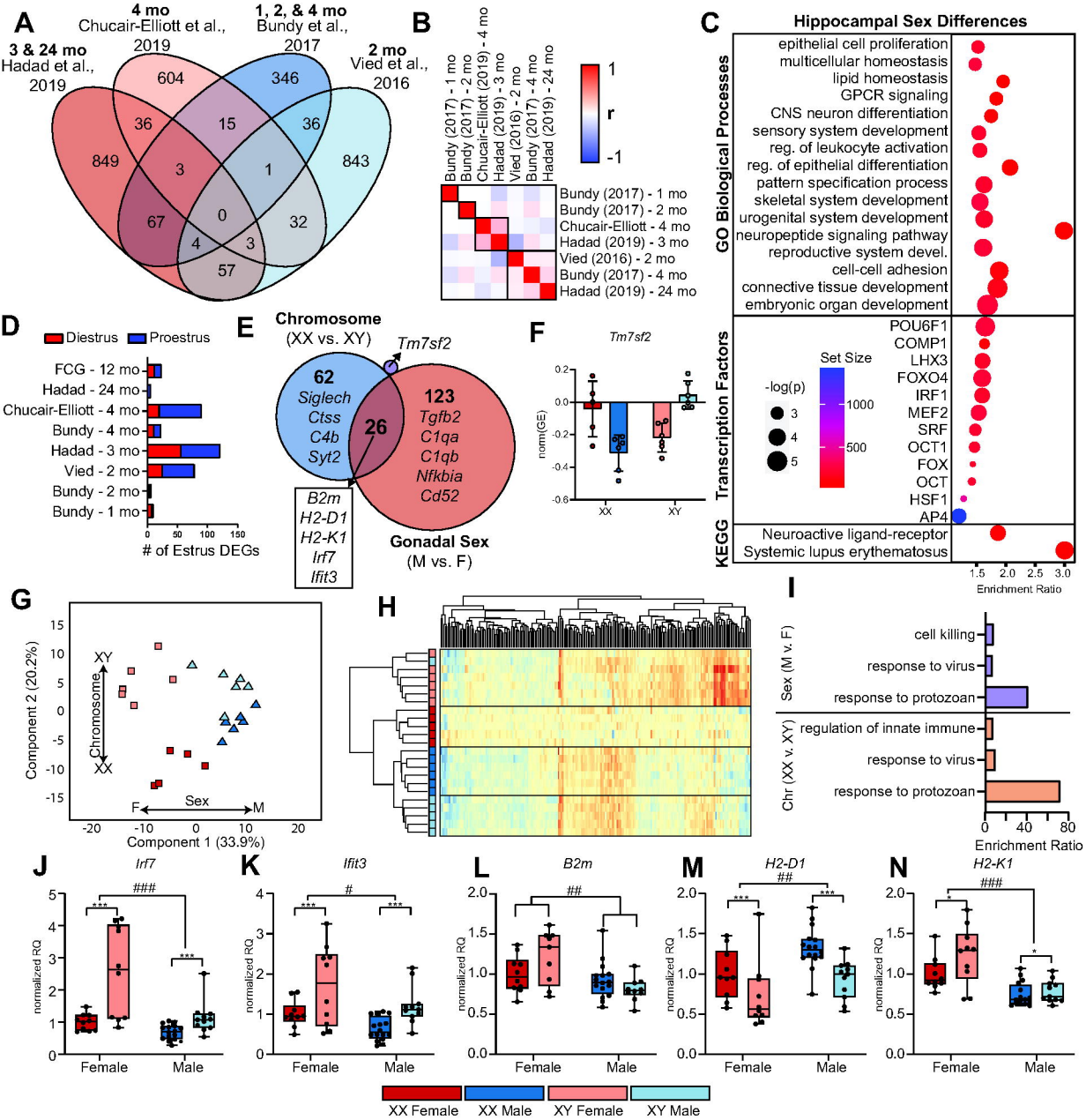
A
4 mo
Chucair-Elliott et al., 2019
1, 2, & 4 mo
Bundy et al., 2017
3 & 24 mo
Hadad et al., 2019
2 mo
Vied et al., 2016
604
346
36
15
36
849
843
3
1
0
67
32
4
3
57
B
Bundy (2017) - 1 mo
Bundy (2017) - 2 mo
Chucair-Elliott (2019) - 3 mo
Hadad (2019) - 3 mo
Vied (2016) - 2 mo
Bundy (2017) - 4 mo
Hadad (2019) - 24 mo
Chucair-Elliott (2019) - 4 mo
r
1
-1
C
Hippocampal Sex Differences
GO Biological Processes
epithelial cell proliferation
multicellular homeostasis
lipid homeostasis
GPCR signaling
CNS neuron differentiation
sensory system development
reg. of leukocyte activation
reg. of epithelial differentiation
pattern specification process
skeletal system development
urogenital system development
neuropeptide signaling pathway
reproductive system devel.
cell-cell adhesion
connective tissue development
embryonic organ development
Transcription Factors
POU6F1
COMP1
LHX3
FOXO4
IRF1
MEF2
SRF
OCT1
FOX
OCT
HSF1
AP4
Set Size
-log(p)
KEGG
Neuroactive ligand-receptor
Systemic lupus erythematosus
Enrichment Ratio
D
Diestrus
Proestrus
FCG - 12 mo
Hadad - 24 mo
Chucair-Elliott - 4 mo
Bundy - 4 mo
Hadad - 3 mo
Vied - 2 mo
Bundy - 2 mo
Bundy - 1 mo
# of Estrus DEGs
E
Chromosome
(XX vs. XY)
Tm7sf2
62
Siglech
Ctss
C4b
Syt2
26
123
Tgfb2
C1qa
C1qb
Nfkbia
Cd52
B2m
H2-D1
H2-K1
Irf7
Ifit3
Gonadal Sex
(M vs. F)
F
Tm7sf2
norm(GE)
XX
XY
G
Component 2 (20.2%)
Component 1 (33.9%)
Chromosome
XY
XX
Sex
F
M
H
I
Sex (M v. F)
cell killing
response to virus
response to protozoan
Chr (XX v. XY)
regulation of innate immune
response to virus
response to protozoan
Enrichment Ratio
J
Irf7
K
Ifit3
L
B2m
M
H2-D1
N
H2-K1
normalized RQ
Female
Male
XX Female
XX Male
XY Female
XY Male

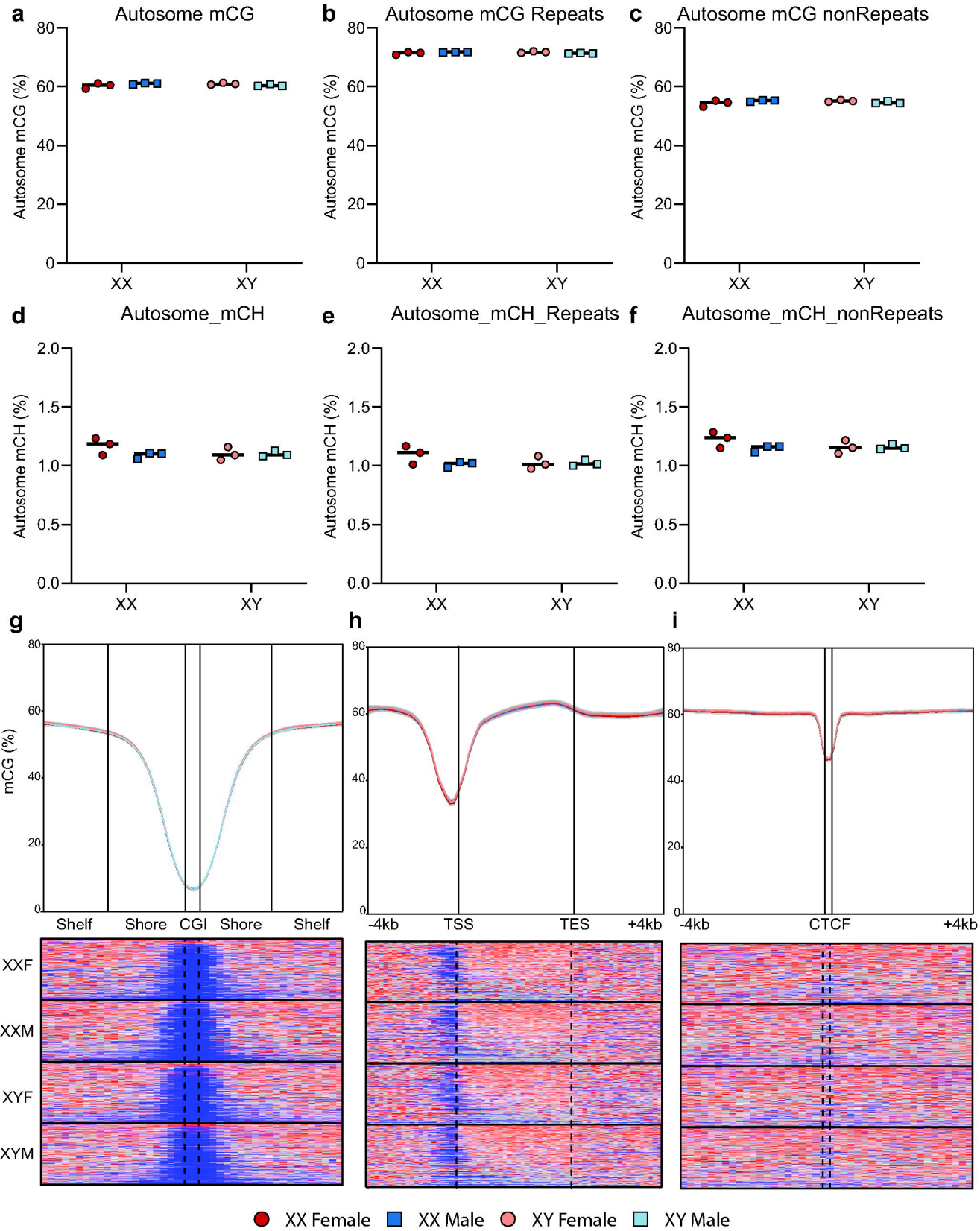
a
Autosome mCG
Autosome mCG (%)
b
Autosome mCG Repeats
c
Autosome mCG nonRepeats
d
Autosome_mCH
Autosome mCH (%)
e
Autosome_mCH_Repeats
f
Autosome_mCH_nonRepeats
XX
XY
g
h
i
mCG (%)
Shelf
Shore
CGI
-4kb
TSS
TES
+4kb
CTCF
XXF
XXM
XYF
XYM
XX Female
XX Male
XY Female
XY Male

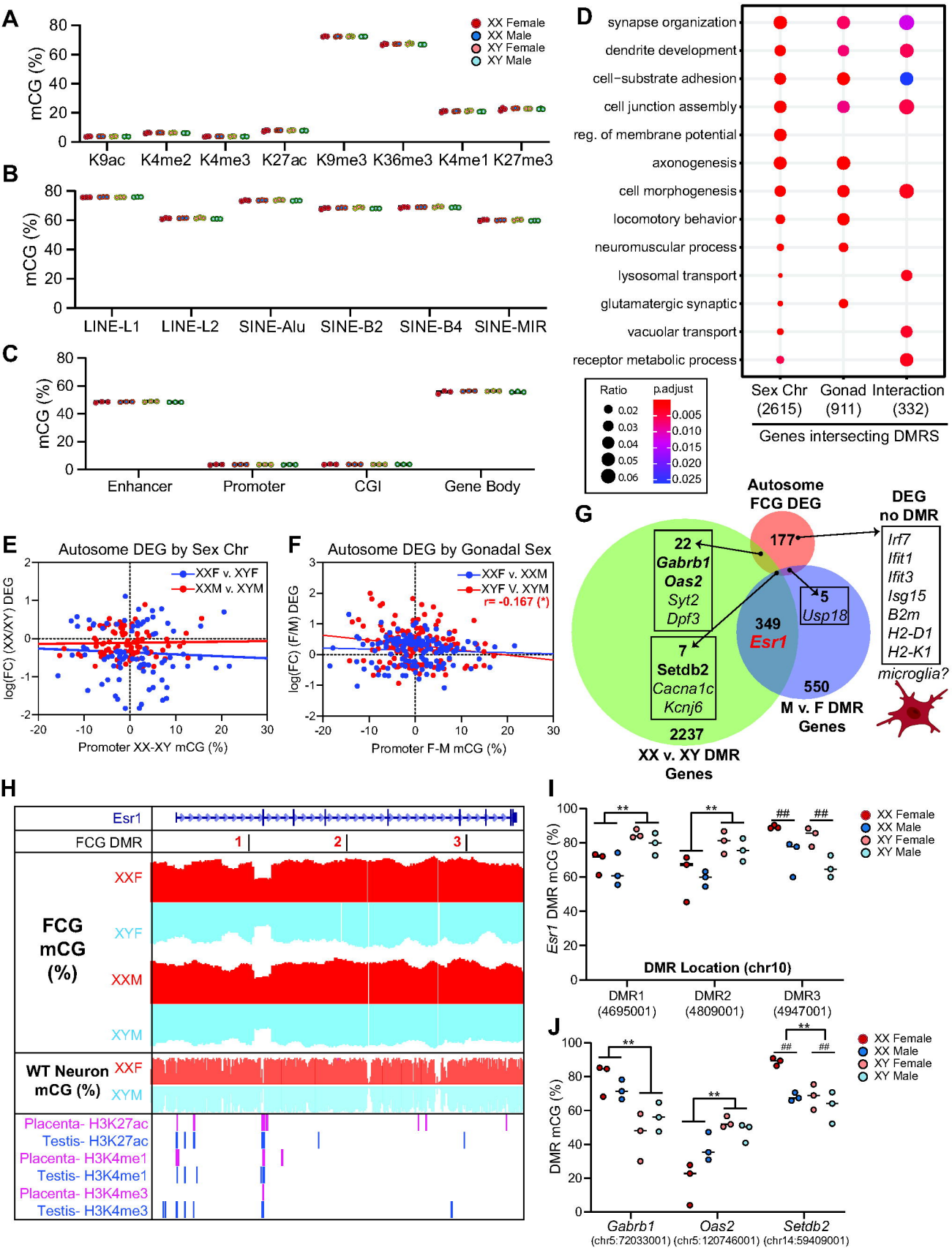
A
mCG (%)
XX Female
XX Male
XY Female
XY Male
K9ac
K4me2
K4me3
K27ac
K9me3
K36me3
K4me1
K27me3
B
LINE-L1
LINE-L2
SINE-Alu
SINE-B2
SINE-B4
SINE-MIR
C
Enhancer
Promoter
CGI
Gene Body
D
synapse organization
dendrite development
cell−substrate adhesion
cell junction assembly
reg. of membrane potential
axonogenesis
cell morphogenesis
locomotory behavior
neuromuscular process
lysosomal transport
glutamatergic synaptic
vacuolar transport
receptor metabolic process
Ratio
p.adjust
Sex Chr (2615)
Gonad (911)
Interaction (332)
Genes intersecting DMRS
E
Autosome DEG by Sex Chr
XXF v. XYF
XXM v. XYM
log(FC) (XX/XY) DEG
Promoter XX-XY mCG (%)
F
Autosome DEG by Gonadal Sex
XXF v. XXM
XYF V. XYM
r= -0.167 (*)
log(FC) (F/M) DEG
Promoter F-M mCG (%)
G
Autosome FCG DEG
DEG no DMR
22
Gabrb1
Oas2
Syt2
Dpf3
177
Irf7
Ifit1
Ifit3
Isg15
B2m
H2-D1
H2-K1
5
Usp18
349
Esr1
7
Setdb2
Cacna1c
Kcnj6
550
M v. F DMR Genes
2237
XX v. XY DMR Genes
microglia?
H
Esr1
FCG DMR
1
2
3
FCG mCG (%)
XXF
XYF
XXM
XYM
WT Neuron mCG (%)
Placenta- H3K27ac
Testis- H3K27ac
Placenta- H3K4me1
Testis- H3K4me1
Placenta- H3K4me3
Testis- H3K4me3
I
Esr1 DMR mCG (%)
DMR Location (chr10)
DMR1 (4695001)
DMR2 (4809001)
DMR3 (4947001)
J
DMR mCG (%)
Gabrb1 (chr5:72033001)
Oas2 (chr5:120746001)
Setdb2 (chr14:59409001)